Doctoral Dissertation

Development of Practical Multispectral Bathymetry for Indonesian Coral Reefs

インドネシアのサンゴ礁における実用的なマルチスペクトル測深法の開発

March, 2017

Masita Dwi Mandini Manessa

Graduate School of Science and Engineering

Yamaguchi University

Acknowledgment

This study would not be possible without the scholarship from the Indonesia Endowment Fund (LPDP) granted to me from September 2013 to March 2017, for which I am very grateful.

Firstly, I will forever be thankful to Professor Masahiko Sekine. Sekine Sensei has been helpful in providing advice during my study. He was and remains my best role model for a scientist, mentor, and teacher. His enthusiasm and love for research is contagious.

Secondly, I would like to express my sincere gratitude to my advisor Dr. Ariyo Kanno for the continuous support of my Doctoral study and related research, for his patience, motivation, and immense knowledge. His guidance helped me in all the time of research and writing of publication and this thesis. I could not have imagined having a better advisor and mentor for my Doctoral study.

Besides my advisor, I would like to thank the rest of my thesis committees Professor Koji Asai, Professor Hideaki Nakamura, Professor Yoshiki Mizukami and Associate Professor Koichi Yamamoto for their insightful comments and encouragement, but also for the question which incented me to widen my research from various perspectives. My special thanks goes to Professor Tatsuku Tanaka and Dr, Takahiro Osawa that give the opportunity to come Yamaguchi University.

I thank my fellow laboratory mates for all the fun we have had; Yudha, Wang, Loc, May, Shahira, Ashraf, and Uyen. All the friend that have graduate earlier that I can mention one by one. The cressos student in Yamaguchi University that all give many kind help: Riri, Dita, Sudi, Edi, and Tiwi. All Indonesia friends that study together in Yamaguchi University. Life won't be fun with them.

Also I thank my colleague in the following institution Hasanuddin University, Indonesia National Institute of Aeronautics and Space (LAPAN), Indonesia Geospatial Agencies (BIG), Udayana University, Bogor Agricultural Institute (IPB), Indonesia Science Institute (LIPI). In particular, I am grateful to Dr. Nurjannah Nurdin, Dr. Eric J. Hochberg, Mr. Gathot Winarso, Mr. Syarif Budhiman, Dr. M. Rokhis Komarudin, Mrs. Marlina Nurlidiasari, Mrs. Sari, Mr. Doddy Yuwono, Mr. Abd

Assyakur, Dr. Takahiro Osawa, Mr. Ari Anggoro, and Mr. Muhammad Hafiz for helping me with the data and the stimulating discussions.

Last but not the least, I would like to thank my family: my parents, my brothers and sister and my big families for supporting me physically and spiritually throughout writing this thesis and my life in general. Especial thank goes to my beloved husband Muhammad Haidar for the patient and support.

Summaries

In the maritime country such us Indonesia, bathymetry data in coastal areas is important for nautical information, coastal area zoning, conservation, and scientific studies. Manual bathymetry survey methods use a boat and a single- or multiple-beam echo sounder. This technique is time-consuming and becomes hazardous in coastal areas, especially in coral reefs, creating the need for a safe and practical method for extracting bathymetry information from these areas. As an alternative, Multispectral Satellite Derived Bathymetry is a remote sensing approach for mapping shallow-water depth; compared with conventional manual survey methods, bathymetry data can be derived more quickly, cheaply, safely, and often at a higher spatial resolution (depending on the spatial resolution of the image).

The primary objective of this thesis was to develop a practical method to estimate the water depth of Indonesia coral reef areas with a small number of the in-situ measurement. The practical method was using Lyzenga's Multispectral Bathymetry (hear after call as "Lyzenga's") SDB Formula and applicable for Worldview-2 image. In order to achieve an accurate estimation, three following steps was performed. First, an investigation for the best atmospheric correction for water depth estimation. Second, an evaluation of Lyzenga's Multispectral Bathymetry under a variety of optical conditions and bottom types. Last, build the water depth estimation formula based on simulated-derived coefficients then test the performance of ten coral reef sites in Indonesia.

The atmospheric noise for multispectral images plays an importance rule for achieving an accurate Bathymetry map. The first part of this study was comparing the effects of three common atmospheric correction methods (i.e: 6S based: Second Simulation of a Satellite Signal in the Solar Spectrum, DOS (Dark Object Subtraction), and Lyzenga et al., 2006 (hear after call as "Lyzenga06")) on the accuracy of Lyzenga's SDB formula using WorldView-2 images of coral reef sites. It was found that the method using radiative transfer simulation (6S) had little effect on accuracy, whereas Dark Object Subtraction had no effect whatsoever because a homogenous

atmosphere was assumed. Pixel-wise correction using near-infrared bands (Lyzenga06) was the only method influencing accuracy, but it significantly reduced the number of valid pixels. In the application, this study recommends the usage of non-correction and Lyzenga06 correction method for each target image. Then, a statistical accuracy comparison can be conducted for each image by using cross-validation, as in this study.

As the second part of this study, a noiseless dataset of above-water remote sensing reflectance from WorldView-2 images over Case-1 shallow coral reef water was simulated using a radiative transfer model. The simulation-based assessment showed that Lyzenga's SDB formula performed robustly, with adequate generality and good accuracy under a range of conditions. As expected, the influence of bottom type on depth estimation accuracy was far greater than the influence of the other optical parameters, namely, chlorophyll-a concentration and solar zenith angle. Further, the Lyzenga's SDB formula, based on the simulation dataset, estimates depth when the bottom type is unknown almost as accurately as when the bottom type is known. Finally, the results of this study give a better understanding on Lyzenga's multispectral bathymetry formula under various optical conditions and a number of bottom types.

Attribute to the good result of Lyzenga's SDB formula on evaluation test. A set of coefficient from simulated dataset fitting (hear after call as "simulated-derived coefficient") was extracted to build the proposed depth estimation formula. Then, the formula was validated using real Worldview-2 images from ten shallow coral reef sites. Two pixels with known depth is needed to convert the relative depth into absolute. The best accuracy was achieved in six sites: Panggang Islands, Gili Mantra Islands, Badi Island, Sarappo Keke Island, Sarappo Lompo, Luwu lulu Islands, and Badi Island. In the shallow areas, the depth estimation was fairly accurate (RMSE 0.45 – 1.66 m), but the error gradually increased with depth. For other sites, the formula was failed (RMSE > 2 meter at any depth). This poor performance might indicate that out zero noise assumption on simulated dataset could not represent the actual condition. Even the tested image has pass atmospheric and surface correction but there was an opportunity that some noise still remain. To test this

suspicion, the simulated database was modified by added an additive noise that represents some actual condition. Then the same procedure of extraction of a set of a simulated-derived coefficient and the application to ten validation sites were also performed. The estimated depth from noisy assumption formula shows better accuracy for all the sites with 0.22– 1.96 m RMSE but the accuracy in the deeper areas (> 5m) still unsatisfactory (RMSE 1.16-10.84 m). In conclusion, the proposed noisy assumed simulated-derived coefficient was applicable for mapping a shallow water area (depth < 5m) and useful for minimizing the risk in bathymetry survey in a hazardous shallow coral reef.

List of Abbreviations

6S	Second Simulation of a Satellite Signal in the Solar Spectrum
BIG	*Badan Informasi Geospasial* (English: Indonesia Geospasial Agency)
DOS	Dark Object Subtraction
IOP	Inherent Optical Properties
KKP	Kementerian Kelautan dan Perikanan (English: Ministry of Marine and Fisheries Affair)
LAPAN	Lembaga Penerbangan dan Antariksa Nasional (English: Indonesia National Institute of Aeronautics and Space)
LIPI	Lembaga Ilmu Pengetahuan Indonesia (English; Indonesia Science Institute)
LLN	Lingkungan Laut Nasional (English: National Coastal Environment)
LPI	Lingkungan Pantai Indonesia (English: Indonesia Coastal Environment)
MLR	Multiple Linear Regression
RS	Remote Sensing
SDB	Satellite based Bathymetry
TOA	Top of Atmosphere
WV2	WorldView-2

List of Contents

List of Figures

List of Tables

Chapter 1. Introduction

1.1. Background and Motivation

In recent years, Indonesia's coral reef ecosystems have experienced an increase in anthropogenic activities, some of which can have a significant impact on the physical condition of the ecosystem. The number and magnitude of anthropogenic activities in coastal and shallow-water areas have become a serious problem regarding the preservation of coral reef ecosystems. By knowing the biogeochemical contents, water clarity, bathymetry, and distribution of benthic habitats within an area, I can estimate and analyze many aspects of the coral reef system, such as changes in bottom type in shallow-water coral reef habitats, the accounting of natural resources, and coastal area zoning, also known as protected marine areas. Sustainable regional planning is required in regions with coral reefs in order to preserve coral reef ecosystems.

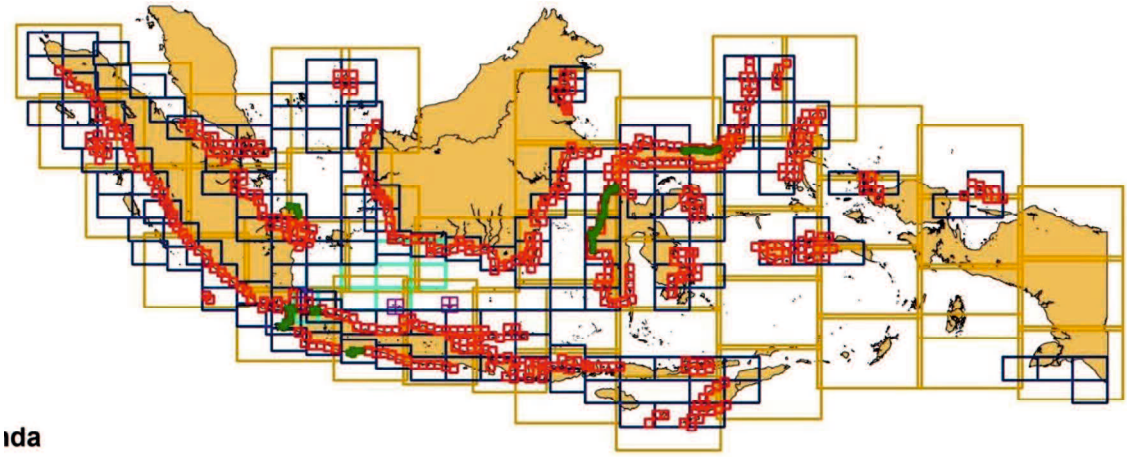

Figure 1-1 Map Index of National Ocean Environment (LLN in bahasa) and Indonesia Coastal Environment (LPI in Bahasa) (Source: BIG, 2015). LLN scale 1:500.000 (Orange rectangle), LLN scale 1:250.000 (Cyan rectangle), LLN scale 1:25.000 (Purple rectangle), LPI scale 1:250.000 (Blue rectangle), LPI scale 1:50.000 (Red rectangle), and LPI scale 1:25.000 (Green rectangle)

Bathymetric or water depth information is a crucial need in Indonesia as an archipelago states. To date, a lack of bathymetry information became the main obstacle in providing the National Ocean Environment (LLN in bahasa) and Indonesia Coastal Environment (LPI in Bahasa) of Indonesia water. Figure 1.1 shows the availability of those map until September 2015, where the detail map (LPI scale 1:25.000) was only cover 10 per cent of the mapping area. Indonesia's government has obtained their bathymetry data from survey measurements (echo sounding) and airborne Light Detection and Ranging (LIDAR). Both methods are time-consuming, expensive, and rely on vessel availability. Furthermore, the government was also facing issues to access remote coral reef areas, which resulted in the acquisition of sparse and few measurements. In these conditions, it is hard to apply the conventional depth estimation methods that require extensive measurement data to build an accurate model. Provide an alternative method that not required a massive field survey data could be a solution for Indonesian Government to map the bathymetry of their large coral reef areas. Satellite-derived bathymetry (SDB), which maps the depth of clear shallow waters (e.g., coral reefs) using a image taken from above and a small amount of in-situ soundings, is an efficient alternative to conventional techniques.

Satellite-derived bathymetry (SDB) is a remote sensing approach for estimating water depth based on the relationships between image pixel values and corresponding depth measurements in analytical or empirical way. The SDB method is a powerful tool for mapping shallow-water depth as, compared with conventional manual survey methods, the bathymetry can be derived at a greater speed, lower cost, and often at a higher spatial resolution (depending on the spatial resolution of the remote image). These techniques are especially suitable for remote areas or hazardous coastal areas (e.g., with high surf) where ship operations are logistically problematic. The obvious advantages over conventional echo sounding methods include the wide data availability, synoptic surface coverage, and high spatial resolution. The only caveat is that remotely sensed images need to be carefully calibrated to ensure the accuracy of extracted depth information.

The feasibility of deriving bathymetric estimates from remote sensing

imagery was first demonstrated using aerial photographs over clear shallow water (Lyzenga 1978). The technique has been expanded to include the use of passive optical multi-spectral satellite imagery including Landsat (Benny and Dawson 1983; Jupp et al. 1985; Lyzenga 1981; 1985), IKONOS (Stumpf, 2003). Moreover, the ready availability of multispectral images has made this method even more feasible. Due to the large surface of areas (Indonesia coral reef) to map, an approach involving multispectral remote sensing seems like an efficient and feasible way to map the bathymetry of the Indonesian coral reef.

Over the past three decades, several empirical methods for deriving bathymetry data from multispectral imagery have been proposed and investigated intensively (Paredes and Spero, 1983; Lyzenga, 1985; Clark et al., 1987; Spitzer and Dirks, 1987; Philpot, 1989; Jupp, 1989; Stumpf et al., 2003; Leckie et al., 2005; Lyzenga et al., 2006; Daniell, 2008; Ribeiro et al., 2008; Su et al., 2008; Su et al., 2013; Vinayaraj et al., 2016). The empirical SDB methods that utilize multispectral data can be categorized into four main techniques: First, the stratified genetic algorithm (SGA) is a development of the depth-of-precision (DOP) model proposed by Jupp (1988). Second, Stumpf et al. (2003) proposed a nonlinear inversion model, which has been modified by Sue et al. (2008) to include automated parameter calibration. Third, in a further modification of the previous method, Sue et al. (2013) combined nonlinear and Geographically Adaptive Inversion models; Vinayaraj et al. (2016) combined linear and Adaptive Geographically Weighted Regression models. Both groups aimed to handle the effects of geographic variation. Finally, the most popular method for use in coral reef environments has been the multiple linear regression method from Lyzenga et al. (2006) (hereinafter referred to as Lyzenga's), which was developed from previously proposed methods (Paredes and Spero, 1983; Lyzenga, 1985; Clark et al., 1987).

The Lyzenga method is based on the simple assumption of a linear relation between water depth and surface reflectance. This method only requires several pixels with known depth, reducing excessive survey work. Combining multiple linearized (i.e., logarithm of radiance or reflectance values) visible bands and known depth pixels into a linear formula for depth estimation, Lyzenga's multispectral

bathymetry model has been widely used and has been successful in many applications (Liceaga-Correa and Euan-Avila, 2002; Flener et al., 2012; Yuzugullu and Aksoy, 2014; Pacheco et al., 2014; Manessa et al., 2016; and Vinayaraj et al., 2016). The application of multiple combinations of bands is done to reduce the negative effects of optical conditions, such as bottom type (i.e. green, brown, or coralline algae species; *Montipora* species; *Enhalus* species; bright sand; rock; and ect.) and water quality, on the estimated depth values. Despite this mitigating step, Lyzenga (2006) posited that this method is only effective when the water quality is less heterogeneous and the number of bottom types is less than the number of bands used as input, which is unrealistic, especially in coral reef environments. Therefore, the generality of this method and its robustness under varying conditions (especially bottom types) is still an essential question.

In general way, the coefficient of the Lyzenga's SDB formula was estimated for each image independently using a number of in-situ measurement, as the same ways with other SDB method (Stumpf, 2003). However, the lack availability of number of in-situ measurement was became a limitation of generating an accurate formula (predictor). To answer the problems, Lyzenga et al. (2006) and Kanno and Tanaka (2012, 2013) demonstrated the application of single set of coefficient to several different image without calibration and with fairly good accuracy. This modification method was labelled as a generalized water depth estimation formula or generalized formula based on Lyzenga's SDB formula.

In this study I used different approach to build the generalized water depth estimation. Despite using an image of a site or multiple sites like the previous study (Lyzenga, 2006, Kanno et al. 2011, and Kanno et al. 2013), a simulated database based method was used to extract a set of coefficient then build the generalized formula. A simulated dataset was build based on radiative transfer theory that represent the Indonesia coral reef environment as our study site. This simulated dataset combined the spectral properties of a number of archived coral reef field reflectance measurements, along with various depths and various modeled Inherent Optical Properties (IOPs) of Case-1 coral reef water scenarios. That could cover all the possibility of surface reflectance that might reflected from Indonesia coral reef

environment.

The multispectral image that used in this study was WorldView-2. It has eight bands centered at 427, 478, 546, 608, 659, 724, 833 and 947 nm, which can be used for the analysis of shallow-water coral reef ecosystems. The Worldview-2 sensor has six visible bands, which provide higher spectral resolution than other common multispectral imagers (e.g., GeoEye-1, WorldView-1, QuickBird, IKONOS, SPOT-5, LANDSAT and ASTER). Common multispectral imagers with three visible bands are less effective in identifying water depth because of the less information in the spectral signatures. By applying the higher spectral resolution available from WorldView-2 imagery, this research intends to estimate water depth more accurately.

1.2. The Study Sites

The Indonesia Archipelago is touched on the Indian and Pacific Oceans as well as many seas, including the Andaman, Java, South China, Sulawesi, Banda, and Arafura Seas (Figure 1-1). A discontinues reef taking the shelf edge separated a large lagoon with many patch reef from open marine settings. The total area of coral reefs in Indonesia is about 85,707 km^2, which consist of 14,542 km^2 fringing reefs, 50,223 km^2 barrier reefs, 1,402 km^2 oceanic platform reefs, and 19,540 km^2 atolls. Made Indonesia as the largest coral reef nation in the world, which is a potential natural resource. The large scale of this coral reef is possible because of the suitable environmental conditions: warm temperatures, year-round sunshine, rich nutrient supply, and clear water (Allen, 2008).

The study area, shown in is located in Indonesia. Based on geographic boundary, our ten validation data: Gili mantra islands, Menjangan island, Gondol Beach, Panggang Island, Badi Island, Sarapo Keke Island, Barang Lompo Islands, Pamanggangan island, Luwu luwu Island and Sorong Island were set into five geographic area, Seribu Islands Archipelago, North Bali Water, Gili Mantra Islands, Spermonde Archipelago, and Papua Coastal. Each geographical area, might consist of one until four coral reef sites, a single image was belong for each site.

Figure 1-2 Map of Indonesia. The red circle with number indicate the location of five geographic area used as a study site: 1. Seribu Islands, 2. North Bali Coast, 3. Gili Mantra Islands, 4. Spermonde Islands, and 5. Papua Coast.

First, Seribu Islands are located in North of Jakarta (the capital city of Indonesia) or Java Sea (5°24' - 5°45' South and 106°25' - 106°40' East), which consist of 110 islands. These islands are remote areas where the distance of the nature reserve zone from Jakarta is approximately 37 nautical miles, and the nearest island (Bidadari Island) is only nine nautical miles away. As a representative of this location Panggang Islands (Figure 1-2) was chosen. Panggang Island is a high dense populated island that focuses on supporting the tourism activities. Due to the beautifulness of coral reef area, this Island became one of destination for marine tourism in Jakarta.

Second, North Bali is the driest area in Bali Islands, due to low rainfall intensity. This condition became a perfect condition for a coral reef to grow. Menjangan Island and Gondol Beach (Figure 1-3) is taken as the sample of the site that represent North Bali coral reef area. First, the Menjangan Island is a small island (about 1.75 km2) near the western edge of Bali Island. This island is a part of 190.23 km2 West Bali Nature Reserve area (114°26'-114°35' East and 8°5'-8°13' South), which conserves animal and vegetation of lowland rain forest. Second, the Gondol Beach is high economic marine areas that been utilized for marine product cultivation such us pearl, and grouper.

Third, the Gili Mantra Islands located on the off the coast of Lombok Island. Geographically, it spans 116°00'–116°08' East and 8°20–8°23' South, encompassing an area to the northwest of Lombok Island. The Gili Mantra Marine Natural Park includes three islands: Gili Trawangan, Gili Meno, and Gili Air (Figure 1-4). Tourism is the dominant economic activity in the islands, and more than 80 percent of families are employed by tourism in some form (Graci, 2007).

Four, the Papua coast is one of the largest coral reef areas in Indonesia. It has the marine natural resources that give it significant potential as a tourist area. However, there are disturbing signs of degradation, primarily as a result of destructive fishing practices (McKenna, 2002). Sorong coastal (Figure 1-5) is the representative of Papua coral reef areas, that plan to be built as one of the connecting port in Papua. Since this year, rapid development in sorong beach have started begin, that can disturbing the coral reef area.

Last, the Spermonde Archipelago (locally also known as Sangkarang Archipelago) is located on a submerged shelf along the west coast of South-West Sulawesi, Indonesia. The coral reef based livelihoods the Spermonde Archipelago in Southern Sulawesi can be seen as representative of many Indonesian and other southeast Asian island groups (Glaeser, 2012). Local communities living in the area have been parts of large trading networks for centuries, which, in combination with a recent rapid population growth, contributed to the overexploitation of marine resources (Ferse et al. 2012). An intensive coral reef destruction has been reported since the past decade, creating a large area of dead coral and rubble in many of the island (personal experience). Five islands (Figure 1-6) in Spermonde Archipelago is used as study site represent the coral reef areas of the center-east of Indonesia especially in Sulawesi area, namely, Badi Island, Sarappo Keke Island, Sarapo Lompo Islands, Pamanggangan island, and Luwu luwu Island. Beside Badi Island, the other four of the islands are a dense habitat island.

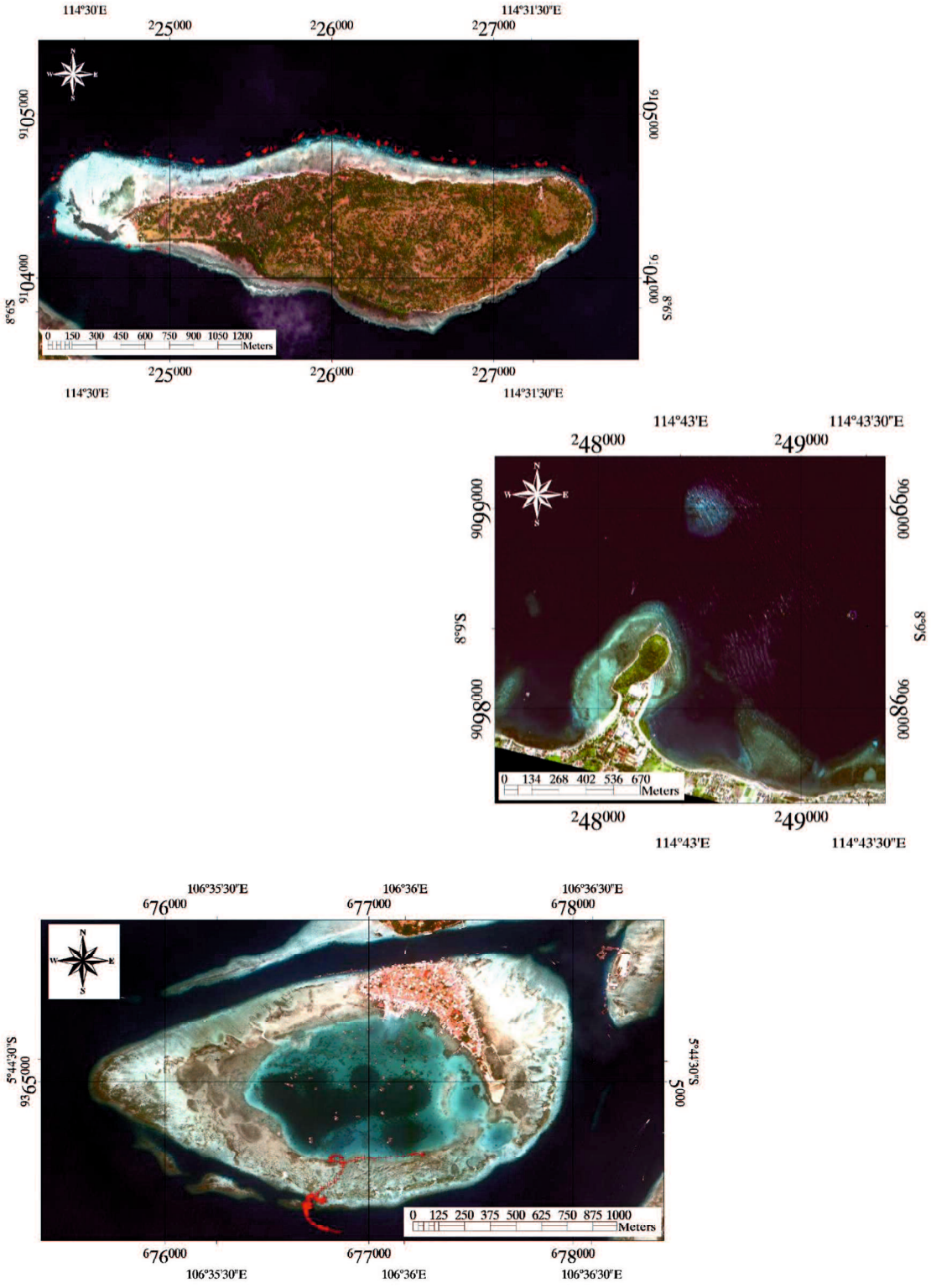

Figure 1-3 Worldview-2 image of Menjangan Island (upper) and Gondol Beach (Middle) and Gondol Beach (lower) in North Bali, Bali. The red mark shows bathymetry measurement location

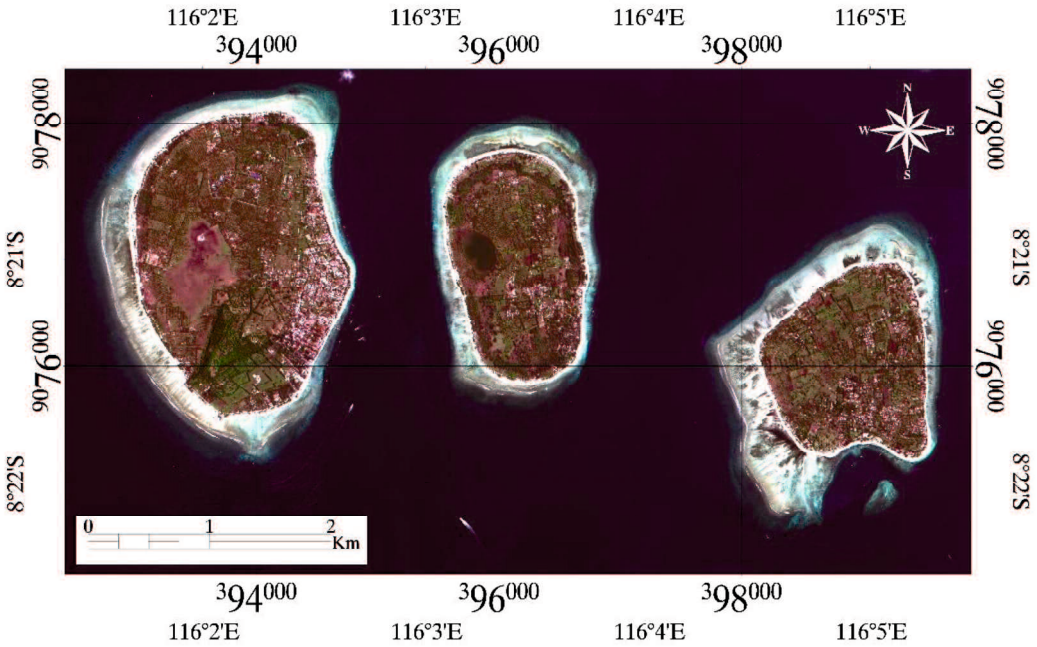

Figure 1-5 Worldview-2 image of Gili Trawangan Island, Gili Meno, Gili Air (West to East:) in Gili Mantra Islands, Lombok. The red mark shows bathymetry measurement location.

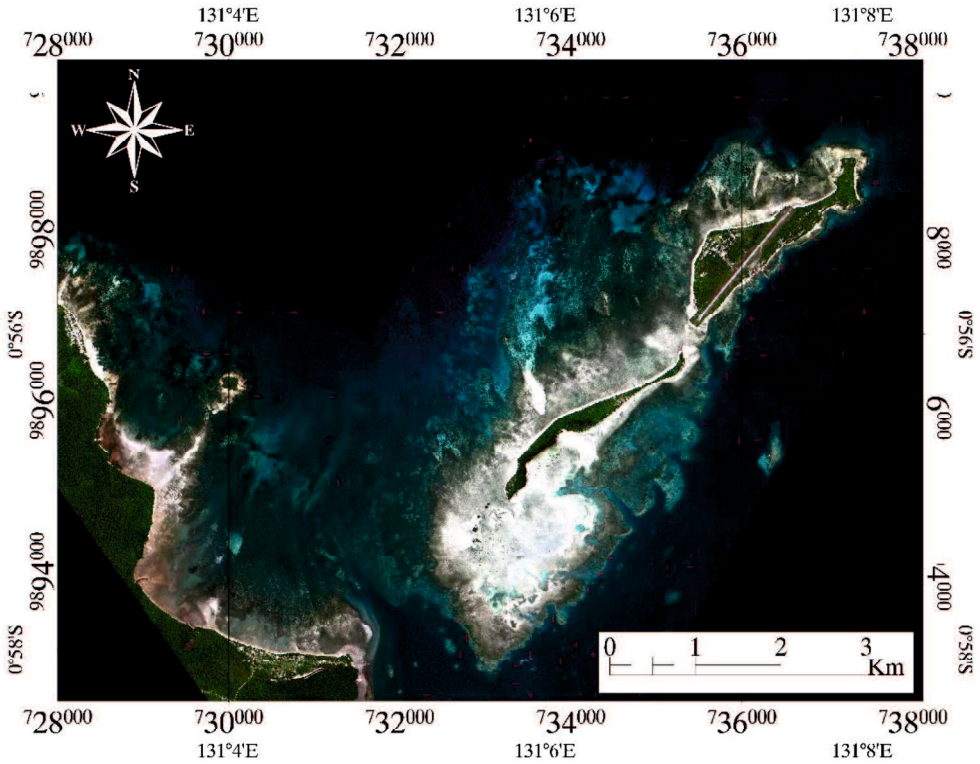

Figure 1-4 Worldview-2 image of Sorong Beach in Papua Coast, Papua Barat. The red mark shows bathymetry measurement location.

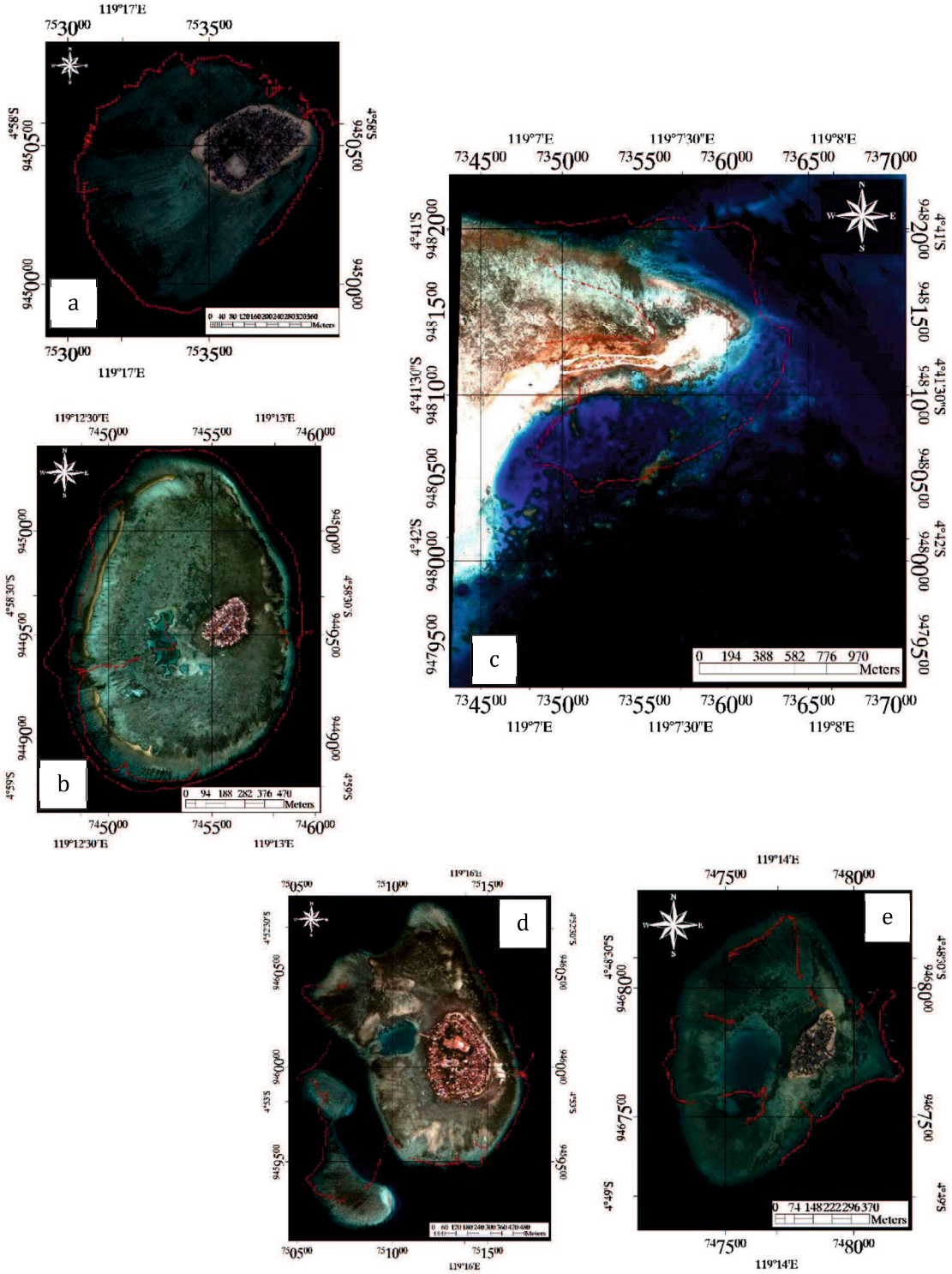

Figure 1-6 Worldview-2 image of Badi Islands (a),Luwu-luwu Island (b),Pamanggangan Islands (c), Sarappo Lompo (d), and Sarappo Keke (e) in Spermonde Islands, Sulawesi. The red mark shows bathymetry measurement location.

1.3. Objectives and Outline of the Thesis

The primary objective of this thesis was to develop a practical method to estimate the water depth of Indonesia coral reef areas that not require an intensive in-situ measurement. The practical method was using Lyzenga's SDB formula and applicable for the Wolrdview-2 image. In order to achieve an accurate estimation, three following steps was performed. First, an investigation for the best atmospheric correction for water depth estimation. Second, an evaluation of Lyzenga's SDB formula under a robust optical condition. Last, build a depth estimation formula based on fix coefficient derived from simulation dataset and Lyzenga's SDB formula then test the performance on ten coral reef site in Indonesia.

Lyzenga's SDB formula is the most popular method among researchers due to its practicality, and it became the reason why this study used this method as the base of the developed method. The basic theory of Lyzenga's SDB formula is importance to be explained. Moreover, three major data was used in this study: In-situ Bathymetry, Multispectral Image, and Simulation dataset. The detail of the data and methodology used in this study described in **Chapter 2**.

It has often been suspected that the atmospheric noise influences the performance of multispectral SDB. However, atmospheric correction performances have rarely been quantified, especially for SDB study. Using ten WV2 images from different coral reef sites, three common atmospheric corrections was compared. The analysis on the influence on SDB was then analyze. The result of this comparison study is described and discussed in Chapter 3. Moreover, since this study used WV2 images with six visible bands, then an analysis on the best pairs for SDB was left as a research gap. Then, a 63 bands pair combination was tested to identify the pair for SDB. An additional work was also done, including the analysis of bottom type classification using the Lyzenga's water column correction and supervised classification. This work was done because the linearity from the Lyzenga's SDB formula as the main topic and the importance of knowing the effect of atmospheric correction and spectral band improvement on bottom type classification.

The simulated based analysis was conducted to evaluate the Lyzenga's SDB formula that been doubt the performance using a simulated dataset of coral reef

environment just above surface reflectance. The simulated dataset is used for three analyses: First, Lyzenga's SDB formula is tested on a simulated dataset that represents a coral reef environment to determine whether Lyzenga's assumptions were unrealistic. In real-world data, the number of bottom types tended to exhibit higher levels of variation than the water quality did. Second, the effect of the quantity of bottom types present at a site is tested, representing the full range of bottom-type diversity that might appear in coral reef environments. Third, Lyzenga's SDB formula is tested in the case in which the bottom type is unknown. Ideally, the pixels with known depth used as input in Lyzenga's SDB formula should represent the whole range of depths and bottom types in the targeted area. However, it difficult to obtain representative input, because of the large area or varied bottom types of coral reef environments. Thus, this analysis becomes importance for evaluating the performance of Lyzenga's SDB formula. **Chapter 4** describe the ability of Lyzenga's SDB formula under robust optical condition.

After evaluating the Lyzenga's SDB formula, a set coefficients was extracted from the Lyzenga's regression model of a simulated dataset. This simulated-based coefficient used to build a water depth estimated formula of Indonesia coral reef environment. Thus, ten coral reef sites that represent Indonesia coral reef was used to test the performance of simulated-derived coefficient. **Chapter 5** describes the application of simulation-derived coefficients for multispectral bathymetry estimation formula on Indonesia coral reefs.

Chapter 6 begins with a synthesis which summarizes the most important findings of the previous chapters. Then followed by a general discussion which aims to put the results in the context of existing paradigms and to identify future strategies.

1.4. Publications

Some parts of the thesis are either published or in the process of being published. Where there are multiple authors, the thesis only contains the portion of these works that were written by the author of this thesis. Moreover, several achieved publication was not included in the thesis because of unrelated content.

1. **Manessa, M.D.M.**, Kanno, A., Sekine, M., and Nurdin, N., (2014). Investigation of WorldView-2 Spectral Cover for Identify Indonesia Coral Reef Stratum Types. In Proceeding of The 11th Hokkaido Indonesian Student Association Scientific Meeting (HISAS) 2014, Sapporo, Japan. (Printed)
2. **Manessa, M.D.M.**, Kanno, A., Sekine, M., Ampou, E.E., Widagti, N., and As-syakur, A.R. (2014). Shallow-water benthic identification using multispectral satellite imagery: investigation on the effects of improving noise correction method and spectral cover. Remote Sensing, 6(5): 4454–4472. doi: 10.3390/rs6054454. (Printed)
3. Poliyapram, V., Raghavan, V., Masumoto, S., Johnson, G., and **Manessa, M.D.M.**, (2014). Investigation of Algorithm to Estimate Shallow Water Bathymetry from Landsat-8 Images. In proceeding of International Symposium on Geoinformatics for Spatial Infrastructure Development in Earth and Allied Sciences 2014. Osaka. (Printed)
4. Winarso, G., **Manessa, M.D.M.**, Budhiman, S., and Kanno, A., (2016). Coral Reef Mapping in Indonesia: Comparison of Seven Supervised Classification Method and the Effect of Site Dependency. In proceeding of Indonesia National Symposium of Remote Sensing (SINASINDERAJA) 2016. Depok. (Printed)
5. **Manessa, M.D.M.**, Kanno, A., Haidar, M., Sekine, M., and Nurdin, N., (2016). Lyzenga Multispectral Bathymetry Formula for Indonesian Shallow Coral Reef: Evaluation and Proposed Generalized Coefficient. In proceeding of SPIE Remote Sensing Conference 2016. Scotland. (Printed)
6. **Manessa, M.D.M.**, Kanno, A., Sekine, M., Haidar, M., Y., Yamamoto, K., Imai, T., and Higuchi, T., (2016). Satellite-Derived Bathymetry Using Random Forest Algorithm and Worldview-2 Imagery. Journal of Geomatics and Planning. 4(2): 117 - 126. (Printed)
7. **Manessa, M.D.M.**, Haidar, M., Budhiman, S., Winarso, G., Kanno, A., Sagawa, T., and Sekine, M., (2016). Evaluating the performance of Lyzenga's water column correction in case-1 coral reef water using a simulated Wolrdview-2 imagery. IOP Conference Series: Earth and Environmental Science, 2nd International

Conference of Indonesian Society for Remote Sensing (ICOIRS) 2016. Yogyakarta. (Printed)

8. **Manessa, M.D.M.**, Kanno, A., Sagawa, T., Sekine, M., Yamamoto, K., Imai, T., Higuchi, T., and Nurdin, N., (201x). Simulation-based Investigation of the Generality of Lyzenga's Multispectral Bathymetry Formula in Case-1 Coral Reef Water. Coastal, Estuary, and Shelf Science. (Submitted)
9. **Manessa, M.D.M.**, Kanno, A., Sekine, M., As-syakur, A.R., Koibuchi, Y., Yamamoto, K., Imai, T., and Higuchi, T., (201x). Effect of Atmospheric Correction Methods on Multispectral Bathymetry. Applied Remote Sensing. (In preparation for submission)
10. **Manessa, M.D.M.**, Kanno, A., Sagawa, T., Sekine, M., and Nurdin, N., (201x). Generalized Multispectral Bathymetry Formula for Indonesian Coral Reef. GIScience & Remote Sensing. (In preparation for submission)

Chapter 2. Methodology

2.1. Lyzenga's Multispectral Bathymetry

The theory of Lyzenga's SDB formula is described as follows [13]. In the case of shallow water, the radiance observed by the satellite using a visible light sensor consists of four components: atmospheric scattering, surface reflection, in-water volume scattering, and bottom reflection as shown in Figure 2-1.

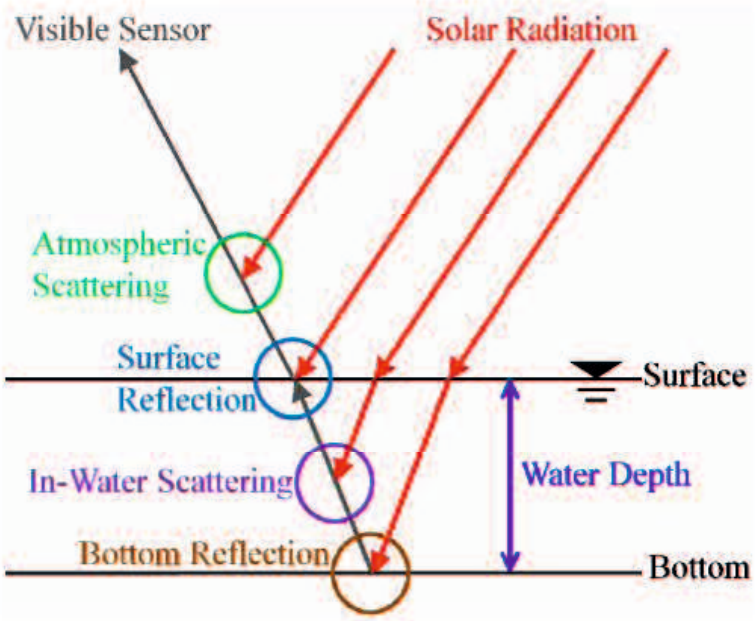

Figure 2-1 Schematic view of radiance components observed by the visible sensor over optically shallow water (Kanno, 2011).

$$Radiance\ at\ TOA = Bottom\ Reflection + In - Water\ Scattering + Surface\ Reflection + Atmospheric\ Scattering \quad \text{Equation 2-1}$$

Or simply written as a symbols as

$$L_{TOA} = B + V + S + A$$

Then the observed spectral radiance (L) or reflectance (R) at the top of atmosphere (TOA) is a function of the wavelength λ and can be expressed as:

$$L_{TOA} = \left(V + (B - V)e^{-kh}\right)TE + S + A \quad \text{Equation 2-2}$$

$$R_{TOA} = \left(V + (B - V)e^{-kh}\right)T + \frac{S}{E} + \frac{A}{E} \quad \text{Equation 2-3}$$

where V is the in-water volume scattering reflectance at infinite depth, B is the bottom reflectance, k is the effective attenuation coefficient, h is water depth, T is the round-trip transmittance through the atmosphere and water surface, V is the down-welling irradiance at the top of the atmosphere, S is the surface reflection component, and A is the path radiance. With the exception of h, all the terms in all equation are functions of λ; however, for notational convenience then it was omitted.

Lyzenga used a simple algorithm to explain bottom reflectance in relation to water depth and the physical properties of light. Several optical assumptions underlying the Lyzenga's method, in particular, it assumes no large changes in water quality and number of bottom types is less than the number of bands use as an input. The prediction formula is an algorithm based on linear regression. Then Lyzenga (1978) proposed a transformation to linearize approximately the relationship between the transformed radiances and the water depth. As following

$$X = \log\left(R_{TOA} - R_{TOA_\infty}\right) \quad \text{Equation 2-4}$$

At infinitive depth, the exponential function (Eq. 2-2 and 2-3) is negligible then can be written as

$$R_{TOA_\infty} = \mathrm{V}T + \frac{S}{E} + \frac{A}{E} \quad \text{Equation 2-5}$$

Substitute Eq 2-2 and 2-5 to Equation 2-4 then following equation obtain

$$X = \log\left(\left((B - V)e^{-kh}\right)T\right) \quad \text{Equation 2-6}$$

Simplified into

$$X = -kh + log(B - V)T$$

Or

Equation 2-7

$$X = -kh + C$$

Where C is a term dependent on the bottom reflectance, an apparent reflectance of deep water due to in-water scattering, round-trip transmittance through the atmosphere and water surface, and downwelling irradiance at the top of the atmosphere. In the case of multispectral image with m band, the variable X, k and C are define as

$$X \equiv (X_1 \dots X_m)$$

Equation 2-8

$$k \equiv (k_1 \dots k_m)$$

Equation 2-9

$$C = (log(B_1 - V_1)T_1 \dots log(B_m - V_m)m)$$

Equation 2-10

Lyzenga's (2006) proposed the propose a depth algorithm of the form

$$\hat{h} = \beta_0 + \beta_1 X_1 + \dots + \beta_M X_M$$

Equation 2-11

where $\beta_0, \beta_0, \dots, \beta_0$ are coefficients estimated by the least-square method using pixels with known depth. Necessary and sufficient condition for $\hat{h}$ in equation 2-11 to satisfy equation 2-10 are as follows:

$$\sum_{i=1}^{M} \beta_i k_i = -1$$

$$\beta_0 + \sum_{i-1}^{M} C_i \beta_i = 0$$

Equation 2-12

If k, V and T are homogeneous for pixel $\hat{h}$, there exist a β that satisfies equation 2-12, provide the number of bottom types is no greater than M. Above algebra explanation about Lyzenga Multispectral Bathymetry was adapted from Lyzenga et al. (2006), and Kanno and Tanaka (2011, 2012).

In application the method was apply as following steps. The first step, above water surface reflectance is corrected by subtracting the remote sensing reflectance of deep water:

$$R_{rs}^{cor}{}_{i} = R_{rs_i} - R_{rs}^{dp}{}_{i} \quad \text{Equation 2-13}$$

where *i* is the specific WorldView-2 band. Second, the corrected surface reflectance is linearized by taking a natural logarithm to yield X_{rs_i}:

$$X_{rs_i} = log\left(R_{rs}^{cor}{}_{i}\right) \quad \text{Equation 2-14}$$

Finally, a multiple linear regression analysis is conducted with depth (h) as the dependent variable and the linearized surface reflectance $\left(X_{rs_i}\right)$ as the independent variable. X_{rs_i} is an image-derived variable that theoretically has a linear relationship with depth (Paredes et al., 1983; Lyzenga et al., 1985). The coefficients β_i (i $= 0, 1, \cdots, 6$) in Eq. (11) were estimated (calibrated) by using least squares fitting on the training data (pixels with measured depth). In other terms, Eq. (11) was built by using multiple linear regression analysis, using depth as the dependent variable and the X_i as the independent variables. Multiple bands of X_i were combined to reduce the effect of inhomogeneity in bottom type and water quality.The complete multispectral bathymetry formula is summarized as follows:

$$\hat{h} = \beta_0 - \sum_{i=1}^{n} \beta_i \left(log\left(X_{rs_i}\right)\right) \quad \text{Equation 2-15}$$

where β_0 is the y-offset; β_i is determined by a regression analysis of depth against linearized reflectance; and n is the number of bands.

2.2. Data

2.2.1. Bathymetry and Tidal Data

Bathymetry data were measured using a single-beam echo sounder and a differential global positioning system (D-GPS). The measured depth data were affected by the tide. Hence, I need to convert the measured depth to mean sea levels (MSL) by subtracting the measured depth from the tide level of tide gauge. The tidal

data was based on the onsite tidal measurement and closes tidal station. Table 2.1 shoes the detail of bathymetry and tidal data in each sites.

Table 2-1 Bathymetry and Tidal data detail in each sites

Sites	Bathymetry			Tidal
	Measurement Date	Number of Measurement	Source	Source
Gili Mantra Islands	2011/09/25	3049	Personal Measurement	Personal Measurement
Gondol Beach	2013/10/12	82	KKP	KKP
Menjangan Island	2013/09/01	266	Personal Measurement	KKP
Panggang Islands	2013/05/24	769	BIG	BIG
Sorong Beach	2012/08/06	218	BIG	BIG
Pamanggangan Island	2012/06/10	671	Hasanuddin University	BIG
Sarappo Keke Island	2012/06/12	273	Hasanuddin University	BIG
Sarappo Lompo Island	2012/06/12	385	Hasanuddin University	BIG
Luwu luwu Island	2012/06/12	686	Hasanuddin University	BIG
Badi Island	2012/06/12	302	Hasanuddin University	BIG

2.2.2. Multispectral Dataset

The WorldView-2 high-resolution commercial imaging satellite was launched on October 8, 2009. The satellite is in a nearly circular, sun-synchronous orbit with a period of 100.2 minutes at an altitude of approximately 770 km. WorldView-2 acquires 11-bit data in nine spectral bands covering panchromatic, coastal, blue,

green, yellow, red, red edge, NIR1, and NIR2. The spectral response of each band is shown in Figure 1 (Updike and Comp, 2001)

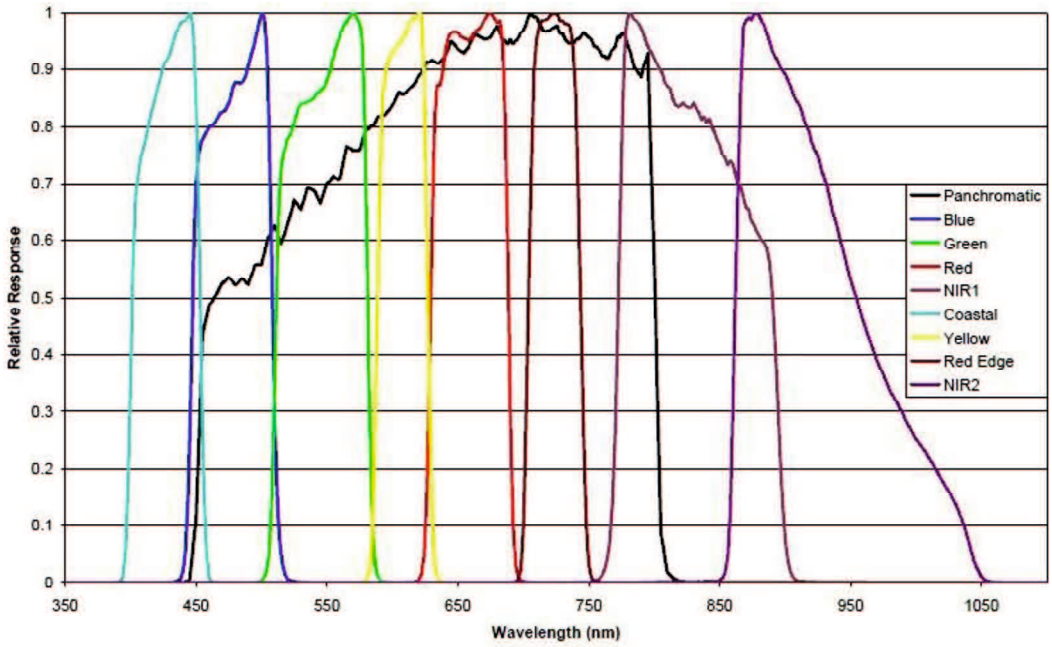

Figure 2-2 WV2 relative spectral response [nm].

In this study, level-2 radiometric-corrected WorldView-2 imagery with six visible bands and two near-infrared bands was used. Table 2-2 shows the imagery information for each site. According to the formulae and directions provided by the satellite data provider DigitalGlobe, the digital number was converted to top-of-atmosphere radiance L_{TOA_i} and reflectance ρ_{TOA_i} by the following formula:

$$L_{TOA_i} = \frac{K_i \,.\, q_i}{\Delta_i} \qquad \text{Equation 2-16}$$

$$\rho_{TOA_i} = \frac{\left(L_{TOA_i} . d_{ES}^2 . \pi\right)}{\left(Esun_i \,.\, \mu_s\right)} \qquad \text{Equation 2-17}$$

where d_{ES} is the Earth-Sun distance during image acquisition, $Esun_i$ is solar spectral irradiance, and μ_s is the cosine of the solar zenith angle during acquisition, K_i is the absolute radiometric calibration factor for a given band, q_i are radiometrically corrected digital numbers, and Δ_i is the effective bandwidth for a given band.

Table 2-2 WorldView-2 Image detail for each sites

Sites	Image ID	Acquisition date	Sun Zenith [degree]	Satellite Zenith [degree]
Gili Mantra	10JAN25024728-M2AS-052647590010_01_P001	2010/01/25	26.6	26.3
Gondol Beach	-	2013/05/04	30.3	13.5
Menjangan Island	-	2011/01/17	30.3	13.4
Panggang Island	13OCT05032942-M2AS-054968372050_01_P001	2013/10/6	7.2	6.609
Sorong Beach	11JUL29020537-M2AS-054968372070_01_P001	2011/7/29	6.27	7.7
Pamanggangan Island	14AUG28024013-M2AS-054968372010_01_P001	2015/08/28	64.5	68.8
Sarappo Keke Island	14AUG28024014-M2AS-054968372020_01_P001	2015/08/28	64.5	68.8
Sarappo Lompo Island	14AUG28024014-M2AS-054968372020_01_P001	2015/08/28	64.5	68.8
Luwu luwu Island	14AUG28024016-M2AS-054968372030_01_P001	2015/08/28	64.4	68.2
Badi Island	14NOV01024111-M2AS-054968372040_01_P001	2014/11/01	71.4	64

2.2.3. Simulation Dataset

2.2.3.1. Dataset description

In this study, a simulated dataset was created to represent multispectral images of a shallow coral reef environment. The simulation dataset is built based on several assumptions specific to the conditions of the Indonesian coral reef ecosystem. First, water is very clear with little suspended matter. Secondly, chlorophyll-α concentration ranges 0.02–5 mg m3. Thirdly, the sky is often clear, implying that

there is no significant noise such as cloud, haze, and smoke. Fourthly, due to the high resolution of the spatial imagery, there is a shorter pixel mixing spectrum. Finally, the water surface is calm with no significant white caps.

As input, Case-1 water conditions were modeled with differing combinations of water depths, chlorophyll concentrations, solar zenith angles, and numbers of bottom types reflectance, defines a follows. First, water depth is define as the high of water column from the top of surface object to the water surface. Second, in the case 1 water, the chlorophyll-a concentration was used as the main indicator to shows the water quality, and mg/m^3 is the unit used in this study. Third, solar zenith angle is the angle between the zenith and the center of the sun's disc. Last, bottom types is a specific object or species cover the ocean crust and submerged, namely, bright sand, rock, mud, green algae, brown algae, coralline algae sp., montipora sp., and enhalus sp..

The simulated dataset was built based on a zero noise assumption. Using the radiative transfer model, the above water remote sensing reflectance was then simulated according to the spectral response of each visible band of the WorldView-2 satellite sensor. Although the WorldView-2 sensor has visible bands with sensitivities greater than 700 nm (band 6), the majority of the spectral data available for coral reef bottom types were limited to 700 nm. Therefore, band 6 was excluded from further analysis. From here forward, all uses of the term “bands” refers to the first five bands of WorldView-2, namely, the coastal blue (band 1), blue (band 2), green (band 3), yellow (band 4), and red (band 5) bands, unless otherwise stated.

2.2.3.2. Radiative transfer model

The Lee et al. (1999) subsurface reflectance model was used to simulate the above water remote sensing reflectance just above the surface at nadir-view. The simulation was done from 400–700 nm at a 1-nm resolution and then rescaled to the spectral response of WorldView-2 bands 1–5. The radiative transfer model used to build the simulation dataset (Lee et al., 1999) was as follows:

$$R_{rs} \approx 0.5r_{rs}/1 - 1.5r_{rs} \qquad \text{Equation 2-18}$$

$$r_{rs} \approx r_{rs}^{dp}\left(1 - e^{-\left[\frac{1}{\cos(\theta_s)} + D_u^C\right]kH}\right) + \frac{\rho}{\pi} e^{-\left[\frac{1}{\cos(\theta_s)} + D_u^B\right]kH}$$ Equation 2-19

where R_{rs} is the above water remote sensing reflectance just above the surface; r_{rs} is the modeled subsurface reflectivity; r_{rs}^{dp} is the subsurface reflectance of optically deep water (infinitive depth); ρ is the bottom reflectance; θ_s is the subsurface solar zenith angle; D_u^c and D_u^B are the optical path-elongation factors for scattered photons from the water column and the bottom, respectively; k is the attenuation coefficient; and H is the depth.

The radiative transfer equation parameters depend greatly on the optical properties of the water, which were expressed through the following equations:

$$r_{rs}^{dp} \approx \big(0.084 + 0.17u(z,\lambda)\big)u(z,\lambda),$$ Equation 2-20

$$u(z,\lambda) = \frac{b_b(z,\lambda)}{a(z,\lambda) + b_b(\lambda z,\lambda)}$$ Equation 2-21

$$k(z,\lambda) = a(z,\lambda)b_b(z,\lambda)\mathrm{L}$$ Equation 2-22

$$D_u^c\,(z,\lambda) \approx \sqrt{1.03(1 + 2.4u(z,\lambda))}$$ Equation 2-23

$$D_u^b(z,\lambda) \approx \sqrt{1.04(1 + 5.4u(z,\lambda))}$$ Equation 2-24

$$b_b(z,\lambda) = b_w(\lambda) + b_{bp}(z,\lambda)$$ Equation 2-25

$$a(z,\lambda) = a_w(\lambda) + a_p(z,\lambda) + a_y(z,\lambda)$$ Equation 2-26

where u is the backscattering diffuse attenuation ratio; a_w, a_p, $and\ a_y$ are the attenuation coefficients for pure water, chlorophyll-bearing particles, and covarying yellow matter (i.e., colored dissolved organic matter; CDOM), respectively; and $b_w\ and\ b_{bp}$ are the backscattering coefficients for water and suspended particles, respectively. Lastly, the IOP parameters were calculated based on several equations below.

We used a new IOP model, which has been referred to in recent publications regarding absorption and scattering in Case-1 waters (Bricaud et al., 1998; Morel and Maritorena, 2001; Morel et al., 2002). The model is characterized as follows:

$$a_p(z,\lambda) = A(\lambda)[Chl(z)]^{E(\lambda)} \quad \text{Equation 2-27}$$

$$a_y(z,\lambda) = a_p(z,\lambda_{440})e^{[-0.0162(\lambda-\lambda_{440})]}, \quad \text{Equation 2-28}$$

$$b_{bp}(z,\lambda) = \breve{B}_p(z,\lambda)b_p(z,\lambda) \quad \text{Equation 2-29}$$

$$\breve{B}_p(z,\lambda) = \ 0.002 + (0.01[0.5 - 0.25log_{10}(Chl(z))]) \quad \text{Equation 2-30}$$

$$b_p(z,\lambda) = c_p(z,\lambda) - a_p(z,\lambda) \quad \text{Equation 2-31}$$

$$c_p(z,\lambda) = 0.407\ [Chl(z)]^{0.795}(\lambda/660)^{v} \quad \text{Equation 2-32}$$

where A and E are numerical constants (Bricaud et al., 1998); *Chl(z)* is the Chlorophyll-a concentration in mgm^3.

2.2.3.3. Optical conditions

The simulated dataset was built by combining the following two input steps: a gridded step and a random step. The aim of the gridded step was to distribute the value of each parameter evenly. Table 2-3 shows the optical conditions used through the gridded step to create a total of 211,200 combinations. The aim of the random step was to ensure that bottom type cases included in the random condition were within the range of conditions that commonly appear in coral reef environments. In this step, water depth, chlorophyll-a concentration, and solar zenith angle were set randomly within the realistic range of optical conditions shown in Table 2-3. The random step produced 211,200 combinations, which was equal to the output number of the gridded step.

As a quality control measure, simulated just-above-surface reflectances with a bottom contribution of less than 25% were excluded from the analysis, because they are less accurate (Carder et al., 2005). The percent of bottom contribution is the ratio of the bottom reflectance part of the remote sensing reflectance at nadir-view just above the surface (R_rs), to the the remote sensing reflectance at nadir-view just above the surface (R_rs), expressed in the following equation:

$$\%\ of\ bottom\ contribution = \left(\left(\frac{0.5\left(\frac{\rho}{\pi}e^{-\left[\frac{1}{\cos(\theta_S)}+D_u^B\right]kH}\right)}{1-1.5\left(\frac{\rho}{\pi}e^{-\left[\frac{1}{\cos(\theta_S)}+D_u^B\right]kH}\right)}\right)\Big/R_{rs}\right)\cdot 100 \qquad \text{Equation 2-33}$$

Table 2-3 Optical conditions for the gridded portion of the simulation dataset.

Input	Setting [units]
Depth	depth = $0.5 \cdot n\ (n = 1, 3, \cdots, 39)$ [m]
Chlorophyll-a concentration	chl = $0.02 * 2^{n/2}\ (n = 1, 3, \cdots, 15)$ [mg/m^3]
Solar zenith angle	sZ = $3 \cdot n\ (n = 0, 3, \cdots, 15)$ [degrees]
Bottom spectral reflectance (Figure 2-3)	Field spectra from 164 types of 5 major classes: coral, algae, dead coral, seagrass, and substrates from Indonesia, Japan, and Australia. Bali, Indonesia: Hochberg et al. (2004); Derawan, Indonesia: Nurlidiasari (2004); Spermonde, Indonesia: Nurjannah Nurdin (Personal archive data); Japan: Sagawa et al. (2010, 2012); Australia: Roelfsema and Phinn (2012).
Water refractive index	1.334

2.3. Atmospheric Correction

2.3.1. DOS (Dark Object Subtraction)

The DOS model is an old atmospheric correction method that is widely used due to its practicality. This method is based on the assumption that some pixels in an image are in complete shadow, and radiance or reflectance values received by the satellite for them are solely due to atmospheric scattering (Chavez, 1988). This method implicitly assumes the homogeneity of the atmosphere. The equation for the DOS method is as follows:

$$\rho_{c.DOS_i} = \rho_{TOA_i} - \rho_{TOA_{haze_i}} \qquad \text{Equation 2-34}$$

where $\rho_{c.DOS-COST_i}$ is the corrected reflectance for band i, and $\rho_{haze\ i}$ is the minimum reflectance value obtained from the histogram of each band.

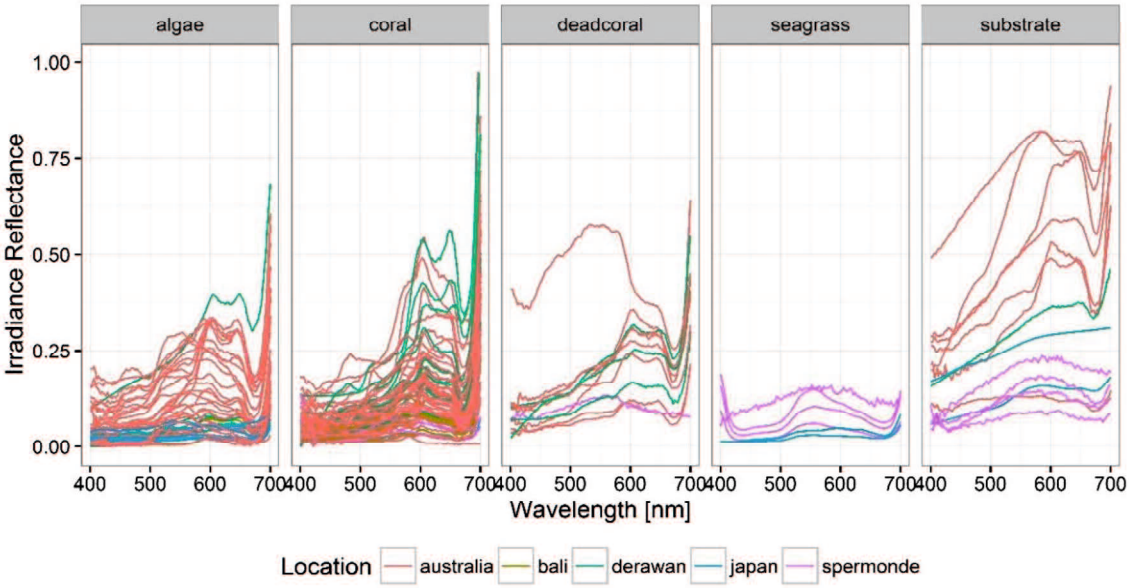

Figure 2-3. Bottom type spectra measured in the field for five different bottom cover classes. The line color denotes the measurement location, as defined in the legend.

2.3.2. *Lyzenga06 correction*

Lyzenga06 correction method is used for multispectral bathymetry and bottom classification. It does not assume the homogeneity of the atmosphere. Instead, it assumes that the reflectance in NIR bands does not depend on water depth even in shallow water because the attenuation coefficient is very large. Thus, this method assumes that pixel-wise variations in NIR bands represent those in atmospheric scattering and sea surface reflection components. If one of the two components is dominant, a correlation between arbitrary visible band reflectance and arbitrary NIR band reflectance is expected.

Because WorldView-2 has two NIR bands, correction can be carried out by using one or both of them. When a single NIR band is used, the correction formula for visible band i can be written as

$$\rho_{c.ly_i} = \rho_{TOA_i} - \alpha_{iNIR}.(\rho_{TOA.NIR} - \bar{\rho}_{TOA.NIR}) \qquad \text{Equation 2-35}$$

where $\rho_{TOA.NIRn}$ is the measured TOA reflectance in the nth NIR band, $\bar{\rho}_{TOA.NIRn}$ is that averaged over the deep water pixels (the pixels belonging to the deep area in the image, which was visually chosen in this study), and α_{iNIRn} is the slope of the simple regression line between visible reflectance and NIR reflectance for deep-water pixels.

When two NIR bands are used, the correction formula is

$$\rho_{c.ly_i} = \rho_{TOA_i} - \alpha_{iNIR1}.(\rho_{TOA.NIR1} - \bar{\rho}_{TOA.NIR1}) - \alpha_{iNIR}.(\rho_{TOA.NIR2} - \bar{\rho}_{TOA.NIR2}) \quad \text{Equation 2-36}$$

2.3.3. 6S code (Second Simulation of a Satellite Signal in the Solar Spectrum)

The 6S (Second Simulation of a Satellite Signal in the Solar Spectrum) is a famous radiative transfer code that calculates the corrected atmospheric reflectance (Vermote et.al., 1997) as

$$\rho_{c.6S_i} = \frac{\left(\frac{1/Tg_i}{T(\theta_s.\theta_v)_i}.\frac{-\pi s \cdot L_{TOA_i}}{\mu_s \cdot Esun} - \frac{\rho_{a_i}}{T(\theta_s.\theta_v)_i}\right)}{\left(1 + \left(\frac{1/Tg_i}{T(\theta_s.\theta_v)_i}.\frac{-\pi s \cdot L_{TOA_i}}{\mu_s \cdot Esun} - \frac{\rho_{a_i}}{T(\theta_s.\theta_v)_i}\right).\ s_i\right)} \quad \text{Equation 2-37}$$

where Tg is total gaseous transmittance, $T(\theta_s)$ and $T(\theta_v\ \theta_s)$ are the downwelling and upwelling of Rayleigh and aerosol scattering, respectively, ρ_a is the atmospheric scattering component, and s_i is the spectral albedo total of the atmosphere.

Although this is often misunderstood, our detailed investigation of the current version (6SV2.1) of 6S found that it assumes a homogeneous and Lambertian Earth surface when calculating $\rho_{c.6S_i}$ in Eq. (6). Eq. (6) is equivalent to the following equation:

$$\rho_{c.6S\,i} = (\mathrm{xa} \cdot L_{TOA} - \mathrm{xb})/(1 + (\mathrm{xa} \cdot L_{TOA} - \mathrm{xb}) \cdot xc) \quad \text{Equation 2-38}$$

Where

$$xa \equiv \left((1/Tg)/\left(T(\theta_s) \cdot T(\theta_v)\right)\right) \cdot (-\pi s/\mu_s \cdot Esun) \quad \text{Equation 2-39}$$

$$xb \equiv \rho_a/\left(T(\theta_s) \cdot T(\theta_v)\right) \quad \text{Equation 2-40}$$

$xc \equiv s$ Equation 2-41

are the values generated by 6S.

2.4. Evaluation Criteria

The accuracy of the depth estimation was evaluated by using the statistical criteria of the standard deviation (σ), coefficient of determination (R^2), and root-mean-square (RMS) error, which can be defined, respectively, as follows:

$$\sigma = \left(\frac{1}{n}\sum_i \left(\hat{h} - \bar{h}_i\right)^2\right)^{0.5} \quad \text{Equation 2-42}$$

$$R^2 = 1 - \sum_i \left(h_i - \hat{h}_i\right)^2 \Big/ \sum_i \left(h_i - \bar{h}\right)^2 \quad \text{Equation 2-43}$$

$$\text{RMS error} = \left(\sum_{i=1}^{n} \left(h_i - \hat{h}_i\right)^2 / n\right)^{0.5} \quad \text{Equation 2-44}$$

where h_i is the measured depth for the ith pixel in the test data, $\hat{h}_i$ is the estimated depth for the ith pixel in the test data, $\bar{h}$ is the mean of the measured depth over the test data, and n is the number of test data items. A large value of R^2 close to 1 and a small value of RMS error close to zero indicate satisfactory estimation accuracy. The average R^2 and RMS error values for 100 instances of cross-validation were used to assess the overall accuracy of MLR-based bathymetry with each atmospheric correction method.

2.5. Bottom Types Classification

2.5.1.1. Lyzenga's Water Column Correction

Transformed radiance (X) bands i and j are a linear function of water depth (Equation 2-42) and are linearly relate each other, for a given bottom types (Lyzenga, 1981). Then If the relationship between reflectance and depth is linear and the bottom type is constant, the scatter plot of transformed reflectance (X) bands i and j will fall ideally in a straight line and expressed as:

$$X_i = mX_j + y \qquad \text{Equation 2-45}$$

The slope (m) of this straight line represents the relative attenuation ($\frac{k_i}{k_j}$) in each combination of bands. The different bottom types represented in a scatter plot should create a similar line, the variation which indicates changes in depth. The gradient of each line would be identical because the ratio of the attenuation coefficients ($\frac{k_i}{k_j}$) is independent of bottom type.

The y-intercept of each line is subsequently used, independent of free of depth, as an index of bottom type; this is known as the depth-invariance index (Yij), which can be written as:

$$Y_{ij} = X_i - \frac{k_i}{k_j} X_j \qquad \text{Equation 2-46}$$

where X_i and X_j represent the transformed radiance at bands i and j, respectively; and ki/kj is the irradiance attenuation coefficient of water in bands i and j. The the ratio of attenuation coefficient (ki/kj) only holds when pixels of the same object at different depths are distributed linearly for the paired bands (Lyzenga, 1978).

2.5.1.2. Supervised Classification

The maximum likelihood classifier is a supervised classification method, which attempts to envisage the output of the bottom-type class. The maximum-likelihood algorithm assumes normality within the training data, and the parametric rule should be approximated by having an appropriate sample size. If the statistical characterization is approximated, then the image classification approach uses the maximum-likelihood decision rule with equal probabilities of the classes (Vanderstraete et al., 2004). The normal distribution of the statistics for each class in each band was a basic assumption in this classification method. The assumption is used to estimate the probability that a given pixel belongs to a particular class. The maximum likelihood method is applied to classify the bottom-type distribution using the depth-invariance indices, and the training area is used as the reference/training data. The following function is calculated for each pixel (Research System Inc., 2009):

$$g_i(x) - \ln p(\omega_i) - {}^1/_2 ln|\Sigma_i| - {}^1/_2 (x - m_i)^t \Sigma_i^{-1} (x - m_i) \quad \text{Equation 2-47}$$

where

i = class

x = n-dimensional data (where n is the number of bands)

$p(\omega_i)$ = probability that class ω_i occurs in the image; it is assumed to be the same for all classes

$|\Sigma_i|$ = determinant of the covariance matrix of the data in class ω_i

Σ_i^{-1} = its inverse matrix

m_i = mean vector

2.5.1.3. Classification Accuracy Test

The accuracy test was referenced to thematic accuracy, which has the non-positional characteristics of spatial data. If the data were to be subjected to hyperspectral or multispectral classification, then thematic accuracy would correlate to classification accuracy (Stehman, 1997). This accuracy refers to the correspondence between the class label and the "true" class, which is generally defined as that observed on the ground during field surveys (Green et al., 2000). In other words, it refers to how much of the class, which is labeled as coral reef on a classified image, is a coral reef *in situ*.

In this assessment, an error matrix (user accuracy) was used to identify object accuracy, and kappa analysis used to identify statistical difference accuracy. The accuracy of the predicted coral reef ecosystem map is represented as user accuracy. A user of this map will find that each time an area labeled as coral reef on the map is visited, there is only an *n*% probability that it is actually coral reef (Green et al., 2000). Moreover, the kappa statistic is an estimator of *n* parameters for a population of subjects and observers (Abraira et al., 1997). The kappa coefficient was first proposed by Cohen (1990). It measures whether two (or more) observers are independent by classifying items or observations into the same set of *n* mutually exclusive and exhaustive categories. It may be of interest to use a measure that summarizes the extent to which the observers agree in their

classifications (Kvalseth, 2011). Based on kappa statistics, one can test whether two datasets have statistically different accuracies (Smith, 2012).

Chapter 3. *Effect of Atmospheric Correction Methods and Multispectral Bands for Coastal Application*

3.1. Introduction

In the coral reef coastal application, the multispectral imagery able to provide the information of bathymetry, bottom type distribution, water quality, and shoreline change and etc. Two importance information to preserve coral reef ecosystems are bathymetry, and bottom type distribution. By knowing the distribution of water depth and objects within an area, we can estimate and analyze many aspects of the coral reef system, such as changes in bottom type in shallow-water coral reef habitats, the accounting of natural resources, and coastal area zoning, also known as protected marine areas. Sustainable regional planning is required in regions with coral reefs in order to preserve coral reef ecosystems. The threats to a coral reef ecosystem are not only from within the local reef environment, but also from the environment around it.

The first step in multispectral image analysis is to calculate a variable proportional to the reflectance just above the water surface (we call it "corrected reflectance" in the following) from the observed TOA (top-of-atmosphere) radiance, for each pixel and band. This step is called "atmospheric correction." Atmospheric correction methods are required to obtain sufficient accuracy in multispectral bathymetry (Martin et al., 2012, Mahiny and Turner et al., 2007).

Atmospheric correction over coastal waters is particularly challenging due to the considerably lower signal-to-noise ratio attainable at the sensor level on shorter wavelengths than that on land (Pacheco et al., 2015). Atmospheric correction has proven to be a crucial step in the processing of high-resolution images for coastal applications (Brando et al., 2009; Eugenio et al., 2015). However, it remains unclear which atmospheric correction method is most suitable for shallow-water bathymetry or bottom type classification.

The first aim of this chapter is to test the effectiveness of three common

atmospheric correction methods for multispectral bathymetry and compare them with the case where no atmospheric correction is carried out, where the corrected reflectance is substituted by TOA reflectance. The methods tested were the DOS (Dark Object Subtraction), Lyzenga06 pixel-wise sun-glint correction method, and a method based on the 6S (Second Simulation of a Satellite Signal in the Solar Spectrum; Vermote et.al., 1997) radiative transfer model. Lyzenga06 correction method was built for shallow-water application (bathymetry and bottom-type classification), whereas DOS and 6S code are general purpose. In this study, I excluded commercially available atmospheric correction methods (MODTRAN, ACORN, QUAC, and FLAASH) for the sake of generality. We were focus on identifying the non-commercial methods that generally and widely used. We used WorldView-2 images of five coral reef sites and the popular multispectral bathymetry method based on MLR (Multiple Linear Regression) (Paredes (1983), Lyzenga et al., (1985)) for the test.

Several studies, for instances Kerr (2002), Lee et al. (2011), Doxani et al.(2012), and Eugenio et al. (2015), have been carried out on SDB using WV2 imagery. Since WV2 imagery has 6 visible bands then choosing the right band combination for SDB was also important. Kerr (2002) has revealed the best pair of WV2 bands for the combination of linear ratio and MLR method. However, identifying the best pair SBD was never done before. Then this study was also examined 63 possible pairs from six visible bands of WorldView-2 image was equally tested as an input to identify the best pair band for SDB and became the second aims.

This paper was also call into question on the effect of atmospheric correction and spectral bands Improvement on bottom type classification. WorldView-2 has already been used for studies involving bottom-type identification in shallow-water coral reef habitats. However, to the best of our knowledge, this is the first time that bottom-type identification has been conducted using WorldView-2 imagery, together with the Lyzenga method and the improved noise correction using the NIR band, as the third aim of this chapter.

3.2. Methods Overview

In attempt to do the evaluation the effect of atmospheric correction and number multispectral bands, three following steps are performed. First, three correction methods mentioned above were applied to ten coral reef sites in Indonesia: Gili Mantra, Gondol Beach, Menjangan Island, Panggang Island, Sorong Beach, Pamanggangan Island, Sarappo Keke Island, Sarappo Lompo Island, Luwu luwu Island, and Badi Island.

The corrected reflectance obtained from each atmospheric correction method (including the no correction cases) was used as an input to MLR-based bathymetry. Because Lyzenga et al.'s method allows three choices of NIR bands, I had a total of six cases, as shown in Table 3-1.

Table 3-1 Six cases of atmospheric correction.

Case	Description
1	Without atmospheric correction (non-correction case)
2	DOS correction
3	6S-based correction
4	Lyzenga06 correction using NIR 1 band
5	Lyzenga06 correction using NIR 2 band
6	Lyzenga06 correction using NIR 1 and 2 bands

Because our aim in this study was not actual depth mapping but accuracy evaluation, not all pixels obtained with the measured depth were used as training data; instead, pixels with measured depths were randomly partitioned with 80% used as training data and 20% as test data. The random partitioning was conducted 100 times, thus defining a cross-validation.

The effectiveness of each atmospheric correction method in terms of improving accuracy was quantified using the change from the non-correction case with R^2 (Eq. 3-1) and the change ratio in terms of RMSE (Eq. 3-2), defined as

$$\Delta_{R^2} = R^2_{atm.cor} - R^2_{no\ atm.cor} \qquad \text{Equation 3-1}$$

$$r_{RMSE} = (RMSE_{atm.cor} - RMSE_{no\ atm.cor})/RMSE_{no\ atm.cor}$$ Equation 3-2

Positive values of these measures increased whereas negative values decreased.

As discussed in Subsection 3.3.2, a significant reduction in valid shallow-water pixels resulted from the execution of certain atmospheric correction methods. In practical bathymetric mapping, a small reduction is as important as satisfactory accuracy. Therefore, the change ratio in the number of valid shallow-water pixels with depth measurements (NVSPM) was also calculated:

$$r_{NVSPM} = (NVSPM_{atm.cor} - NVSPM_{no\ atm.cor})/NVSPM_{no\ atm.cor}$$ Equation 3-3

Second, WV2 have six visible bands, 63 different pairs (= 6 combinations one band + 15 combinations of two bands + 20 combinations of three bands + 15 combinations of four bands + 6 combinations of five bands + 1 combination six bands) could be used as an input for Equation 2-15. We tested the performance of each pair to estimate the water depth.

Third, after the linearization (Equation 2-14), the known object pixels are applied to predict the ratio of the attenuation coefficients (ki/kj); sand is used because it is easily identified. The radiance value extracted from sand at various depths is used as input in calculating the attenuation coefficients (ki/kj). Then, the attenuation coefficient is calculated for each band pair. The rule of band pairing is that a band only pairs once with another band. Thus, three visible bands create three band pairs, while six visible bands create 15 band pairs. For each Lyzenga's correction method, this research derived ratios of attenuation coefficients from the transformed radiance (X) values. Then, the variable calculated above is added to the calculated depth-invariance index. A pair of bands is needed as an input with an attenuation coefficient for the same band pair. Each pair of spectral bands produces a single depth-invariant band. The data used in the classification process are the result of the depth-invariance index derived from Equation 2-43. The inputs for the classification process are the three and 15 depth-invariant bands from the three and six visible bands, respectively.

3.3. Results and Discussion

3.3.1. Atmospheric Correction on Multispectral Bathymetry

3.3.1.1. Results without Atmospheric Correction

Figure 3-1 shows a scatterplot of measured depth versus estimated depth at each site for the case with no atmospheric correction. The Menjangan site showed poor estimation (R^2 = 0.14): overestimation in shallow water and underestimation in deep water. However, at the other nine locations, MLR-based bathymetry estimated depth with 0.74-1.14 m RMS error and 0.73-0.96 R^2. This result, with no atmospheric correction, was used as the benchmark for evaluating the performances of atmospheric correction methods.

3.3.1.1. DOS and 6S-based Methods

In contrast with Lyzenga06 correction method, there was no data removal from the DOS and the 6S-based methods (Figure 3-2). Moreover, the DOS method exhibited no effect, and the 6S-based method yielded little effect, on accuracy, as shown in Figure 3-4. Although Martin (2012) proved that the DOS and the 6S-based methods can satisfactorily correct for reflectance, our study indicates these methods do not improve the accuracy of MLR-based bathymetry. Below, I investigate the theoretical reasons for why the DOS has no effect and the 6S-based method has little influence on accuracy.

X_i , defined by Eq. (12) for the case with no atmospheric correction, written as

$$X_{noAtmosphericCorrection\,i} = log\left(\rho_{TOA\,i} - \bar{\rho}_{TOA\,\infty_i}\right) \quad \text{Equation 3-4}$$

Using Eq. (3), DOS is shown to have no effect on X_i as follows:

$$X_{DOS\,i} = log\left(\rho_{c\,DOS_i} - \bar{\rho}_{c\,DOS\infty_i}\right) \quad \text{Equation 3-5}$$

$$= log\left(\left(\rho_{TOA_i} - \rho_{TOA_{haze_i}}\right) - \left(\bar{\rho}_{TOA\infty_i} - \rho_{TOA_{haze_i}}\right)\right)$$

$$= log\left(\rho_{TOA_i} - \bar{\rho}_{TOA\,\infty_i}\right) = X_{noAtmosphericCorrection\,i}$$

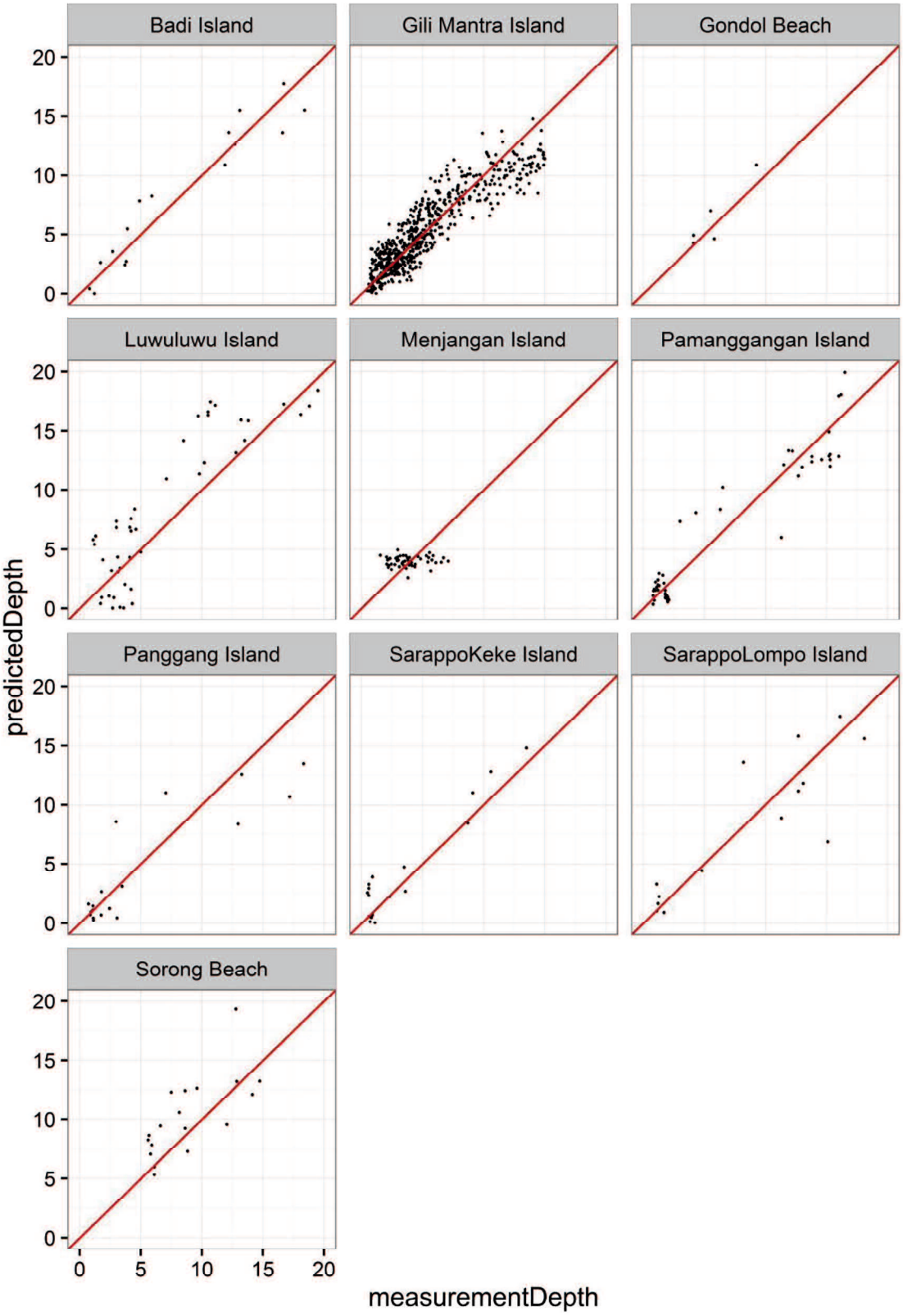

Figure 3-1 Scatterplot of the estimated and measured depths for each site when no atmospheric correction was applied.

Table 3-2 Atmospheric parameters calculated by 6S for each site. Some of the products of these parameters are also shown for discussion

Site	6S coefficients				
	xa	xb	xc	xa.xb	xb.xc
Gili Mantra Islands	0.003059	0.0515	0.093568	0.000158	0.004819
Gondol Beach	0.002814	0.050741	0.093571	0.000143	0.004748
Menjangan Island	0.003329	0.048554	0.093568	0.000162	0.004543
Panggang Islands	0.00288	0.055803	0.093581	0.000161	0.005222
Sorong Beach	0.003261	0.053888	0.093586	0.000176	0.005043
Pamanggangan Island	0.003185	0.060821	0.093586	0.000194	0.005692
Sarappo Keke Island	0.003185	0.060865	0.093586	0.000194	0.005696
Sarappo Lompo Island	0.003185	0.060813	0.093586	0.000194	0.005691
Luwu luwu Island	0.003188	0.060406	0.093586	0.000193	0.005653
Badi Island	0.002871	0.05471	0.093586	0.000157	0.00512

Thus, I show that theoretically, DOS has no effect on MLR-based bathymetry. Similarly, using Eq. (7) for 6S, I can derive

$$X_{6S\,i} = log\left(\rho_{c\,6S_i} - \bar{\rho}_{c\,6S\infty_i}\right) \qquad \text{Equation 3-6}$$

$$= log\left(\left(\frac{\text{xa}\cdot L_{TOA_i} - \text{xb}}{\left(1+\left(\text{xa}\cdot L_{TOA_i} - \text{xb}\right)\cdot xc\right)}\right) - \left(\frac{\text{xa}\cdot \bar{L}_{TOA\infty_i} - \text{xb}}{\left(1+\left(\text{xa}\cdot \bar{L}_{TOA\infty_i} - \text{xb}\right)\cdot xc\right)}\right)\right)$$

$$= log\left(\frac{L_{TOA_i} - \bar{L}_{TOA\infty_i}}{1+\left(\text{xa}\cdot L_{TOA_i} - \text{xb}\right)\cdot xc}\right) - C$$

$$= X_{noAtmosphericCorrection\,i} - C - log\left(1 - xb\cdot xc + xa\cdot xc\cdot L_{TOA_i}\right)$$

where $C \equiv log\left(xa\cdot\left(1+\left(xa\cdot \bar{L}_{TOA\infty_i} - xb\right)\cdot xc\right)\right)$ has a constant value for all the pixels in an image. Because the offset change in X_i in Eq. (11) does not change the linear form of the predictor, the constant offset C does not change the result of MLR-based bathymetry. Therefore, the effect of 6S-based correction is controlled only by the magnitudes of products $xb\cdot xc$ and $xa\cdot xc$. If these products are small in comparison with unity, $X_{6S\,i}$ approaches $X_{noAtmosphericCorrection\,i} - C$, and MLR-bathymetry is only slightly affected. Table 3-2 proves that these products were considerably smaller than 1 for all tested sites, and hence explains why there was

only a slight effect of the method on MLR-bathymetry shown in Figure 3-4. In summary, the atmospheric correction methods with the assumption of a homogenous atmosphere have no practical effect on MLR-based bathymetry.

3.3.1.2. Effectiveness of Lyzenga06 Correction Method

After applying each atmospheric correction method to the five sites and estimating the water depth, the number of data items for each site was reduced, as shown in Figure 3-2. For Lyzenga et al.'s method, a significant reduction of 2%-90% occurred. As an example Image of Gili Mantra Islands (Figure 3-3) was chosen to visually show the data reduction. The Lyzenga et al.'s correction method transformation generates a non-value (NaN) pixel for two object types, which are dense seagrass and bright sand (marked in Figure 3-3b). Sand reflectance in very shallow water does not follow the assumption that reflectance in the NIR band is absorbed completely by the water. Reflectance emitted from the sand in any NIR band is higher than the absorption properties of the water. Meanwhile, the dense seagrass reflectance is similar or slightly lower in value to the reflectance of the deep-water area, especially for low wavelengths, *i.e.*, coastal and blue band. The reflectance has low value and appears dark (Figure 3-3a) because the areas of seagrass absorbed the light. Based on Equation (2-36) of the Lyzenga et al.'s correction method, the calculated visible bands, which are subtracted from the NIR band after multiplication with the $\alpha(\lambda)$ coefficient, produce a negative value of the log function in this case. In order to describe the NaN pixel that appears in the Lyzenga et al.'s correction method, we perform a simple algebraic description, as below:

$$\log(L(\lambda)_i - \alpha(\lambda)_{i1}.L_{NIR1} - \alpha(\lambda)_{i2}.L_{NIR2}) = NaN$$

$$L(\lambda)_i < (\alpha(\lambda)_{i0} + \alpha(\lambda)_{i1}.L_{NIR1} + \alpha(\lambda)_{i2}.L_{NIR2}), \text{ then}$$

$$(L(\lambda)_i - \alpha(\lambda)_{i1}.L_{NIR1} - \alpha(\lambda)_{i2}.L_{NIR2}) = negative\ value$$

$$\log(L(\lambda)_i - \alpha(\lambda)_{i1}.L_{NIR1} - \alpha(\lambda)_{i2}.L_{NIR2}) = \log(-value) = NaN$$

Based on above explanation, such significant reduction is known to be mainly due to use of the NIR band. Unfortunately, the assumption that NIR band reflectance does not depend on water depth does not hold for shallow pixels with bright bottoms. This failure led to the overestimation of $\rho_{TOA.NIRn}$ in Eq. (2-36) and a

negative value of $\rho_{ci} - \bar{\rho}_{c\infty_i}$ in Eq. (2-35). It thus became impossible to calculate the log function in Eq. (2-14), resulting in data removal.

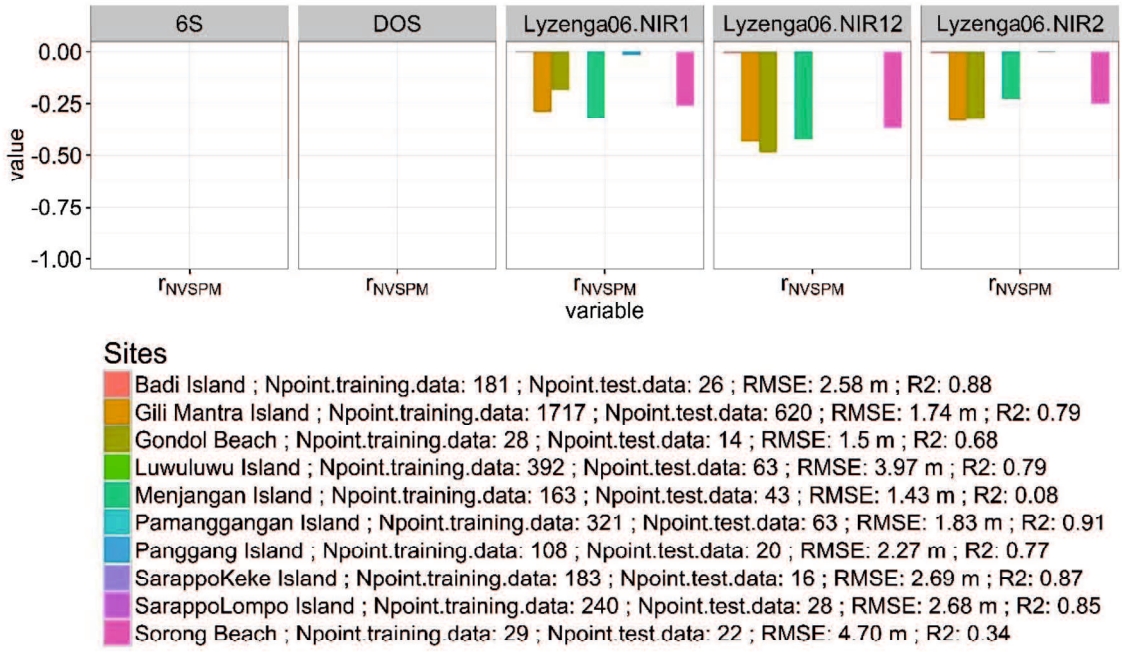

Figure 3-2 Reduction in the number of valid data items as a result of each atmospheric correction method, for each site. rNVSPM is the change ratio in the number of valid shallow-water pixels with depth measurements.

In other cases of coral reef ecosystems with different bottom-type characteristics, the reflectance of the bottom object is low in the NIR band. High reflectance of bottom type in shallow water is not only due to the high reflectance of the bottom, but also the adjacent effect. It is referred to as the effect of high reflectance emitted from objects in the coastal area, which are very close to the water body and being scattered in the atmosphere above the water area. The information recorded by the satellite not only consists of information of the water and spectral object below the surface, but also of the spectral object near the water body.

Figure 3-4 shows two measures of accuracy change, r_{RMSE} and Δ_{R^2}, defined in Eqs. (3-1) and (3-2), for each site. For a fair comparison, these measures were evaluated using only the pixels with measured depth that were not removed by any correction method. The result showed that atmospheric correction can decrease or

increase the accuracy of estimation depending mainly on the site in question.

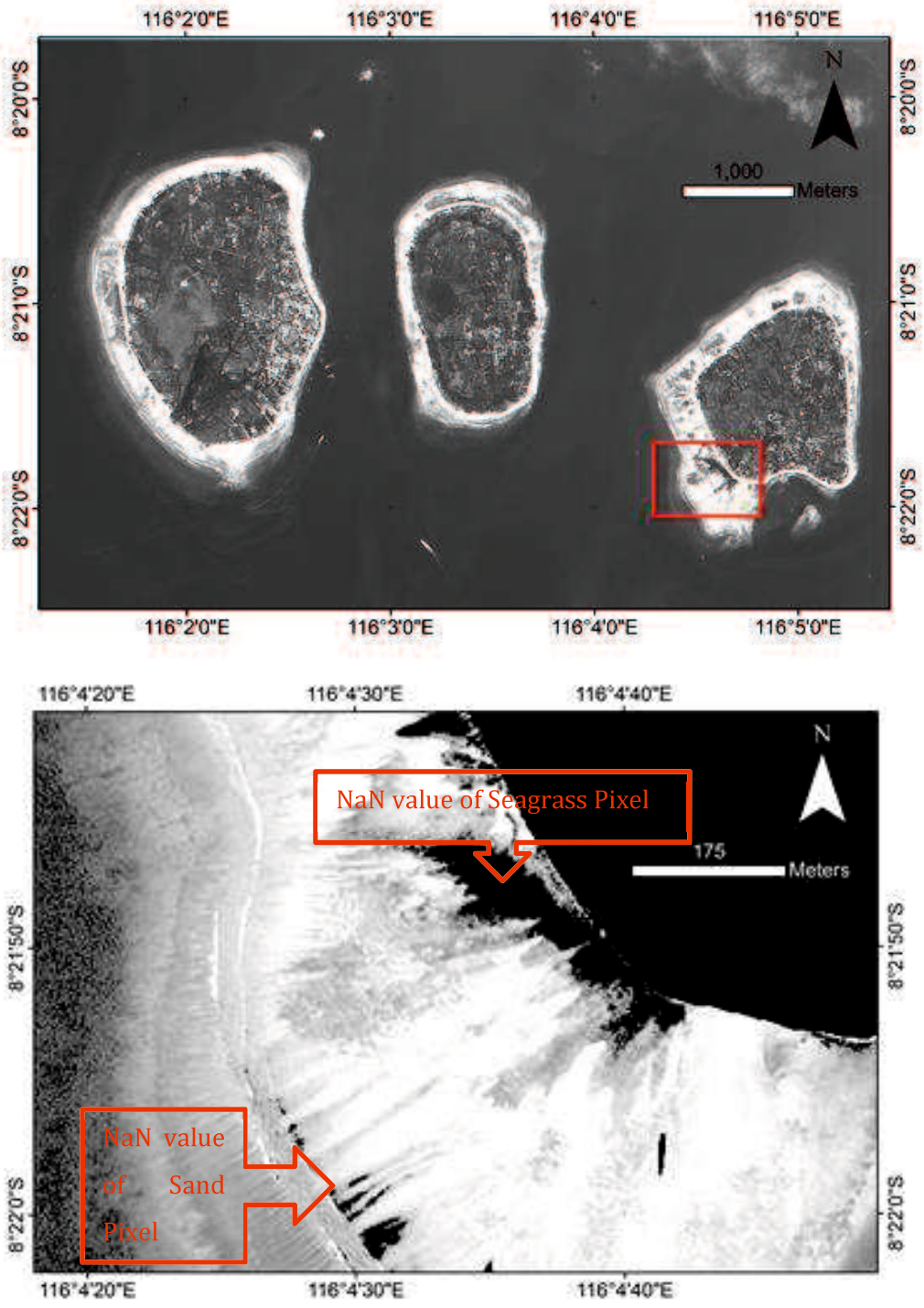

Figure 3-3 Visualization of WorldView-2 spectral reflectance; (a) Reflectance (b) transformed radiance of band 2 (Xi) in Lyzenga's correction. Images are represented using the band blue.

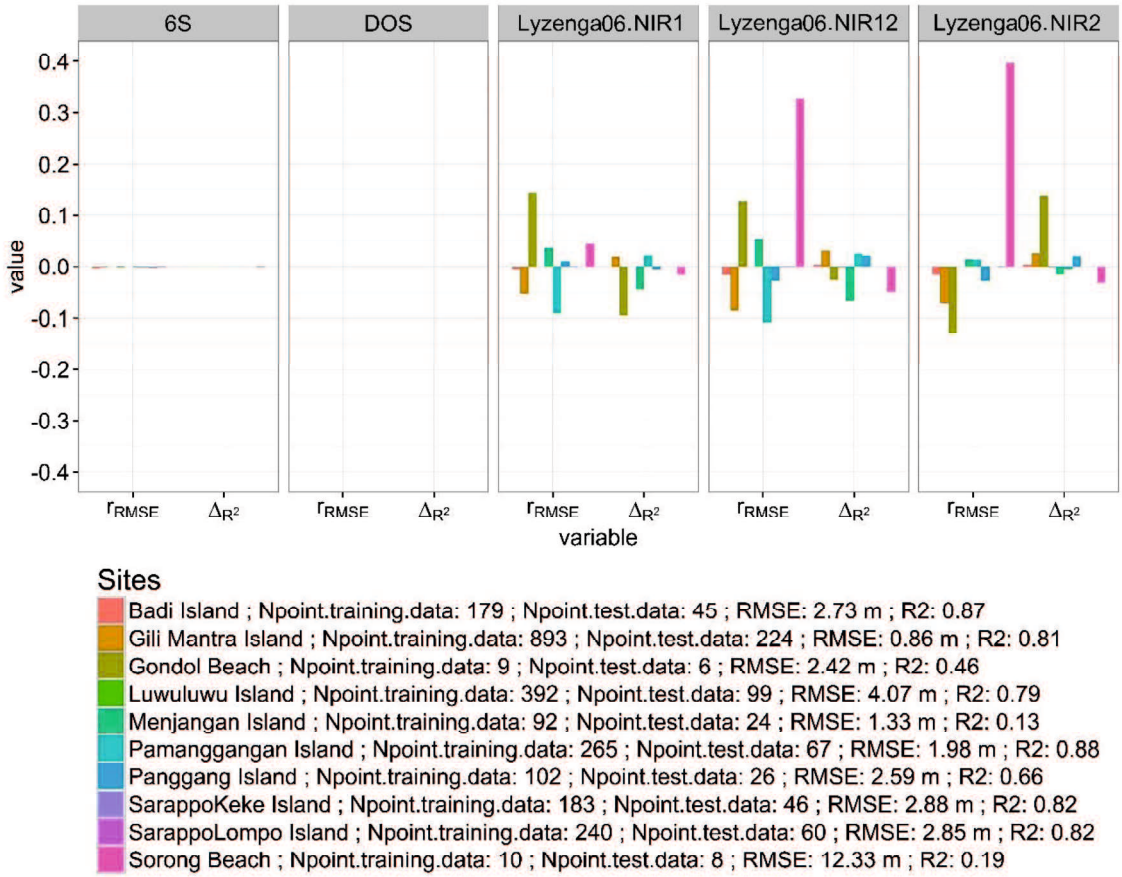

Figure 3-4 The RMSE change ratio (r_{RMSE}) and R^2 change (Δ_{R2}) from the non-correction case for each atmospheric correction method and site. The summary of MLR-based bathymetry for non-correction case is shown in the legend.

The ranges of the RMSE change ratio (r_{RMSE}) and the R^2 change (Δ_{R^2}) were -0.17-0.39 and -0.13-0.13, respectively. These minimum and maximum values were obtained from the Gondol Beach and Sorong site. This sites had a very small amount of data (15 points: nine for training and six for validation for Gondol Beach and 18 points: ten for training and eight for validation for Sorong Beach) that may have yielded unstable results. If I ignore this site, the ranges were -0.08-0.05 and -0.06-0.035, respectively.

As described in Section 2.3, Lyzenga et al.'s correction method theoretically assumes a linear relationship between each visible band and NIR bands in deep water. We investigated whether site-dependent variations in r_{RMSE} and Δ_{R^2} were related to how well the assumption held. For this purpose, I defined a new

variable $\overline{R_\infty^2}$, which is the band-averaged value of R^2 of the regression line (described in Section 2.3) that relates each visible band reflectance value with NIR band reflectance, and was built using deep-water pixels. This R^2 can also be described as the square of the correlation coefficient of visible band reflectance with NIR band reflectance for deep-water pixels. Thus, $\overline{R_\infty^2}$ indicates how well the assumption by Lyzenga et al. (2006) holds.

Figure 3-5 shows scatterplots between $\overline{R_\infty^2}$ and r_{RMSE} and also $\overline{R_\infty^2}$ and Δ_{R^2}. If I exclude the Gondol Beach and Sorong Beach site, which had unstable r_{RMSE} and Δ_{R^2} values as described above, the difference in r_{RMSE} between the best and worst sites, for a specific NIR band combination, ranged from 0.054 – -0.085, whereas that in Δ_{R^2} ranged from 0.0314 – -0.062. The r_{RMSE} and Δ_{R^2} values of each band combination may seem to have had negative and positive correlations with $\overline{R_\infty^2}$, respectively, encouraging the hypothesis that the performance of Lyzenga06 method depends on the soundness of their theoretical assumption. However, as I only had three sites, this hypothesis requires further analysis with a greater number of sites or images.

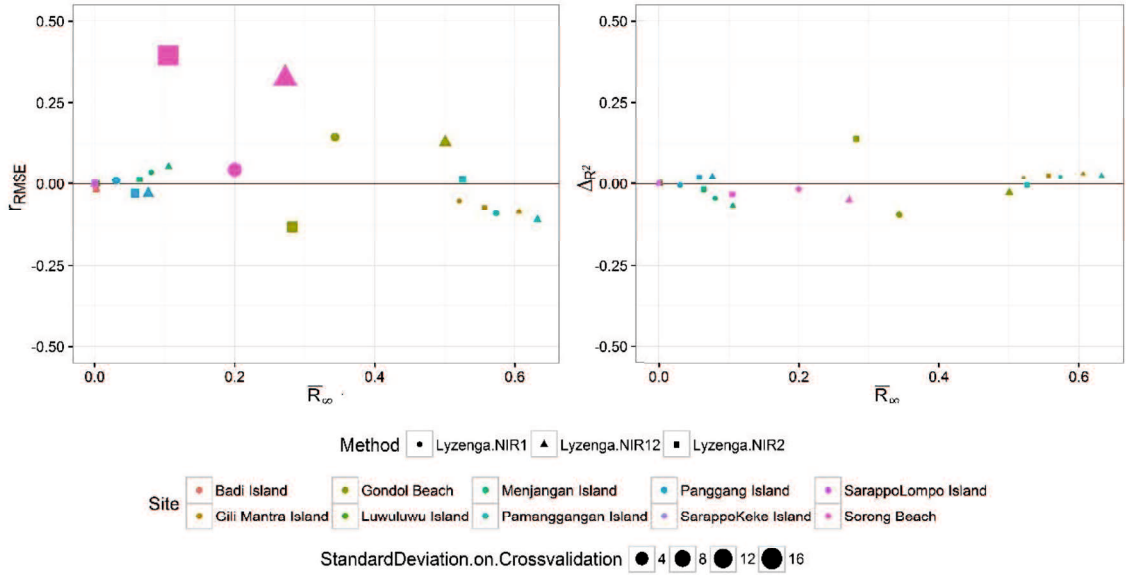

Figure 3-5 Scatterplot between $\overline{R_\infty^2}$ (band-averaged value of the square of the correlation coefficient between visible band reflectance and NIR band in deep-water pixels) versus RMSE change ratio (r_{RMSE}) and R^2 change (Δ_{R^2}).

In Figure 3-5, we can observe that the best NIR band combination depended on the site. The combination of two NIR bands did not always yield the best result. Excluding the unstable Gondol Beach site, the difference in r_{RMSE} between the best and worst combinations ranged from 0.019 – -0.043, depending on the site. That in Δ_{R^2} ranged from -0.004 – 0.0314. These values were in the same order of magnitude as the differences between the best and worst sites shown above. Because the effect of the NIR band combination was shown to be as large as that of the site (or the image), I recommend carefully choosing the best combination for each site by a statistical method (e.g., cross-validation).

3.3.2. Best combination bands for SDB

Figure 3-6 – 3-8 shows the performance of SDB under 63 possible combinations of Worldview-2 bands for nine sites, Gili Mantra Islands, Menjangan Island, Gondol Island, Badi Island, Pamanggangan Island, Panggang Island, Lululuwu Island, Sarappo Keke Island, and Sarappo Lompo Island. As a result, the rank of the best pair is varied between each tested site. Thus, this result needs to be interpreted with caution as a following. In contrast with the previous study (Kerr, 2002), the best performance was not always given by the usage of all the visible bands. Although six visible bands of WV2 were expected to estimate the depth accurately, it was not predicted that the six bands would also give the best accuracy compared with less number of bands as an input. This is not particularly unexpected considering that some bands contain more noise or less bottom reflectance information than other, such as RedEdge bands having less bottom reflection information especially in the deeper depth due to high absorption value.

Interestingly, for evaluated sites the usage of band green, yellow, and red shows better estimation accuracy. Meanwhile, the other bands namely coastal, blue, and rededge had a tendency to give the adverse effect of poor estimation accuracy. As shown in Figure 3-6 – 3-8, even though the short wavelength namely coastal and blue band are sensitive to water depth and penetrate into the deeper water, the high noise is also included. This problem is an issue of WV2 coastal band that claims to be useful for shallow-water mapping.

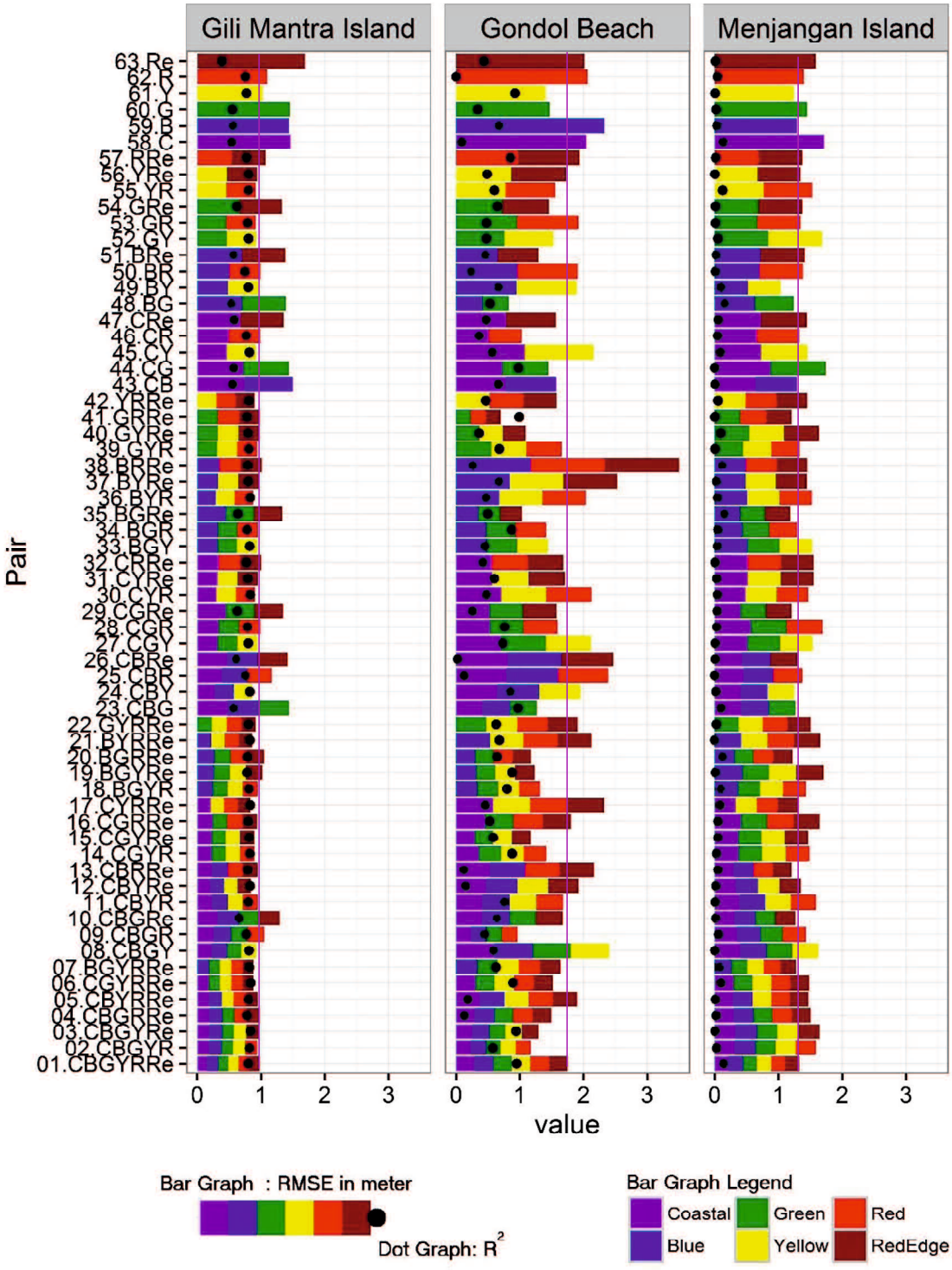

Figure 3-6 Graph of SDB estimation accuracy of SDB of 63 combination bands of Gili Mantra Island, Gondol beach and Menjangan Islands**.** The color bar is the RMSR in meter, and black dot is R^2**.** Example: 01.CBYGRRed is combination number 1 consisting of Coral, Blue, Yellow, Green, Red, and Red Edge bands, for Gili Islands the RMSR is 0.8 m and R^2 is 0.9**.**

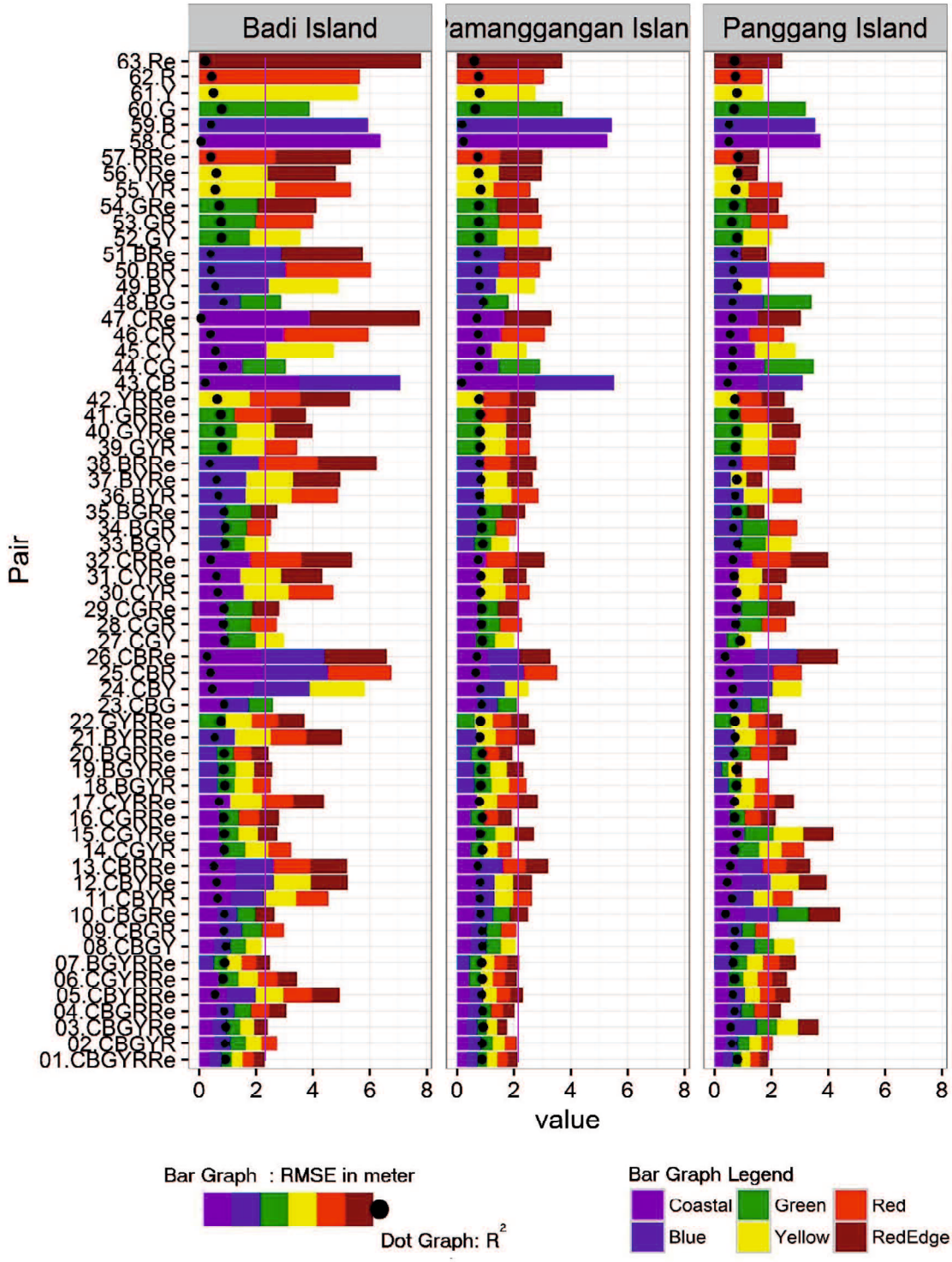

Figure 3-7 Graph of SDB estimation accuracy of SDB of 63 combination bands for Badi Island, Pamanggangan Island, and Panggang Island.

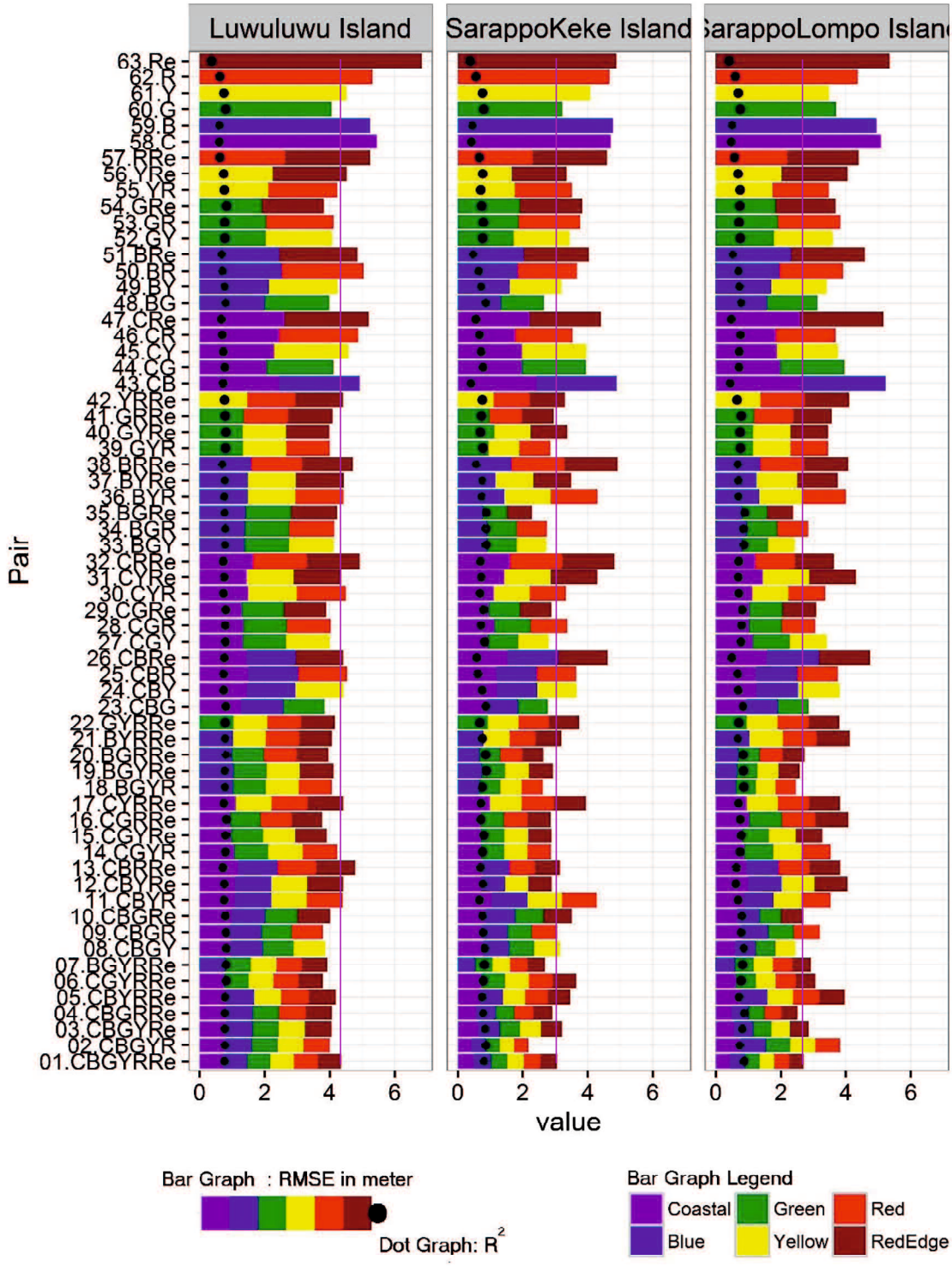

Figure 3-8 Graph of SDB estimation accuracy of SDB of 63 combination bands for Lululuwu Island, Sarappo Keke Island, and Sarappo Lompo Island.

3.3.3. Effect of Lyzenga06 Correction Method and Spectral Improvement on Bottom Types Classification

In the Gili Mantra Islands site, sand, rubble, seagrass, and live coral reefs were the most abundant bottom types in the shallow coral reef ecosystem. Although these features have different spectral characteristics and they can be separated as homogeneous pixels, in reality, there can be significant intermixing between them, even with spatial resolution of 2 × 2 m. Furthermore, complex feature combinations, categorized as mixed bottom type, define inseparable objects in the field observations. A training point for five bottom types was created as a reference for the maximum likelihood classification Based on combinations of the depth-invariance bands from non-correction and Lyzenga06 correction methods, using different numbers of visible bands, the classification results were obtained (Figure 3-9).

Visual interpretation of Figure 3-9-a and 3-9-b, based on the combined depth-invariance indices of the three visible bands, shows a complex distribution, but most of which is misclassified. Both methods for this number of visible bands show the misclassification of rubble and seagrass. The combined depth-invariance indices of the three visible bands are unable to separate this information because seagrass and rubble are always presented with different percentage cover in each pixel. Figure 3-9-c and 3-9-d shows that the combination of depth-invariance indices for the six visible bands for each method could differentiate the coarse bottom-type classification. The mixed bottom type is frequently misclassified as seagrass; however, in the Lyzenga06 correction, the number of misclassifications is reduced.

The techniques of accuracy assessment are based on statistical calculations derived from the confusion matrix, which compares the output of classified and control pixel data. Classification accuracies for each method, obtained with WorldView-2 imagery, are provided in Table 3-3, together with the overall accuracy and kappa coefficient. Individual bottom types exhibit different classification accuracies. Values of class definition similarity, at the coarse descriptive level, vary from 58% to 98%. These numbers represent the degree of uniformity among the factors defining each bottom type class. For instance, rubble is always very well classified (e.g., 93% to 98% user accuracy). Conversely, mixed bottom is poorly

classified with the combined depth-invariance indices of the three visible bands (*i.e.*, 66% to 69%), but the accuracy is higher for the six visible bands (*i.e.*, 74% to 80%). The trigger could be because of the heterogeneity of bottom objects and because the low spectral data of mixed objects does not allow the objects to be separated accurately. The accuracy of identification of sand and seagrass is high (*i.e.*, 72% to 97%) for both methods and combined depth-invariance indices. Coral identification exhibits wide variation in accuracy (*i.e.*, 58% to 86%). The highest overall accuracy of WorldView-2 imagery analysis is achieved using the Lyzenga81 correction method with the combined depth-invariance indices of the six visible bands. This achieved an overall accuracy of 90% and it remained significantly high throughout the analysis (>80%) for each bottom type. The value of the overall kappa statistic exhibits a moderate value (0.71 and 0.73) for the application of three visible bands and it is high for the application of six visible bands (0.81 and 0.86). This statistic estimates the percentage of successful classifications compared with a random chance classification assignment.

Table 3-3. Comparison of accuracy of bottom-type identification.

	Lyzenga06 with 3 Visible Bands	**Non-correction with 3 Visible Bands**	**Lyzenga06 with 6 Visible Bands**	**Non-correction with 6 Visible Bands**
Coral	78.08%	58.46%	88.56%	89.22%
Mix Bottom	60.49%	62.57%	76.45%	87.61%
Rubble	99.80%	100.00%	100.00%	100.00%
Sand	90.18%	80.35%	94.02%	94.46%
Seagrass	90.97%	93.40%	90.97%	93.40%
Overall Accuracy	89.31%	92.86%	89.31%	92.86%
Kappa	0.87	0.91	0.87	0.91

Based on the classification results for all the cases, the rubble is located relatively close to the shoreline, as is seagrass that is mixed with rubble and sand in numerous parts of the island. On the other hand, corals were identified along the edge of the shallow area bordering the deeper water (escarpment area).

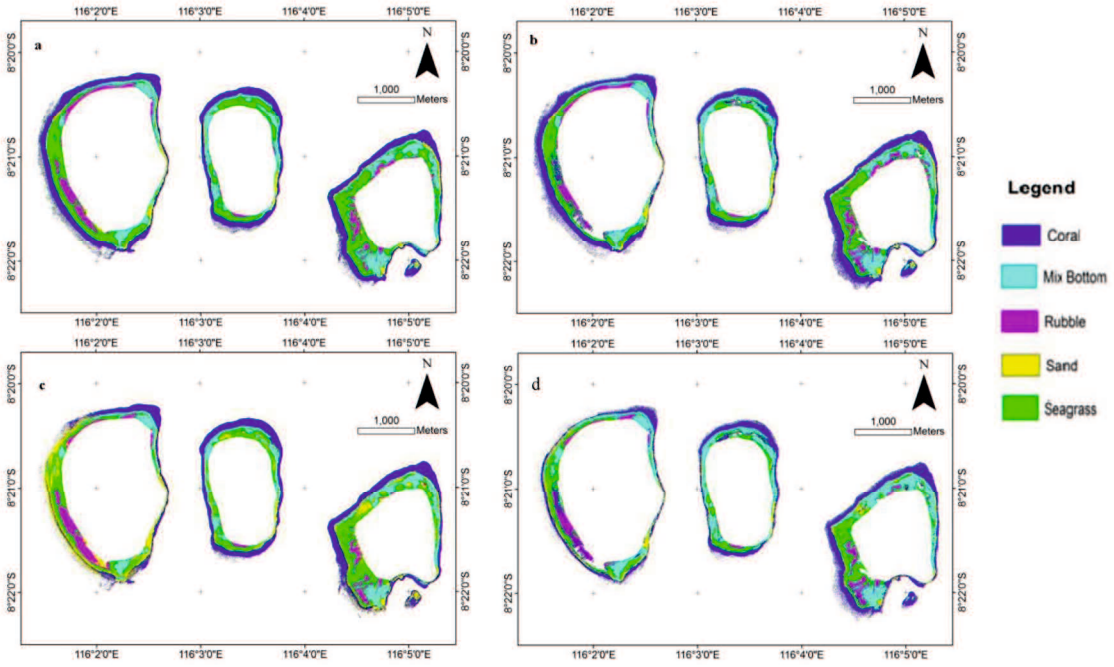

Figure 3-9 Image Classification of Bottom Type in Gili Mantra Islands. (Upper Right) Non-correction method with three bands, (Bottom Right) Lyzenga06 correction method with three bands, (Upper Right) Non-correction method with six bands, (Bottom Right) Lyzenga06 correction method with six bands

Table 3-4 shows that the most influential factor for improving the accuracy in this case is spectral resolution rather than the method of image noise correction. The improvement of spectral resolution from three to six bands could enhance the overall accuracy by 28% and 16% for the non-correction and Lyzenga06 correction methods, respectively. On the other hand, it is not clear which noise correction method gives better overall accuracy; the Lyzenga06 correction method is slightly (2%) better for the case with three bands and the Lyzenga06 correction method is slightly (4%) better for the six band case. However, the noise correction method significantly affects the classification accuracy for some bottom types. For example, the accuracy for coral in the three-band case changes by 10% depending on the choice of the noise correction method. For the three visible bands, many misclassifications occur for both methods and each object except rubble.

Table 3-4. Effect of improvement on accuracy.

	Improvement by Lyzenga's Method in 3 Visible Bands	Improvement by Lyzenga's Method in 6 Visible Bands	Improvement by Spectral Coverage in non-correction	Improvement by Spectral Coverage in Lyzenga06
Coral	19.62%	−0.66%	30.76%	10.48%
Mix Bottom	−2.08%	−11.16%	25.03%	15.96%
Rubble	−0.20%	0.00%	0.00%	0.20%
Sand	9.83%	−0.43%	14.10%	3.84%
Seagrass	−7.38%	−2.44%	2.98%	7.92%
Overall Accuracy	2.45%	−3.55%	14.57%	8.57%
Kappa	0.03	−0.04	0.18	0.10

Theoretically, the Lyzenga06 correction method is able to increase the accuracy of bottom-type identification. However, the enhanced method could only improve the low spectral resolution, whereas for the high spectral resolution, this method reduces the accuracy. Additionally, the result shows that the non-correction algorithm is the best method for identifying bottom type using the applied combined depth-invariance indices of the six visible bands in the Gili Islands' shallow-water coral reef ecosystem. The trigger could be because the NIR band applied in the Lyzenga06 correction is sensitive to bottom spectral reflectance and the adjacent effect; thus, the theory does not hold for correcting sea-surface scattering and atmospheric noise. In summary, spectral resolution is more important than noise correction for improving the accuracy of bottom-type identification.

The classification level applied in this research is a coarse description of the bottom type (e.g., coral, seagrass, rubble, sand, and mixed bottom). It is possible to implement an intermediate–fine description classification level using high-resolution WorldView-2 imagery, if supported with appropriate field data. Applying the method for a large number of bottom materials poses some problems because of the similarity in the reflectance of several materials, such as vegetation and mud (Lyzenga, 1981).

3.4. Conclusion

First, this study compared the effects of three atmospheric correction methods on the performance of MLR-based bathymetry, using WorldView-2 images of five coral reef sites. As a result, I found that Lyzenga06 pixel-wise atmospheric correction method was the only one that influenced accuracy. The correction method that used a radiative transfer model (6S) had little effect, and the Dark Object Subtraction method had no effect at all. We also provided theoretical evidence for this result. Unfortunately, Lyzenga06 atmospheric correction method had the disadvantage of significant data reduction. Moreover, the change in accuracy by this method depended on the site and NIR band combination, and sometimes turned negative.

Second, considering the six visible bands of WV-2 images, 63 possible pairs were evaluated to identify the best pair as an input in estimating the water depth. As a result, each band pair give different performance on estimating the water depth. For each evaluated sites, the best band pair was different shows the site dependency factor. Overall, a better accuracy was achieved when a multiple (>2) and excluding the rededge bands from the input.

Third, Lyzenga's bottom-type identification method was applied to WorldView-2 imagery for the first time. The Lyzenga06 correction method, which utilizes the near infrared (NIR) bands, was more accurate than the non-correction method only for the case of three visible bands. This result indicates that the superiority of the Lyzenga06 correction method is case-dependent. Moreover, the used of six visible bands in the identification accuracy was better than only three bands, regardless of the correction method. This result shows that a large number of visible bands of multispectral data, used for water-column correction, improve the accuracy of bottom-type identification in shallow-water coral reefs.

In practice, for water depth estimation, one of the non-correction methods and Lyzenga06 correction method (with three possible NIR-band combinations) and multiple bands input for each target image is recommended, depending on acceptable data reduction and the required accuracy. The recommendations for bottom type classification are the usage of higher spectral resolution image (multiple bands) and the non-correction methods. Then, a statistical accuracy

comparison can be conducted for each image by using cross-validation, as in this study.

Chapter 4. *Simulation-Based Derivation of a Robust Set of Coefficients of Lyzenga's SDB Formula*

4.1. Introduction

Although Lyzenga's SDB formula has been successful in many applications (Flener et al., 2012; Yuzugullu Aksoy, 2014; Vinayaraj et al., 2016), the robustness under varying conditions is still an essential question that is currently considered a research gap. One place where such highly variable conditions can be encountered is coral reef environments, which can exhibit a wide range of water quality features and unique bottom types in terms of spectral characteristics and spatial distributions. The goal of this study is to assess the influence of variable optical conditions on Lyzenga's multispectral bathymetry retrievals in the context of Case-1 shallow coral reef waters. The evaluation was carried out by using a simulated WorldView-2 above water reflectance dataset that combined the spectral properties of a number of archived coral reef field reflectance measurements, along with various depths and various modeled Inherent Optical Properties (IOPs) of Case-1 coral reef water scenarios. The simulated dataset is used for three analyses: First, Lyzenga's bathymetry formula is tested on a simulated dataset that represents a coral reef environment to determine whether Lyzenga's assumptions were unrealistic. In real-world data, the number of bottom types tended to exhibit higher levels of variation than the water quality did. Second, the effect of the quantity of bottom types present at a site is tested, representing the full range of bottom-type diversity that might appear in coral reef environments. Third, Lyzenga's SDB formula is tested in the case in which the bottom type is unknown. Ideally, the pixels with known depth used as input in Lyzenga's bathymetry formula should represent the whole range of depths and bottom types in the targeted area. However, it difficult to obtain representative input, because of the large area or varied bottom types of coral reef environments. Thus, this analysis becomes importance for evaluating the performance of Lyzenga's bathymetry formula.

4.2. Methods Overview

This empirical model of Lyzenga et al. (2006) was used to predict the shallow-water bathymetry present in the simulated dataset. After quality control (Subsection 2.1.3), the simulation dataset was analyzed to investigate the performance of Lyzenga's multispectral bathymetry model under a wide range of bottom types. The analysis procedure was as follows.

First, water depths were estimated by applying the least squares method of Equation 13 to the dataset. The residual (r) for each data point was determined as the difference between the estimated and true depth value. The relationship between the optical conditions and the magnitude of the residuals was then investigated, as described further on in Subsection 4.3.2. To identify the effect of the number of bottom types on the depth estimation, 100 possible combinations of bottom types ranging in number from 1 to the maximum number of archived bottom types were selected randomly. For each combination, a cross validation of 100 repeated random sub-sample validations was done by randomly splitting the dataset into training and test datasets at a training:testing ratio of 9:1 (described in detail in Subsection 4.3.3). The average RMS values for 100 instances of cross validation were used to assess the overall accuracy of the depth prediction (further described in Subsection 4.3.3). To testing the possibility in predicting the depth of unknown bottom types, leave one cross validation was performed. Each bottom type was excluded from the dataset then performed the fitting. Afterward, the excluded bottom type data was used as tested data (described in detail in Subsection 4.3.4).

4.3. Results and Discussion

4.3.1. Simulation Dataset Overview

Figure 4-1 presents a portion of the simulated dataset, which was described in Subsection 2.2.3. Each row in the dataset represents a different optical condition and each column represents a variable. The figure shows only a subset of the dataset (9 variables and 10 rows) for the purpose of providing a general familiarization with the data structure. The actual size of the dataset was 422,400 rows and 43 columns.

The simulation dataset was built from the grid and random part as described in Subsection 2.2.3.

	bottomType	sZ	depth	chl	Rrs.1	Rrs.2	Rrs.deep.1	Rrs.deep.2	X.1	X.2
1	b20Acroporasp1	9.00000	9.500000	3.62038672	0.002680210	0.003570291	0.002554158	0.003127315	-8.978819	-7.721995
2	b106AcroporaBrown	21.00000	3.500000	1.81019336	0.006786564	0.008029328	0.003032999	0.003286691	-5.585049	-5.351162
3	b31Diploria	3.00000	13.500000	3.62038672	0.002556764	0.003178085	0.002554158	0.003127315	-12.857861	-9.888216
4	b88Rubble2	27.00000	2.500000	0.02828427	0.051535121	0.061878491	0.013438783	0.005398007	-3.267637	-2.873860
5	b39Sinulariasp1	33.00000	9.500000	1.81019336	0.003507052	0.004060598	0.003032999	0.003286691	-7.654192	-7.164058
6	b82EncrustingBrown	23.39635	10.838328	1.34748458	0.003688293	0.004324447	0.003340716	0.003402740	-7.964524	-6.989283
7	b31Diploria	22.37604	7.361004	2.89887279	0.002721657	0.003490258	0.002685512	0.003172463	-10.227970	-8.054103
8	b96AcroporaYellow1	9.00000	15.500000	0.90509668	0.004260249	0.004658980	0.003826375	0.003564127	-7.742755	-6.817135
9	b124AcroporaTurf	16.05605	12.626797	2.01191406	0.003506864	0.004766180	0.002933820	0.003247082	-7.464548	-6.489638
10	b54Seriotoporastelata	45.00000	19.500000	0.22627417	0.007762574	0.006937514	0.006399595	0.004211701	-6.598083	-5.904988

Figure 4-1 Simulation dataset screen shot; the information for bands 3 to 5 was excluded because of space limitations. The variable names in each column are abbreviations: bottomType is the bottom type symbol; sZ is the solar zenith angle in degrees; depth is the water depth in meters; chl is the chlorophyll-a concentration in mg m^{-3}; Rrs.n is the above water remote sensing reflectance just above the surface in band n; Rrs.deep.n is the deep water remote sensing reflectance just above the surface at band n; and X.n is the linearized above water remote sensing reflectance just above the surface at band n.

Table 4-1 shows the data removal that occurred following the surface reflectance linearization and quality control steps. The data removal results were spectrally dependent (i.e., different for each band). In the quality control step, the opposite situation occurred, where low bottom contributions at long wavelengths (band 5) led to the removal of ~70% of the initial data items. In this data reduction step, the depth range of the dataset was reduced significantly from 0.5–19.5 m initially to 0.5–10.5 m. These results show that longer wavelength bands and areas of deeper water yielded small bottom contributions because of their characteristically high attenuation coefficients. The low bottom contribution of these samples can be explained by the maximum depth of bottom reflectance detectability. As shown in Table 4-1, after quality control, the maximum depth was less than 10.5 m and data at deeper depths were defined as having a low bottom contribution. Similar results were found by Carder et al. (2005). The findings may also explain the poor bathymetry estimations from actual satellite imagery for depths greater than 10.5 m. However, to confirm this, further investigation is needed. Meanwhile, in the linearized reflectance step, the majority of data removal

occurred because of the low (< 25%) bottom contribution in the short wavelength range (bands 1 and 2), and this was caused by dark object reflectance that was lower than that of deep water. The data removal of these spectra caused a significant removal of 141 of the 164 total bottom type objects, as shown in Table 4-1. This is a known issue that commonly appears in the application of Lyzenga's SDB formula (Manessa et al., 2014).

Table 4-1 Summary of all data removed as a result of quality control requirements and reflectance linearization (Equation 12). The initial data contained 422,400 rows. The number of rows removed is shown in the "Number of data" column.

Band	After quality control (> 25% of the % bottom contribution)				After depth variable linearization $log(R_{rs}^{cor}{}_i)$			
	No. of data (rows)	% of initial dataset	Depth range in meters	No. of bottom types	No. of data (rows)	% of initial dataset	Depth range in meters	No. of bottom types
Band 1	253,998	60%	0.5 – 19.5	164	89,209	22%	0.5 – 10.5	144
Band 2	305,784	73%	0.5 – 19.5	164	106,826	25%	0.5 – 10.5	141
Band 3	344,031	82%	0.5 – 19.5	164	121,338	28%	0.5 – 10.5	163
Band 4	189,854	45%	0.5 – 16.5	164	122,538	29%	0.5 – 10.5	164
Band 5	124,440	29%	0.5 – 10.5	164	122,538	29%	0.5 – 10.5	164
All Bands	122,538	29%	0.5 – 10.5	164	88,080	21%	0.5 – 10.5	137

4.3.2. Performance of Lyzenga's Multispectral Bathymetry Model

4.3.2.1. Depth Estimation Accuracy

4-2(a) presents a scatter plot between the measured water depth and the estimated water depth (the result of regression fitting) for all data items. For greater visual understanding of the relationship shown in Figure 4-22(a), a subset of 500 points were randomly selected and presented in Figure 4-22 (b). The differences between the measured and estimated depth values were defined as residuals and are summarized in Table 4-2. The maximum residual was around 1 m and the RMS

residual was less than 0.4 m, as shown in Table 3. In the varying water quality and bottom type conditions of 137 different spectra, Lyzenga's SDB formula was able to achieve good depth prediction accuracy. This provides support for the performance of Lyzenga's SDB formula under this wide range of optical conditions.

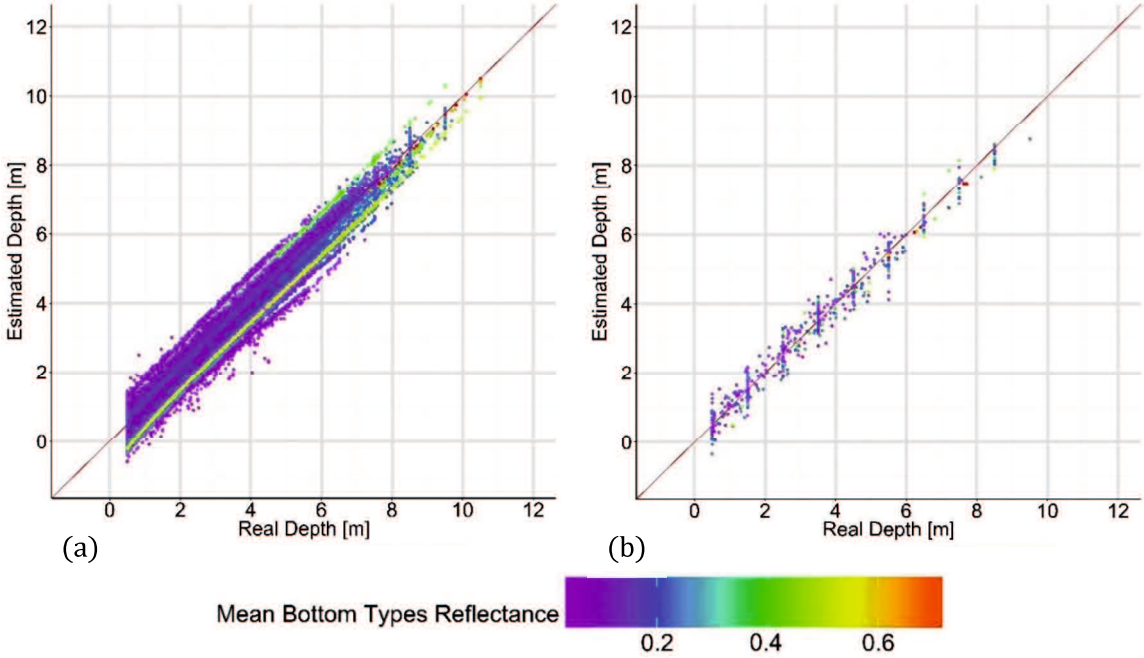

Figure 4-2 Scatter plot of the estimations (fitted values) of water depth versus the measured water depth for (a) all data and (b) a subset of 500 randomly selected points displayed for greater visual understanding. The color indicates the average spectral reflectance of each bottom type. The red line is y = x, which indicates the parity of the model predictions with real depth.

This finding on the generality of Lyzenga's multispectral bathymetry appears to be well-supported by previous studies, in which the application of Lyzenga's SDB formula on real coastal environment images acceptably estimates water depth (Liceaga-Correa and Euan-Avila, 2002; Pacheco et al., 2014; and Vinayaraj et al., 2016). The accuracies achieved in previous studies are 0.78–0.88 m and 0.8–2.63 m for R^2 and RMSE, respectively. The accuracy of real images is far higher that of the simulation-based analysis (Table 3), as the optical conditions and bottom types are less varied. The resistance parameters, (i.e., image spatial and spectral resolution, image noise, data quality, and site dependency) contribute significantly to the

accuracy achieved in real-image analysis; whereas, in this study, resistance parameters were excluded, as the simulated dataset is assumed to be zero-noise. Thus, these resistance parameters could well be responsible for several failures (Stumpf et al., 2013; Manessa et al., 2016) in applying Lyzenga's SDB formula to real images.

Table 4-2 Statistical summary of the residual ($\boldsymbol{r}$) data between the estimated and measured water depth values.

RMS (m)	Σ	R^2	Mean absolute depth (m)	Maximum absolute depth (m)
0.359	0.359	0.977	0.283	2.944

4.3.2.2. Relationship between the accuracy and optical condition

Since the simulation dataset was free of noise, the average of the estimated depth residuals was equal to zero. Thus, as Deakin and Kildea (1999) explain, RMS could be broken down as follows:

$$RMS^2 = \left(\frac{1}{n}\sum_i (r_i - \bar{r_i})^2\right) + (\bar{r_i} - r_i)^2, \qquad \text{Equation 4-1}$$

or, alternatively, in words,

$$RMS^2 = \ estimate\ of\ standard\ deviation + \ (estimate\ of\ bias)^2.$$

The mean component of RMS corresponds to the bias caused by the bottom type, while the standard deviation component corresponds to the errors caused by other optical conditions (depth, chlorophyll-a concentration, and solar zenith angle). It follows that the contribution rate of bottom type to RMS is calculated by:

$$\boldsymbol{contribution\ rate\ of\ bottom\ types\ on\ RMS} = \frac{\boldsymbol{mean\ absolute}}{\boldsymbol{RMS}} \qquad \text{Equation 4-2}$$

Table 4-3 shows the minimum, median, and maximum of the summary statistics for each bottom type and the contribution rate of the bottom type to the RMS. First, the results show that for any bottom type, the RMS was less than 1 m. Second, the residuals were dominated by effects from the bottom types (Figure 4-3: contribution rate of bottom type to the RMS error), while water depth, solar zenith angle, and chlorophyll concentration contributed to the residuals to a lesser degree (a maximum of 18%). An additional indication of bottom types contributing highly

to the RMS is that 98 out of 137 bottom samples provided a bottom type contribution rate of greater than 0.9 to the RMS. Moreover, Figure 4-3 shows that in the case of the bottom type with the highest RMS (bottom type ID "b155Encrusting20ms"), the effect of chlorophyll-a concentration and solar zenith angle on RMS was only 0.17 m, far smaller than the 1-m effect of bottom type. Since the majority of the RMS values of the residuals from the depth prediction were distributed close to the parity line (y = x), it can be understood that the bottom type had the greatest influence of all variables on RMS.

Table 4-3 The statistic of residual for each bottom types

Statistic	Minimum	Median	Maximum
RMS [m]	0.05207	0.25774	0.95117
Mean (bias) [m]	-0.82109	-0.00482	0.93329
Mean Absolute [m]	0.03941	0.25217	0.93329
Standard Deviation	0.02489	0.06379	0.48959
Contribution rate of bottom type on RMS	0.72453	0.95964	0.99732
Number of data	98	660	1092

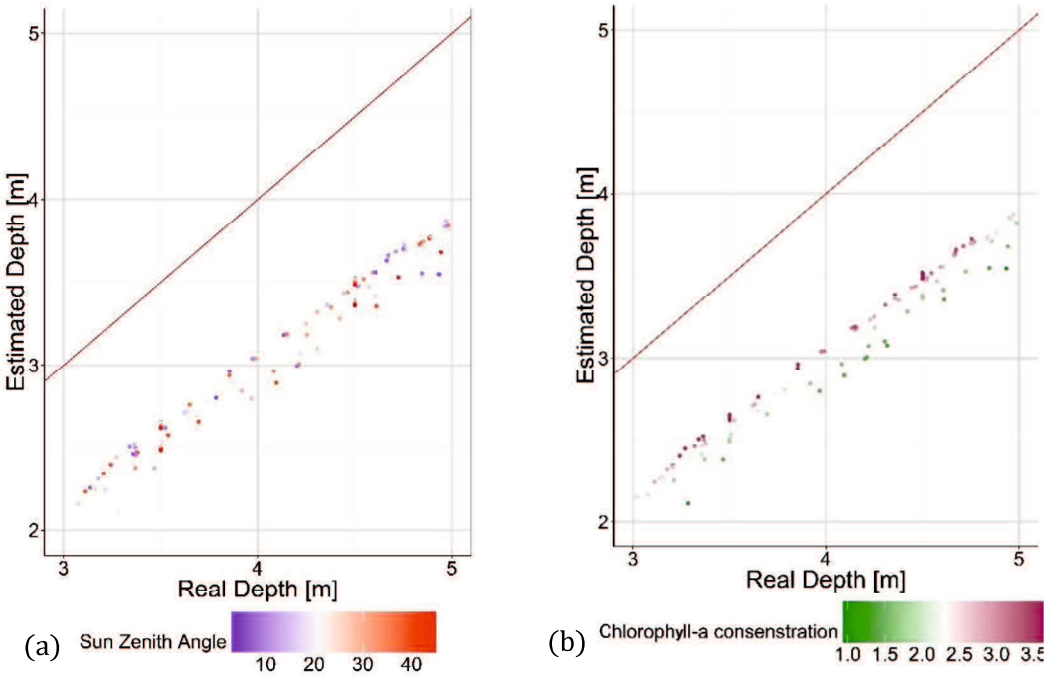

Figure 4-3 Scatter plot of the measured versus estimated depths for the bottom type ID of "b155Encrusting20ms." This bottom type exhibited the highest RMS residual value (0.95117 m). The plots are color-coded by the (a) solar zenith angle (degrees) and (b) chlorophyll-a concentration (mg m^{-3}).

4.3.3. Effect of Number of Bottom Types on the Depth Prediction Accuracy

Figure 4-7 presents the performance of Lyzenga's SDB formula under a number of bottom type conditions. Results showed that as the number of bottom types increased, the RMS of the bathymetry prediction increased. The model provided its best performance on the uniform distribution (one bottom type), with an RMS error of 0.02 m (Figure 4-4), and performance declined (RMS error increased) significantly with the each additional bottom type. This rate of increasing error (decreasing accuracy) with increasing number of bottom types became significantly smaller after approximately 15 bottom types and reached a plateau around 30 bottom types. This trend occurred because at high bottom type diversity, there was a high probability of a bottom type with spectral properties being added to the group of bottom types (i.e., at a certain number of bottom types, the spectral diversity becomes robust to change with the addition of more bottom types). As shown in Figure 2-3, many bottom types had very similar spectral characteristics.

These results offer unprecedented evidence for the use of Lyzenga's SDB formula for diverse coral reef environments. Doubts about the performance of Lyzenga's method for diverse bottom types (Stumpt, 2003 and Sue et al., 2013) and a number of bottom type greater than the number of bands (Lyzenga et al., 2006) were not proven. However, it is natural that less diverse bottom types gives better estimation accuracy than more diverse bottom types.

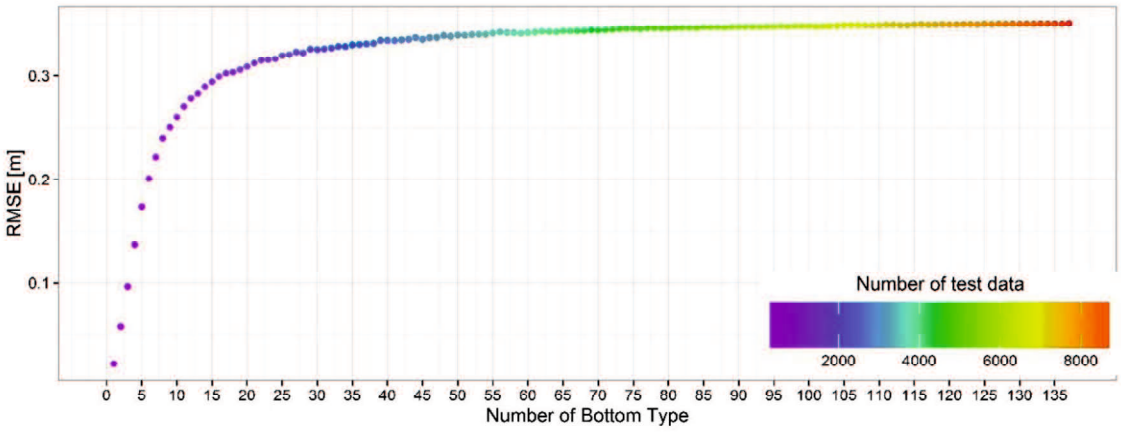

Figure 4-4. RMS error (RMSE) estimation from 100-sample cross validations of each instance of bottom type quantity.

4.3.4. The Performance of Lyzenga's For Water Depth Estimation for the Unknown Bottom Type

Figure 4-5 shows the comparison between RMS residual when all the bottom types used in fitting and RMS of error when one bottom type excluded in fitting, almost the plotted point fall closet to the straight line of x = y. Moreover, the removal of bottom type in the fitting was increased the error but not too significant. This result shows that even the bottom type is unknown this model still able to predict the water deep of the unknown bottom type almost as accurate when the bottom type is known in the model.

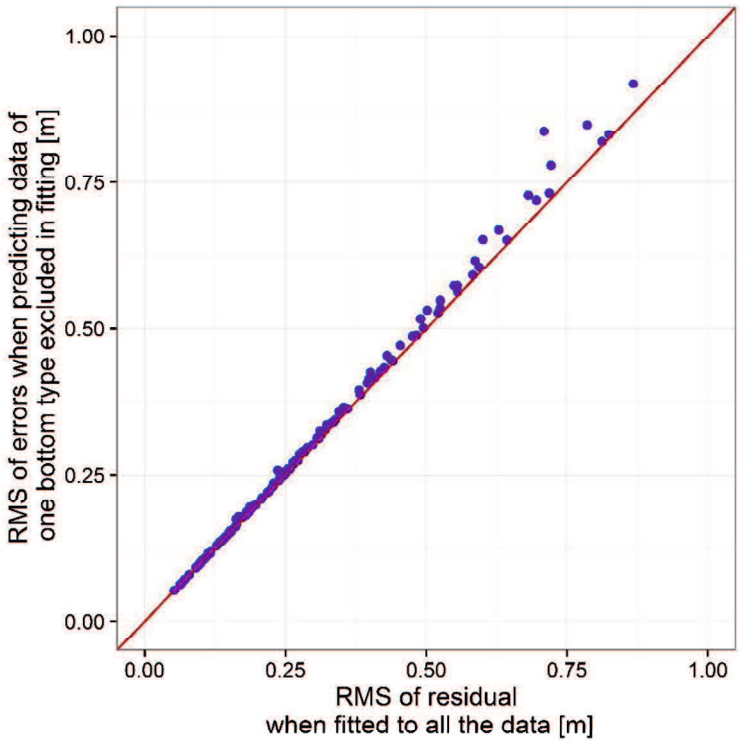

Figure 4-5 Scatter plot of RMS residual when all the bottom types used in fitting versus RMS of error when one bottom type excluded in fitting. Each point represent a one bottom type. The red line is a straight line y = x.

Table 4-4 shows the statistic of residual of water depth estimation of each bottom type in the minimum, center, and maximum for both cases of all bottom types was known or the tested bottom type excluded in the calibration of estimation model. The incensement rate of error because the tested or unknown bottom type was excluded from model calibration. It is interesting to note from that the maximum RMS residual when the bottom type is excluded was 1.03 m, which just 0.08 meter higher than if all the bottom types is used (RMS residual = 0.95 m). This result has confirmed that our water depth estimation model or formula was general enough to predict a water depth from a coral reef area with unknown bottom types.

This result confirmed that our water-depth estimation model was general enough to predict water depth from a coral reef area with unknown bottom types. However, careful attention must be paid to bottom type diversity of the model prediction input. Excluding one bottom type of 134 still made the input (simulated

dataset of 133 bottom types) diverse enough for model prediction; thus, the depth of the excluded bottom type could still be estimated accurately. These result points to the likelihood that Lyzenga's SDB formula can still estimate the depth of an unknown bottom type because the known depth used as input for building the model has a bottom type that represents (or is similar to) the unknown bottom type. Further studies that consider realistic cases, such as less diverse bottom types as input, need to be performed.

Table 4-4 Statistic of RMS residual of estimated depth of each bottom type based on estimation model using all the bottom types data and without the estimated bottom type.

	Minimum	Median	Maximum
RMS when all the bottom types is used in training data (=A) [m]	0.05207	0.25774	0.95117
RMS when one bottom type is excluded in training data (=B) [m]	0.05213	0.26066	1.03373
Incensement Ratio of RMS rate of error (= B / A - 1)	0.00101	0.01715	0.19958
Increase value of RMS (= B – A) [m]	0.00005	0.00487	0.12788

4.4. Conclusions

In this study, a WorldView-2 above-water remote sensing reflectance dataset was simulated for Case-1 waters of a coral reef environment. The simulation dataset was used to verify the generality of the Lyzenga et al. (2006) multispectral bathymetry model under varying bottom type, solar zenith angle, and water quality (represented by chlorophyll-a concentrations) conditions. First, for a wide range of bottom types and variable optical conditions (solar zenith angles and chlorophyll-a concentrations), Lyzenga's SDB model was sufficiently general and able to accurately estimate water depth. Lyzenga et al. (2006) noted that the application of this method was limited to some bottom types, where the number of bottom types is no greater than the number of multispectral bands. Surprisingly, the results of this study contradict the previous result; the simulation-based analysis shows that this model still works well (R^2 = 0.97 and RMS residual 0.4 m) for 137 bottom types, which is much greater than the number of multispectral bands used (5 visible bands

of WorldView-2 image). Second, the number and combination of bottom types (bottom type diversity) dominantly influenced the performance of Lyzenga's multispectral bathymetry model (72–99 % contribution to RMS residual), whereas other optical conditions (solar zenith angles and chlorophyll-a concentrations) made only minor contributions (maximum 18% contribution to RMS residual). Third, Lyzenga's depth estimation accuracy became poorer with the cumulative increase of the number of bottom types. Interestingly, beyond a certain number of bottom types (~30), the change in accuracy reached a plateau for any increase in bottom type number. Lastly, the depth of an unknown bottom type can be predicted accurately (~0.13 m RMS residual incensement) if the prediction model was built based on diverse bottom type conditions (133 bottom types).

This study provides a basis for other research efforts aimed at the usage of Lyzenga's multispectral bathymetry for mapping shallow coral reef bathymetry. However, it should be noted that this promising result was performed under a zero-noise assumption. In reality, multispectral imagery contains noise, especially in the shorter wavelength bands due to Rayleigh scattering. Thus, further studies that consider the noise contribution must be performed..

Chapter 5. *Evaluation of Applicability of Simulation-Derived Coefficients to Indonesian Coral Reefs*

5.1. Introduction

Until now, Indonesia only had a single large-scale bathymetry map (1:250.000) for the entire nation and detailed maps (1:50.000 or 1:25.000) of a few locations. A straightforward and cost-efficient bathymetry mapping of the Indonesian coral reef is urgently needed. To address this problem, I present a simulation-derived coefficient for Lyzenga's SDB formula that requires few in-situ measurement data to adjust coefficients. The simulation dataset corresponding to the Indonesian coral reef and Worldview-2 Imagery spectral response was built to extract the coefficient. Then, the formula was validated using real Worldview- 2 images from ten shallow coral reef sites: the Gili mantra islands, Menjangan Island, Gondol Beach, Panggang Island, Badi Island, Sarappo Keke Island, Sarappo Lompo Island, Pamanggangan Island, Luwu luwu Island and Sorong Island in Indonesia.

This chapter presents a simulation-derived coefficient for depth estimation formula using a multispectral image and limited survey data. We limited the target areas to Indonesia shallow coral reefs. We used a multiple linear regression (MLR) model to establish our formula. The first step consisted in building a simulation dataset that represents the surface reflectance over Indonesia. Then, I tested the performance of our simulated dataset to estimate the depth. If it showed satisfying results, then the coefficient of the MLR model was extracted from the simulation. These coefficients were used to build the depth estimation formula. For the final step, a Worldview-2 image including depth measurements was used to evaluate the performance of .proposed estimation formula based on simulation-derived coefficients.

5.2. Methods Overview

The WV2 imagery of ten sites were processed in three steps before being submitted to the depth estimation formula from simulation-derived coefficients. First, a pre-processing step is the sensor calibration, where digital numbers are converted into units comparable to the band-averaged spectral reflectance or TOA (top of atmosphere) reflectance. Secondly, the TOA reflectance was atmosphere-corrected by applying the Lyzenga's SDB formula. Lastly, the transformed reflectance (X_i) was calculated using Eq. 2-4.

The coefficients of β are derived from the regression analysis between the depth and the transformed reflectance of a simulated dataset. The coefficients indicate the intercept (β_0) and slope (β_i). For each site, the intercept (β_0) coefficient needs to be adjusted using two pixels (minimum) with measurement depth ($\acute{h}$) according to the following formula:

$$\beta_0 = \frac{\sum_n^{minimum\ n}(\hat{h}_n - \acute{h}_n)}{n} \qquad \text{Equation 5-1}$$

5.3. Results and Discussion

5.3.1. Performance of Proposed Derived Coefficients

Considering that the simulation dataset (Chapter 4) shows a good fit with the estimated depths, the coefficients from the MLR of Lyzenga's SDB formula were extracted. Then, the depth estimation formula using the simulation-derived coefficients for Worldview-2 images is presented as:

$$\hat{h}(m) = \beta_0 - 0.5225 \cdot X_{coastal} + 1.1021 \cdot X_{blue} - 0.7364 \cdot X_{green} - 5.1219 \cdot X_{yellow} - 5.7963 \cdot X_{red} \qquad \text{Equation 5-2}$$

The proposed equation shows the influence of each band on bathymetric estimations, with high coefficients corresponding to a strong influence.

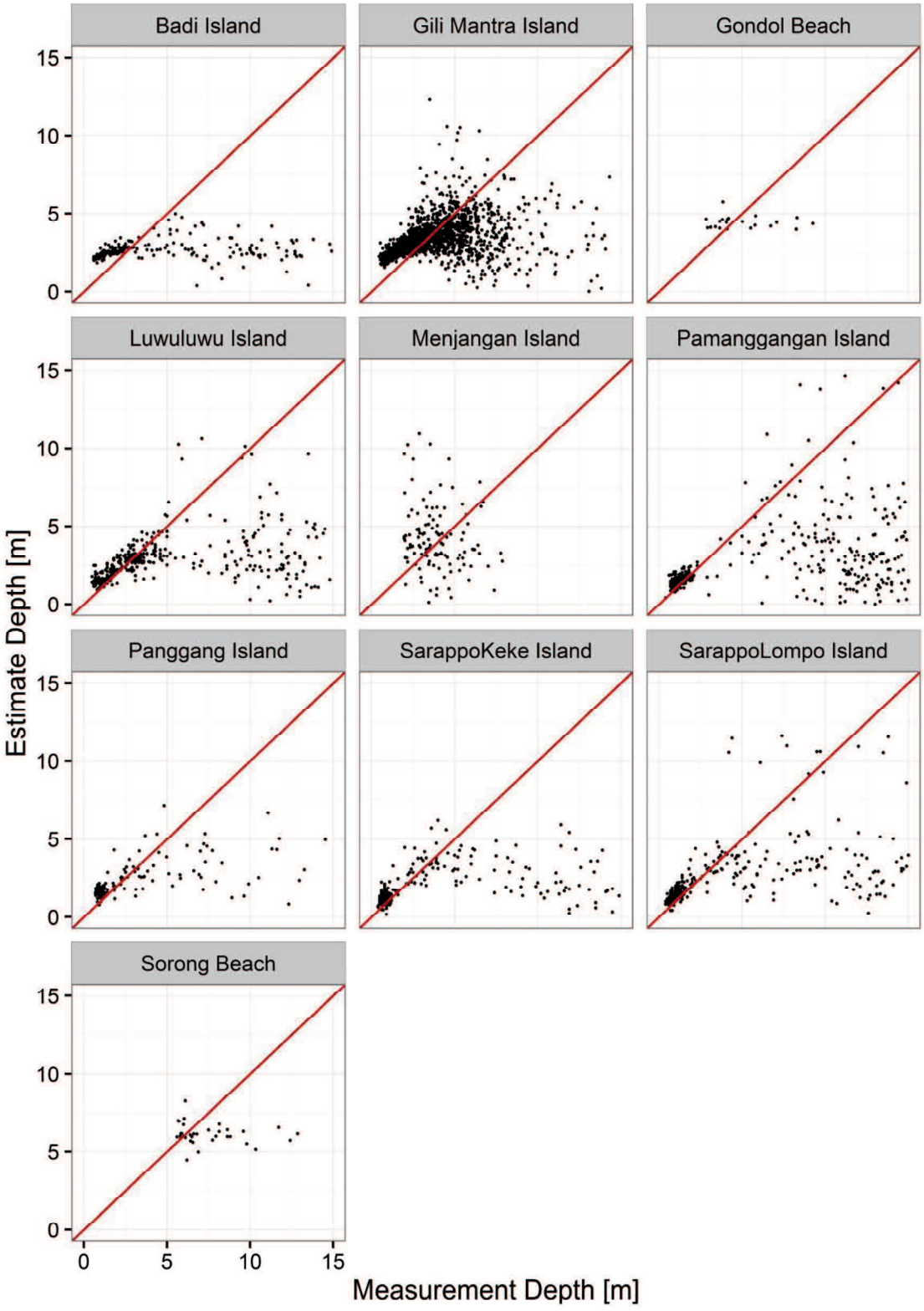

Figure 5-1 Scatterplot of depth estimation using simulated-derived coefficient for each site. The red line is a straight line y = x.

Table 5-1 The calculated β_0 for each site using five pixels with known depth

Sites	β_0
Gili Mantra Island	1.364
Gondol Beach	3.402
Menjangan Island	1.969
Panggang Island	4.728
Sorong Beach	5.775
Pamanggangan Island	0.209
Sarappo Keke Island	0.128
Sarappo Lompo Island	0.102
Luwu luwu Island	0.726
Badi Island	1.159

Table 5-1 shows the β_0 for each tested site. The β_0 or intercept was calculated from five pixels with measured depths to adjust the intercept (β_0) coefficient and to represent the problem of the limited measurement data in Indonesia.

After applying the estimation formula based on the simulated-derived coefficient for each site, the depth estimation value was obtained. Then, the measured depths were plotted against estimated depths for each location (Figure 5-1). The R^2 and RMSR between actual depth and estimated depth varied across locations and depth range. The best performance was achieved only at six sites: Panggang Islands, Gili Mantra Islands, Badi Island, Sarapo Keke Island, and Luwu lulu Islands, at shallow depth range between 0.5 – 5 meter with RMS error less than 1 meter. Moreover, the error was rapidly increased at the deeper depth. Several processes may have caused these accuracy problems. First, a measurement error of the single beam echosounder occurred in the reef edge (deep) area, where there was some delay in receiving the signal. Secondly, the deeper coral reef area displayed high noise caused by the absorption and scattering of light. Thirdly, the simulation

dataset was not able to represent the conditions of the deep area (> 5 m).

Meanwhile, the depth estimation at other three sites: Gondol Beach, Menjangan Island, and Badi island sites failed. This failure might attribute to the noise of the tested images, as describe further in subsection 5.3.2. Since the simulated dataset was built under a no-noise assumption, then it is clear that the formula was only applicable to a less noisy image.

Table 5-2. Statistics for RMS residual (accuracy) [m] of estimated depth at depth range in each site

Sites	Depth range [m]							
	0 -1	2 - 3	4 - 5	6 -7	8 - 9	10 - 11	12 - 13	14 - 15
Gili Mantra Island	1.29	0.95	1.43	3.13	5.11	7.78	10.75	11.34
Gondol Beach	NA	1.23	0.81	1.95	4.30	NA	NA	NA
Menjangan Island	NA	3.58	2.90	4.02	4.79	NA	NA	NA
Panggang Island	0.70	0.80	1.67	3.86	5.62	7.22	9.45	NA
Sorong Beach	NA	NA	1.01	2.00	4.26	6.16	NA	NA
Pamanggangan Island	0.45	0.44	1.52	2.88	5.96	8.01	10.90	12.04
Sarappo Keke Island	0.55	0.81	1.52	3.42	5.72	8.21	10.51	12.35
Sarappo Lompo Island	0.55	0.70	1.29	3.88	4.71	6.65	10.78	10.57
Luwu luwu Island	0.81	0.59	1.13	3.82	5.66	6.70	9.57	10.40
Badi Island	1.33	0.68	1.66	3.82	6.32	7.71	10.16	11.94

5.3.2. Noisy Condition Assumption

As described in Section 5.3.1, the formula was not applicable in the all tested site. Moreover, the estimated depth was accurate in the shallow area, while large errors gradually increased with depth. We investigated whether the noise assumes in the simulated dataset was not represent the actual condition of the tested image. For this purpose, I build another simulated dataset with an additive noise added. This refers to the concept of noise in an optical remote sensing system that additive in nature and normally distribute. Gaussian Noise is a statistical noise that has a

probability density function of the normal distribution (also known as Gaussian distribution). It is represented the condition of noise that creates because of natural processes which introduce noise.

The noise level is set based on standard deviation of the residual of used in the Lyzenga06 correction as following

$$\rho_{TOA_\infty} = \alpha_0 + \alpha_1 \cdot \rho_{NIR1_\infty} + \alpha_2 \cdot \rho_{NIR2_\infty} + residual \qquad \text{Equation 5-3}$$

where $\rho_{TOA_\infty}$is the TOA reflectance of visible band deep water pixels, ρ_{NIRn_∞} is TOA reflectance of NIR band deep water pixels, α is regression coefficients.

The Standard deviation of the residual of above model shows the level of error introduced just by the atmospheric correction and represented remaining noise after the atmospheric correction. Table 5-3 shows the standard deviation of the residual for all evaluated sites and also the minimum, maximum, and average value.

Table 5-3 Standard deviation of the residual for ten evaluated sites

Sites	Residual standard error				
	Coastal	**Blue**	**Green**	**Yellow**	**RedEdge**
Gili Mantra Island	0.000872	0.0009429	0.0008904	0.0005778	0.0008079
Gondol Beach	0.0007799	0.001082	0.0008938	0.00108	0.0007838
Menjangan Island	0.001314	0.001906	0.001274	0.0009522	0.001187
Panggang Island	0.001392	0.001859	0.001291	0.001137	0.007963
Sorong Beach	0.01499	0.01858	0.01676	0.01614	0.01294
Pamanggangan Island	0.001259	0.001848	0.001497	0.001256	0.001305
Sarappo Keke Island	0.0009984	0.001231	0.000841	0.0006723	0.0007249
Sarappo Lompo Island	0.0007681	0.001094	0.000781	0.0005120	0.0005609
Luwu luwu Island	0.001067	0.002472	0.001675	0.0007226	0.001231
Badi Island	0.001112	0.002082	0.001424	0.0007176	0.0009497
Minimum	0.000768	0.000943	0.000781	0.000512	0.000561
Mean	0.002455	0.00331	0.002733	0.002377	0.002845
Maximum	0.01499	0.01858	0.01676	0.01614	0.01294

Table 5-4 Noise cases for noisy assumption simulated dataset and the accuracy assessment

No	Noise Cases	Noise (standard deviation value)					RMSE (m)		
		Coastal	Blue	Green	Yellow	RedEdge	Min	Mean	Max
1	Zero noise	0	0	0	0	0	6.76	3.91	2.14
2	Residual Minimum	0.00076	0.00094	0.00078	0.00051	0.000561	4.12	2.98	1.66
3	Residual Mean	0.00245	0.00331	0.00273	0.00237	0.002845	4.14	2.97	1.69
4	Residual Maximum	0.01499	0.01858	0.01676	0.01614	0.01294	5.02	3.13	1.82
5	Equal Sd. 0.01	0.01	0.01	0.01	0.01	0.01	4.72	3.06	1.77
6	Equal Sd. 0.005	0.005	0.005	0.005	0.005	0.005	4.41	3	1.72
7	Equal Sd. 0.001	0.001	0.001	0.001	0.001	0.001	4.13	2.97	1.68
8	Equal Sd. 0.0001	0.0001	0.0001	0.0001	0.0001	0.0001	4.17	3.02	1.71
9	Equal Sd. 0.00001	0.00001	0.00001	0.00001	0.00001	0.00001	6.61	3.86	2.13
10	Combina-tion Sd1	0.001	0.00001	0.00001	0.0001	0.001	4	3.02	1.55
11	Combin-ation Sd2	0.0001	0.000001	0.00001	0.0001	0.001	3.99	2.87	1.55
12	Combina-tion Sd3	0.001	0.0001	0.00001	0.0001	0.001	3.99	3.02	1.56

Table 5-4 shows that the overall response to this noise assumption approach is positive as expected, where accuracy is increasing. The minimum residual of standard deviation from residual the Lyzenga06 correction shows to be more

accurate with RMSE of 4.12m, 2.98m, and 1.66m for the minimum, average, and maximum, respectively. This improvement reaches 1-2m more accurate that the zero noise assumption. Then the coefficients from a simulated dataset with the additive noise of minimum residual of standard deviation were used for the proposed noisy assumption water depth estimation formula.

Besides the minimum, maximum and average of standard deviation from residual the Lyzenga06 correction, this study also tested several standard deviation values that range from 0.01 – 0.00001 as shown in Table 5-4 (case 5 – 9). In order to evaluate the range of optimum noise level that needs to be added into the simulation dataset. As a result, the accuracy is achieved maximum at noise range from 0.001 – 0.0001 value of standard deviation. Moreover, a different noise level for each band was also tested (Table 5-4, case 10-12). For this case, the accuracy found to be better but not significant. This fact shows that the accuracy level still able to improve if the noise level is different for each specific band, and further investigation is needed to reveal the most appropriate noise level at each band.

Finally, a simulation-derived coefficient was extracted from the simulated dataset with an additive noise of minimum standard deviation of residual. Last, estimate the depth from the ten sites using the proposed noisy assumed formula. The depth estimation formula using the noisy assumed simulation-derived coefficients for Worldview-2 images is presented as:

$$\hat{h}(m) = \beta_0 + 0.06538 \cdot X_{coastal} + 0.75803 \cdot X_{blue} + 1.9524 \cdot X_{green} - 3.07569 \cdot X_{yellow} - 0.90543 \cdot X_{red} \quad \text{Equation 5-4}$$

Table 5-5 shows the RMS residual of estimated depth using noisy assume formula; almost all the site shows accuracy improvement using the noisy assume formula. From nine of ten sites, the noisy assume formula give a better accuracy with 0.04 – 5.61 m less error. Compared with the shallow area (< 5 m) the accuracy was significantly increased in deeper area (> 5 m). This finding strength our confidence that the poor performance of simulated-derived coefficient (subsection 5.3.1) was due noise factor of tested image. Even, our tested image has pass atmospheric and surface noise correction; there was a big opportunity that the noise not perfectly

removed.

Table 5-5 Statistics for RMS error [m] of estimated depth at depth range in each site using the formula of simulated-derived coefficients of noisy assumed simulated dataset.

Sites	Depth range [m]							
	0 -1	**2 - 3**	**4 - 5**	**6 -7**	**8 - 9**	**10 - 11**	**12 - 13**	**14 - 15**
Gili Mantra Island	0.81	0.49	0.80	1.90	3.64	5.68	7.77	9.02
Gondol Beach	NA	0.91	0.43	2.08	4.44	NA	NA	NA
Menjangan Island	NA	1.97	1.96	3.59	4.46	NA	NA	NA
Panggang Island	0.34	0.41	1.39	3.89	5.25	7.42	9.00	NA
Sorong Beach	NA	NA	0.70	2.52	4.28	6.91	NA	NA
Pamanggangan Island	0.22	0.31	0.75	1.16	2.26	4.23	6.05	8.15
Sarappo Keke Island	0.28	0.71	0.81	2.08	4.01	6.16	7.40	9.15
Sarappo Lompo Island	0.27	0.69	0.98	1.83	3.69	5.13	7.06	9.05
Luwu luwu Island	0.55	0.49	0.89	2.18	4.27	5.57	8.09	9.51
Badi Island	0.82	0.48	1.81	3.44	5.57	7.31	9.43	10.84

Even the proposed noisy assumed formula still far from our expectation, specifically in deeper mapping area (> 5 m). These discrepancies can be neglected because the targeted mapping area is dominated by a very shallow water depth. Table 5-6 shows that more than 65 - 89 % of the targeted mapping area in the evaluated site have a depth ranging from 0-5 m., except for Gondol and Pamanggangan Site. As the final word, we are suggesting the usage of proposed noisy assumed formula shown in Equation 5-4 to be applied to mapping only the shallower part of the coral reef environment, as our experiment indicates that the error is less than 1 meter. This error level was accepted for the usage of bathymetry map of conservation area or shipping line (IHO, 2005), but could be used for detail map such as a harbor construction based map.

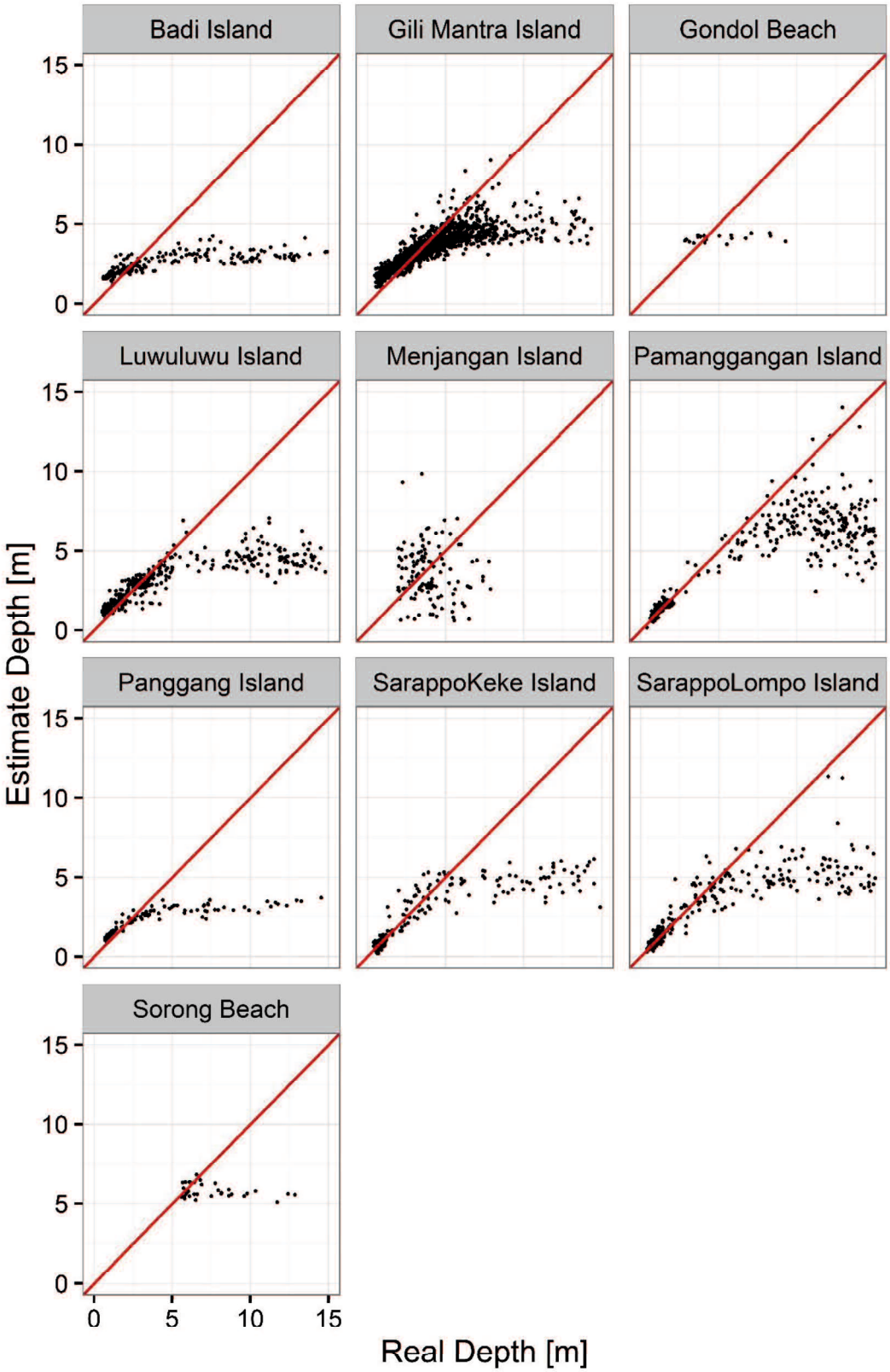

Figure 5-2 Scatterplot of depth estimation using proposed noisy assumed formula for each site. The red line is a straight line y = x.

Table 5-6 Targeted mapping area of shallow coral reef in ten evaluated sites**.** The percent number shows the persentage of area at specific depth range over the entire shallow water area (0-25 m)

Sites	Shallow Water area in m^2 and percent				
	0 -25 m	Shallow water 0 – 5 m		Deep water 6 – 25 m	
Gili Mantra Island	4,649,072	2,912,840	63%	1,736,232	37%
Gondol Beach	590,672	62,480	11%	528,192	89%
Menjangan Island	949,984	818,040	86%	131,944	14%
Panggang Island	7,221,984	4,660,360	65%	2,561,624	35%
Sorong Beach	24,483,892	18,492,364	76%	5,991,528	24%
Pamanggangan Island	4,822,856	1,712,880	36%	3,109,976	64%
Sarappo Keke Island	706,556	497,560	70%	208,996	30%
Sarappo Lompo Island	1,235,340	924,856	75%	310,484	25%
Luwu luwu Island	1,581,952	1,218,736	77%	363,216	23%
Badi Island	561,940	390,936	70%	171,004	30%

5.4. Conclusion

In summary, the formula of the simulation-derived coefficients shows the possibility to estimate the water depth of Indonesian shallow waters with a limited number of measurements. Unfortunately, the image noise (atmospheric, surface, or sensor) might control the performance of the proposed method. Moreover, the best performance was achieved at shallow depth (± less than 5 meters) sites. Thus, another coefficient was derived from a simulated dataset with additive noise was also tested. The formula from noisy assumed simulation-derived coefficients give a better estimation accuracy; it shows that the tested image was noise contained and a zero noise assumption formula could not work perfectly. The present finding has importance implication for solving the problem of the difficulty in collecting

measurement depth data of hazardous shallow coral reef water. In eight from ten of the tested sites, an area with 0-5 m depth range was covered more than 65% of the targeted mapping area (shallow coral reef at 0-25 m depth range).

Future work will concentrate on improving the formula so that it overcomes the poor depth estimations in deep waters. Moreover, it is also necessary to test the method in a larger number of sites or images.

Chapter 6. *General Discussion and Conclusion*

Given the importance of the coral reef ecosystems for life quality and the global climate, efficient and adequate information about the biogeochemical contents, water clarity, bathymetry, and distribution of benthic habitats of coral reef ecosystems are important for government agencies and the public. Satellite-based imaging systems with multispectral bands within the visible spectrum reliably provide information at spatial scales needed to implement spatially based conservation actions for coral reef locations, such as the Indonesia coral reef area. This work has demonstrated the application of very high-resolution multispectral imagery with less in-situ data to estimate bathymetry in the shallow-water coral reef environments.

For the Satellite derived bathymetry based on Worldview-2 multispectral images, this study affirms that atmospheric correction methods should carefully be applied to WV2 imagery before the development of bathymetric, in order to increase the accuracy of the final products. Preprocessing methods alter the estimated radiance and reflectance values to account for known sources of error in the data, resulting in values that more closely estimate the true radiance and reflectance. Ideally, the evaluation of atmospheric correction is compared the retrieved reflectance from satellite images with ground-based measurements for a variety of targets, however, since there were no ground-based measurements then the evaluation was the focus on the performance on accuracy improvement compared with without atmospheric correction. Thus, it is surprising that applying atmospheric correction procedures prior to fitting the depth derivation model sometimes could not improve the retrieved water depths.

Selecting a proper atmospheric correction method became an essential step in multispectral SDB. Base on the result of this study that the method using radiative transfer simulation (6S) had little effect on accuracy, whereas Dark Object Subtraction had no effect whatsoever, because a homogenous atmosphere was assumed. Pixel-wise correction using near-infrared bands (Lyzenga06) was the only

method influencing accuracy, but it significantly reduced the number of valid pixels. Then the recommendation is using one of the non-correction methods and Lyzenga06 correction method (with three possible NIR-band combinations) for each target image, depending on acceptable data reduction and the required accuracy.

A previous study on Lyzenga's SDB formula shows a good fit in estimating a water depth. However, there was no scientific publication evaluating the performance of the Lyzenga's SDB formula under a variety of optical conditions and bottom types that it applies to use for an unknown environment. A simulated dataset was used to evaluate the Lyzenga's SDB formula. Simulated dataset was represented multispectral images of a shallow coral reef environment and build using Lee's radiative transfer model. This study provides a basis for other research and this study effort aimed at the usage of Lyzenga's for mapping shallow coral reef bathymetry.

Lyzenga (2006) in the paper mention that the application of this method was limited to some bottom types, where the number of bottom types is no greater than the number of multispectral bands. Surprisingly, the result of this study said; differently, the simulated-based analysis shows that this model still works perfectly (0.97 of R2 and 0.4 m of RMSR) under 137 bottom types, which much higher than the number of multispectral bands been used (five visible bands of WV2). But still, the influence of bottom types plays the most significant role in Lyzenga's model, compared with the water quality. It means that a variety of water quality on images was less affecting the accuracy of the retrieved water depths. An importance information for several researchers that doubt the performance of Lyzenga's SDB formula under diverse water quality. Moreover, the bottom spectral variance became the main issue on Lyzenga's model, where more variance the spectral signature less accurate the retrieved water depths obtained.

The last simulation based experiment conduct in this study was testing the set of simulation-derived coefficients for estimating the water depth of unknown bottom type. As became the goal to proposed a simulation-derived coefficient for water depth estimation formula that able to predict a depth with less in-situ

measurement. That means no in-situ measurement used for model fitting to obtain the coefficient (Lyzenga's SDB formula based), and in-situ measurement was only for converting the relative depth to absolute depth or as intercept adjustment. Even the simulation dataset build based on 137 different bottom types there still a high opportunity that some bottom type appear in targeted coral site was not included. Then to test this issue, every bottom type (from 137 bottom types) has been excluded from the simulation dataset model fitting; then the excluded bottom types was used as tested data. As a result, the maximum RMS residual was 1.03 m when the bottom type excluded, which just 0.08 meter higher than if all the bottom types are used (RMS residual = 0.95 m). This performance has confirmed that our water depth estimation model or formula was general enough to predict a water depth from a coral reef area with unknown bottom types.

As the final works, we extracted the coefficient from the fitting of simulation dataset used then tested the performance of ten evaluated coral reef sites. The result was varied across locations, and depth range, wherein few location the estimation is failed. Moreover, the other site shows the best performance at shallow depth (± less than 5 meters), and error gradually increased follow with depth. This result was far from the expectation if refer to the simulation analysis result. This poor performance on the application on real WV2 imagery shows an opposite result from the simulation analysis where the formula was able to estimate the depth of unknown bottom type accurately (maximum RMS error ± 1m). Since those promising result of the simulated based analysis was performed under a zero noise assumption. In reality, multispectral imagery always contains noise even after a correction method been performed. Then a simulation-derived coefficient based on a noisy assumption for water depth estimation formula was built from the simulated dataset with additive noise. Minimum two pixels with known depth for each image is needed to adjust the intercept of depth estimation formula, as this study used five pixels with known depth. As a result, the retrieved water depths accuracy was improved (± less than 5 meters: RMSE 0.22– 1.96m) compared with the zero noise assumption. In fact, by adding a noise component to the simulated dataset, the accuracy significantly improved. By optimizing noise component in further studies,

there is room for improving the accuracy.

As a recommendation, for mapping a very shallow area (less than 5 meters), the depth estimation formula from noisy assumed simulation-derived coefficients shows to give a good accuracy with error ranging from 0.26 - 0.92 meter. This will help to remove the risk of measuring a depth data in a shallow coral reef environment. Since in the most shallow coral reef site (refer to the ten coral reef site used in this study), the area of 0 – 5meter depth is cover more than 60% of targeted mapping area.

References

Abraira, V., Vargas, A.P.D., and Cajal, H.R. (1999). Generalization of the kappa coefficient for ordinal categorical data, multiple observers and incomplete designs. Questiio: 23, 561–571.

Allen, G.R. (2008). Conservation hotspots of biodiversity and endemism for Indo-Pacific coral reef fishes. Aquatic Conservation: Marine and Freshwater Ecosystems. 18(5): 541--556.

Baker, K. S., and Smith, R. C. (1982). Bio-optical classification and model of natural waters. 2. Limnology and Oceanography, 27(3), 500-509. doi: 10.4319/lo.1982.27.3.0500

Brando, V. E., Anstee, J. M., Wettle, M., Dekker, A. G., Phinn, S. R., and Roelfsema, C. (2009). A physics based retrieval and quality assessment of bathymetry from suboptimal hyperspectral data. Remote Sens. Environ 113 (4): 755-770. doi:10.1016/j.rse.2008.12.003.

Bricaud, A., Morel, A., Babin, M., Allali, K., and Claustre, H. (1998). Variations of light absorption by suspended particles with chlorophyll a concentration in oceanic (Case-1) waters: Analysis and implications for bio-optical models. J. Geophys. Res. Oceans, 103(C13): 31033–31044. doi: 10.1029/98JC02712

Carder, K.L., Cannizzaro, J.P., and Lee, Z. (2005). Ocean color algorithms in optically shallow waters: Limitations and improvements. Proc. SPIE 5885: 588506. doi: 10.1117/12.615039

Chavez, P. S. 1988. An improved dark-object subtraction technique for atmospheric scattering correction of multispectral data. Remote Sens. Environ 24 (3): 459-479. doi:10.1016/0034-4257(88)90019-3.

Clark, R.K., Fay, T.H., and Walker, C.L. (1987). Bathymetry calculations with Landsat 4 TM imagery under a generalized ratio assumption. Appl. Opt., 26(19): 4036–4038. doi: 10.1364/AO.26.4036_1

Cohen, J. A coefficient of agreement for nominal scales. (1960). Educ. Psychol. Meas.: 20, 37–46.

Daniell, J.J. (2008). Development of a bathymetric grid for the Gulf of Papua and adjacent areas: A note describing its development. J. Geophys. Res. Earth Surf., 113: F01S15. doi: 10.1029/2006JF000673

Deakin, R.E. and Kildea, D.G. (1999). A note on standard deviation and RMS. Australian Surveyor, 44(1): 74–79.

Eugenio F., J. Marcello and J. Martin. (2015). High-resolution maps of bathymetry and benthic habitats in shallow-water environments using multispectral remote sensing imagery. IEEE Trans. Geosci. Remote Sens. 53 (7): 3539-3549. doi:10.1109/TGRS.2014.2377300.

Flener, C., Lotsari, E., Alho, P., and Käyhkö, J. (2012). Comparison of empirical and theoretical remote sensing based bathymetry models in river environments. River Research and Applications, 28(1): 118–133. doi: 10.1002/rra.1441

Ferse, S.C.A., Glaser, M., Neil, M., Schwerdtner Máñez, K. (2012). To cope or to sustain? Eroding long-term sustainability in an Indonesian coral reef fishery. Regional Environmental Change. Doi: 10.1007/s10113- 012-0342-1

Green, E.P.; Mumby, P.J.; Clark, C.D.; Edwards, T.M. (2000). Remote Sensing Handbook for Tropical Coastal Management, Coastal Management Sourcebooks, 3. UNESCO Publishing: Paris, France.

Glaeser, B., and Glaser, M. (2011). People, fish and coral reefs in Indonesia: A contribution to social-ecological research. Gaia, 20(2): 139-141.

Jupp, D. L. B. (1988, September). Background and extensions to depth of penetration (DOP) mapping in shallow coastal waters. In Proceedings of the Symposium on Remote Sensing of the Coastal Zone (pp. IV-2).

Hochberg, E.J., Atkinson, M.J., Apprill, A., and Andréfouët, S. (2004). Spectral reflectance of coral. Coral Reefs, 23(1): 84–95. doi: 10.1007/s00338-003-0350-1

Kanno, A. and Tanaka, Y. (2011). Modified Lyzenga's Method for Estimating Generalizes Coefficients of Satellite-based Prediction of Shallow Water Depth. IEEE Geoscience and Remote Sensing Letters, 9(4): 715-719. doi: 10.1109/LGRS.2010.2051658

Kanno, A. and Tanaka, Y. (2013). Generalized Lyzenga's Predictor of Shallow Water 1 Depth for Multispectral Satellite Imagery. Marine Geodesy, 36(2): 1-12. Doi: 10.1080/01490419.2013.839974

Kvalseth, T.O. (2011). Kappa Coefficient of Agreement. In International Encyclopedia of Statistical Science; Lovric, M., Ed.; Springer: Berlin, Germany, pp. 710–713.

Leckie, D.G., Cloney, E.E., Jay, C., and Paradine, D. (2005). Automated mapping of stream features with high-resolution multi-spectral imagery: an example of the capabilities. Photogramm. Eng. Remote Sens., 71(2): 145–155.

Lee, Z., Carder, K.L., Mobley, C.D., Steward, R.G., and Patch, J.S. (1999). Hyperspectral remote sensing for shallow waters: 2. Deriving bottom depths and water properties by optimization. Appl. Opt., 38(18): 3831–3943. doi: 10.1364/AO.38.003831

Liceaga-Correa, M. A., & Euan-Avila, J. I. (2002). Assessment of coral reef bathymetric mapping using visible Landsat Thematic Mapper data. International Journal of Remote Sensing, 23(1), 3-14. doi: 10.1080/01431160010008573

Lyzenga, D.R., N. P. Malinas, and F. J. Tanis. (2006). Multispectral bathymetry using a simple physically based algorithm, IEEE Trans. Geosci. Remote Sens. 44 (8): 2251–2259. doi:10.1109/TGRS.2006.872909.

Lyzenga, D.R. 1978. Passive remote sensing techniques for mapping water depth and bottom features. Appl. Opt. 17(3): 379–383. doi:10.1364/AO.17.000379.

Ma, R., Duan, H., Liu, Q., and Loiselle, S.A. (2011). Approximate bottom contribution to remote sensing reflectance in Taihu Lake, China. Journal of Great Lakes Research, 37(1): 18-25. doi: 10.1016/j.jglr.2010.12.002.

Mahiny, A.S., and Turner, B. J. (2007.) A comparison of four common atmospheric correction methods. Photogrammetric Eng. & Remote Sens. 73 (4): 361-368. doi:10.14358/PERS.73.4.361

Manessa, M.D.M., A. Kanno, M. Sekine, E.E. Ampou, N. Widagti, and A.R. As-syakur. (2014). Shallow-water benthic identification using multispectral satellite imagery: Investigation on the effects of improving noise correction method and spectral cover. Remote Sens.6 (5): 4454–4472. doi:10.3390/rs6054454.

Martin, J., Eugenio, F., Marcello, J., Medina, A., Bermejo, J.A. and Arbelo, M. (2012), November. Atmospheric correction models for high resolution WorldView-2 multispectral imagery: A case study in Canary Islands, Spain. In SPIE Remote Sens. (pp. 85340O-85340O). International Society for Optics and Photonics.

McKenna, S.A., Allen, G.R., and Suryadi, S. (eds.). (2002) A Marine Rapid Assessment of the Raja Ampat Islands, Papua Province, Indonesia. RAP Bulletin of Biological Assessment 22. Conservation International, Washington, DC.

Morel, A. and Maritorena, S. (2001). Bio-optical properties of oceanic waters: A reappraisal. J. Geophys. Res., 106(C4): 7163–7180. doi: 10.1029/2000JC000319

Morel, A., Antoine, D., and Gentili, B. (2002). Bidirectional reflectance of oceanic waters: accounting for Raman emission and varying particle scattering phase function. Appl. Opt., 41(30): 6289–6306. doi: 10.1364/AO.41.006289

Nurlidiasari, M. (2004). The application of QuickBird and multi-temporal Landsat TM data for coral reef habitat mapping case study: Derawan Island, East Kalimantan, Indonesia. Thesis, International Institute for Geo-Information Science and Earth Observation, Enschede, The Netherlands.

Pacheco, A., Horta, J., Loureiro, C., and Ferreira, Ó. (2015). Retrieval of nearshore bathymetry from Landsat 8 images: a tool for coastal monitoring in shallow waters. Remote Sens. Environ. 159: 102-116. doi:10.1016/j.rse.2014.12.004.

Paredes, J. M and Spero, R. E., (1983). Water depth mapping from passive remote sensing data under a generalized ratio assumption. Appl. Opt. 22(8): 1134-1135. doi: 10.1364/AO.22.001134

Philpot, W.D. (1989). Bathymetric mapping with passive multispectral imagery. Appl. Opt., 28(8): 1569–1578. doi: 10.1364/AO.28.001569

Research System Inc. (2009). ENVI Online Help. Research System Inc.: Boulder, CO, USA.

Ribeiro, S. R. A., Centeno, J. A. S., and Krueger, C. P. (2008). An estimate of depth from a bathymetric survey and IKONOS II data by means of artificial neural network. Boletim de Ciências Geodésicas 14: 171–185.

Roelfsema, C.M., and Phinn, S.R. (2012). Spectral Reflectance Library of Selected Biotic and Abiotic Coral Reef Features in Heron Reef. Pangaea, Bremerhaven, Germany.

Sagar, S., V. Brando, M. Sambridge. (2014). Noise estimation of remote sensing reflectance using a segmentation approach suitable for optically shallow waters. IEEE Trans. Geosci. Remote Sens. 52(12):7504-7512. doi:10.1109/TGRS.2014.2313129.

Sagawa, T., Boisnier, E., Komatsu, T., Mustapha, K.B., Hattour, A., Kosaka, N., and Miyazaki, S. (2010). Using bottom surface reflectance to map coastal marine areas: a new application method for Lyzenga's model. Int. J. Remote Sensing, 31(12): 3051–3064. doi: 10.1080/01431160903154341

Sagawa, T., Mikami, A., Aoki, M.N., and Komatsu, T. (2012). Mapping seaweed forests with IKONOS image based on bottom surface reflectance. Proc. SPIE, 8525: 85250Q. doi: 10.1117/12.975678

Smith, R.B. (2012). Remote Sensing of Environment; MicroImages Inc.: Lincoln, NE, USA.

Spitzer, D. and Dirks, R.W.J. (1987). Bottom influence on the reflectance of the sea. Int. J. Remote Sens., 8(3): 279–290. doi: 10.1080/01431168708948642

Stehman, S.V. (1997). Selecting and interpreting measures of thematic classification accuracy. Remote Sens. Environ.: 62, 77–89.

Stumpf, R.P., Holderied, K., and Sinclair, M. (2003). Determination of water depth with high-resolution satellite imagery over variable bottom types. Limnol. Oceanogr., 48(1): 547–556. doi: 10.4319/lo.2003.48.1_part_2.0547

Su, H., Liu, H., and Heyman, W.D. (2008). Automated derivation of bathymetric information from multi-spectral satellite imagery using a non-linear inversion model. Mar. Geod., 31(4): 281–298. doi: 10.1080/01490410802466652

Su, H., Liu, H., Wang, L., Filippi, A.M., Heyman, W.D., and Beck, R.A. (2013). Geographically adaptive inversion model for improving bathymetric retrieval from satellite multispectral imagery. IEEE Trans. Geosci. Remote Sens., 52(1): 465–476. doi: 10.1109/TGRS.2013.2241772

Updike, T., and Comp, C., (2010). A Radiometric Use of WorldView-2 Imagery, Technical Note, Digital Globe.

Vanderstraete, T.; Goossens, R.; Ghabour, T.K. (2004) Coral reef habitat mapping in the red sea (Hurghada, Egypt) based on remote sensing. EARSeL eProc.: 3, 191–206.

Vermote, E. F., D. Tanré, J. L. Deuzé, M. Herman, and J.J. Morcette. (1997). Second simulation of the satellite signal in the solar spectrum, 6S code: An overview. IEEE Trans. Geosci. Remote Sens. 35(3): 675-686. doi:10.1109/36.581987.

Vermote, E., D. Tanré, J. L. Deuzé, M. Herman, J. J. Morcrette, and S. Y. Kotchenova. (2006). Second simulation of a satellite signal in the solar spectrum – vector (6S codeV), 6S code User Guide Version 3.

Vinayaraj, P., Raghavan, V., and Masumoto, S. (2016). Satellite-Derived Bathymetry using Adaptive Geographically Weighted Regression Model. Marine Geodesy 39(6): 458–478. doi: 10.1080/01490419.2016.1245227.

Yuzugullu, O. and Aksoy, A. (2014). Generation of the bathymetry of a eutrophic shallow lake using WorldView-2 imagery. J. Hydroinf., 16(1): 50–59. doi: 10.2166/hydro.2013.133

Appendix Bottom Irradiance Spectral

No	Bottom Type Name	Bottom Type Symbol	Site	Class
001	MUD	b0MUD	derawan	substrate
002	Algae.1	b01PadinaarborescensHolmes	japan	coral
003	coralline_algae	b02Corallinealgae1	bali	algae
004	coralline_algae.1	b03Corallinealgae2	bali	algae
005	CA	b04Corallinealgae3	derawan	algae
006	Coralline_Algae	b05Corallinealgae4	world	algae
007	Algaebrown	b06Eckloniacava	japan	algae
008	seagrass	b07Gelidiumcrinale	japan	algae
009	green_macroalgae	b08Greenmacroalgae	world	algae
010	HALIMEDA	b09Halimeda1	derawan	algae
011	halimeda	b10Halimeda2	world	algae
012	SPONGE	b11Sponge	derawan	algae
013	PADINA	b12Padina	derawan	algae
014	Algae.2	b13brownRockalgae	japan	algae
015	Algae.3	b14greenRockalgae	japan	algae
016	seagrass.1	b15Sargassumfusiforme	japan	algae
017	Sargassum_horneri	b16Sargassumhorneri	japan	algae
018	Algaebrown.1	b17Sargassumringgoldianum	japan	algae
019	tuft_algae	b18Tuftalgae	world	algae
020	Algae	b19Undariapinnatifida	japan	algae
021	acropora	b20Acroporasp1	world	coral
022	Acropora_formosa	b21Acroporasp2	spermonde	coral
023	ACROPOR	b22Acroporasp3	derawan	coral
024	Acropora_sp	b23Acroporasp4	bali	coral
025	Acropora_sp.1	b24Acroporasp5	bali	coral
026	acropora_palma	b25Acroporasp6	world	coral
027	OTHER	b26Coral1	derawan	coral
028	coral	b27Coral2	bali	coral
029	porites.1	b28Coral3	world	coral
030	CYAN	b29Cyanobacteria	derawan	coral
031	Cymodocea_sp	b30Cymodoceasp	spermonde	coral
032	Diploria_clivosa	b31Diploria	world	coral
033	GALAXY	b32Galaxeasp	derawan	coral
034	HELIOPORA	b33Heliopora	derawan	coral
035	macropora	b34Macropora	world	coral
036	porites	b35Poritessp1	world	coral
037	Porites_sp	b36Poritessp3	bali	coral
038	BRANPOR	b37Poritessp4	derawan	coral

No	Bottom Type Name	Bottom Type Symbol	Site	Class
039	MASSPOR	b38Poritessp5	derawan	coral
040	Sinularia_sp	b39Sinulariasp1	bali	coral
041	SINULARIA	b40Sinulariasp2	derawan	coral
042	soft_coral	b41Softcoral1	bali	coral
043	soft_coral.1	b42Softcoral2	bali	coral
044	OTHER_SC	b43Softcoral3	derawan	coral
045	Syringodium_sp	b44Syringodiumsp2	spermonde	coral
046	XENIA	b45Xenia	derawan	coral
047	Dead_Acropora	b46DeadCoral1	spermonde	deadcoral
048	deadcoral	b47DeadCoral2	world	deadcoral
049	DCBL	b48DeadCoralBleaching	derawan	deadcoral
050	DCCA	b49DeadCoralCorallineAlgae	derawan	deadcoral
051	DCTA	b50DeadCoralTuftAlgae	derawan	deadcoral
052	deadcoral_acropora	b51Poritessp6	world	deadcoral
053	Enhalus_sp	b52Enhalussp	spermonde	seagrass
054	Halophila_sp	b53Halophilasp	spermonde	seagrass
055	Seriotopora_stelata	b54Seriotoporastelata	spermonde	seagrass
056	syringodium_filiforme	b55Syringodiumsp1	world	seagrass
057	thalassia_testidinum	b56Thallasiasp1	world	seagrass
058	Thallasia_sp	b57Thallasiasp2	spermonde	seagrass
059	Z_asia	b58Zasiatica	japan	seagrass
060	Zcau	b59Zcaulescens	japan	seagrass
061	batu	b60Rock	japan	substrate
062	Rubber_..6_months.	b61Rubble1	spermonde	substrate
063	Sand_broken_shell	b62Rubble2	spermonde	substrate
064	Rubber_.6_Minus_12_months.	b63Rubblealgae	spermonde	substrate
065	SAND	b64Sand1	derawan	substrate
066	sand	b65Sand2	world	substrate
067	sand.1	b66Sand3	world	substrate
068	Sand	b67Sand4	spermonde	substrate
069	pasir	b68Sand5	japan	substrate
070	Montipora	b69Montipora	australia	coral
071	Chlorodesmis	b70Chlorodesmis	australia	algae
072	MontiporaBlue	b71MontiporaBlue	australia	coral
073	MontiporaBrown	b72MontiporaBrown	australia	coral
074	Gorgonian	b73Gorgonian	australia	coral
075	SoftCoral	b74SoftCoral	australia	coral
076	SandORrock	b75SandORrock	australia	substrate
077	FolioseCoral	b76FolioseCoral	australia	coral
078	MontiporaPurple	b77MontiporaPurple	australia	coral
079	DeadBranching	b78DeadBranching	australia	deadcoral

No	Bottom Type Name	Bottom Type Symbol	Site	Class
080	Laurencia	b79Laurencia	australia	algae
081	Gorgonian	b80Gorgonian	australia	coral
082	FluoresentCoral	b81FluoresentCoral	australia	coral
083	EncrustingBrown	b82EncrustingBrown	australia	coral
084	DigitateCoral	b83DigitateCoral	australia	coral
085	ChlorodesmisShaded	b84ChlorodesmisShaded	australia	algae
086	ChlorodesmisNotShaded	b85ChlorodesmisNotShaded	australia	algae
087	AcroporaLight	b86AcroporaLight	australia	coral
088	BrownCoral	b87BrownCoral	australia	coral
089	Rubble2	b88Rubble2	australia	substrate
090	FireCoral	b89FireCoral	australia	coral
091	Acropora	b90Acropora	australia	coral
092	MontiporaGreen	b91MontiporaGreen	australia	coral
093	DeadPlate200	b92DeadPlate200	australia	deadcoral
094	DeadPlate100	b93DeadPlate100	australia	deadcoral
095	CoralLine	b94CoralLine	australia	algae
096	AcroporaBrown1	b95AcroporaBrown1	australia	coral
097	AcroporaYellow1	b96AcroporaYellow1	australia	coral
098	AcroporaTurf1	b97AcroporaTurf1	australia	coral
099	AcroporaBrown2	b98AcroporaBrown2	australia	coral
100	AcroporaYellow2	b99AcroporaYellow2	australia	coral
101	AcroporaTurf2	b100AcroporaTurf2	australia	deadcoral
102	RubbleOrturf	b102RubbleOrturf	australia	substrate
103	CoralEncrusting	b103CoralEncrusting	australia	coral
104	Coraline	b104Coraline	australia	algae
105	MontiporaBlue	b105MontiporaBlue	australia	coral
106	AcroporaBrown	b106AcroporaBrown	australia	coral
107	DigitateGreen	b107DigitateGreen	australia	coral
108	GreenAlgae	b108GreenAlgae	australia	algae
109	AcroporaBlue	b109AcroporaBlue	australia	coral
110	AcroporaLightBrown	b110AcroporaLightBrown	australia	coral
111	AcroporaLight	b111AcroporaLight	australia	coral
112	AcroporaBrown	b112AcroporaBrown	australia	coral
113	Halimeda	b113Halimeda	australia	algae
114	Coraline	b114Coraline	australia	algae
115	Rock	b115Rock	australia	substrate
116	MassiveLive	b116MassiveLive	australia	coral
117	FolioseTurf	b117FolioseTurf	australia	deadcoral
118	FolioseLive	b119FolioseLive	australia	coral
119	DigitateLive	b120DigitateLive	australia	coral
120	DigitateDead	b121DigitateDead	australia	deadcoral

No	Bottom Type Name	Bottom Type Symbol	Site	Class
121	AcroporaTurf	b122AcroporaTurf	australia	deadcoral
122	AcroporaLive	b123AcroporaLive	australia	coral
123	AcroporaTurf	b124AcroporaTurf	australia	deadcoral
124	AcroporaLive	b125AcroporaLive	australia	coral
125	AcroporaBlue	b126AcroporaBlue	australia	coral
126	Lobophora	b127Lobophora	australia	algae
127	Porites	b128Porites	australia	coral
128	TurfOnPorites	b129TurfOnPorites	australia	coral
129	LiveEncrusting	b130LiveEncrusting	australia	coral
130	TurfEncrusting	b131TurfEncrusting	australia	algae
131	LaurenciaGreen	b132LaurenciaGreen	australia	algae
132	LaurenciaRed	b133LaurenciaRed	australia	algae
133	Halimeda	b134Halimeda	australia	algae
134	Cholorodesmis	b135Cholorodesmis	australia	algae
135	Caulerpa	b136Caulerpa	australia	algae
136	Caulerpa2	b137Caulerpa2	australia	algae
137	Caulerpa3	b138Caulerpa3	australia	algae
138	Dictyota	b139Dictyota	australia	algae
139	DictyotaSand	b140DictyotaSand	australia	algae
140	Turbinaria	b141Turbinaria	australia	algae
141	Enteromorpha	b142Enteromorpha	australia	algae
142	AlgaeSand	b143AlgaeSand	australia	substrate
143	AlgaeNoSand	b144AlgaeNoSand	australia	algae
144	AlgaeGreen	b145AlgaeGreen	australia	algae
145	Turbinaria	b146Turbinaria	australia	algae
146	Sand	b147Sand	australia	substrate
147	SandBMA	b148SandBMA	australia	substrate
148	Pocillopora	b149Pocillopora	australia	coral
149	LaurenciaRed	b150LaurenciaRed	australia	algae
150	LaurenciaGreen	b151LaurenciaGreen	australia	algae
151	FuzzyAlgae	b152FuzzyAlgae	australia	algae
152	Porites	b153Porites	australia	coral
153	RedSponge	b154RedSponge	australia	coral
154	Encrusting20ms	b155Encrusting20ms	australia	coral
155	Encrusting50ms	b156Encrusting50ms	australia	coral
156	Encrusting50msshade	b157Encrusting50msshade	australia	coral
157	Turf	b158Turf	australia	algae
158	Encrusting	b159Encrusting	australia	coral
159	BrownAcropora	b160BrownAcropora	australia	coral
160	BlueAcropora	b162BlueAcropora	australia	coral
161	PinkSponge	b163PinkSponge	australia	coral

No	Bottom Type Name	Bottom Type Symbol	Site	Class
162	TurfOnMassive	b164TurfOnMassive	australia	algae
163	AcroporaLightBrown	b165AcroporaLightBrown	australia	coral
164	AcroporaDarkBrown	b166AcroporaDarkBrown	australia	coral
165	MontiporaGreen	b167MontiporaGreen	australia	coral